CLASSIFICATION OF LUNG SOUNDS USING WAVELET-BASED NEURAL NETWORKS

by

Mete Yeğiner

B.S. in Physics,
Boğaziçi University, 1999

Submitted to the Institute of Biomedical Engineering
in partial fulfillment of the requirements
for the degree of
Master of Science
in
Biomedical Engineering

Boğaziçi University
September, 2002

ACKNOWLEDGMENTS

I would like to express my gratitude to Assoc. Prof. Yasemin P. Kahya for her supervising supports and encouragements in all the stages of my study. I will always remember hours-long exciting discussions on respiratory sound papers and preparations of conference papers until midnights.

I would like to thank Prof. Günseli Kılınç and her assistants for their help during respiratory sound recordings in Cerrahpaşa Medical School. We would not be able to take reliable data without their help.

I wish to thank members of Lung Acoustics Laboratory (LAL), Koray Çiftçi, Uğur Çini and Sameer Alsmadi for their time-independent encouraging friendships at every hour of the day, no matter how early or late (!).

My gratitude to my family is beyond words. Behind all those figures, tables and equations are there the endless support and warmness of them.

CLASSIFICATION OF LUNG SOUNDS USING WAVELET-BASED NEURAL NETWORKS

ABSTRACT

Computer-based systems for diagnosing diseases have been widely used in various areas of medicine in the last decades and similar studies have been performed to parameterize and increase the reliability of lung-sound based diagnosis by using computational techniques.

In this study, two types of classifiers, namely wavelet-based neural network and conventional artificial neural network (ANN), are used and compared for the classification of healthy and two-class pathological lung sounds which are acquired using two microphones on the chest wall along with the air-flow signal. The inputs of classifiers are organized using two different methods, 'even-odd partitioning' and 'leave-one-out'.

The lung sound signals belonging to inspiratory or expiratory phases are divided into thirty segments with 25% overlapping. In wavelet-based classifiers, the signals belonging to segments are decomposed to five levels using wavelet transforms and the reconstructed signal at each level is represented by AR parameters at the input of the network along with a volume constant indicating the sub-phases (early, mid, and late) of the respiratory cycle. The outputs of five networks belonging to five octaves are later combined to determine the performance of the classifier with respect to the frequency intervals used.

For the ANN, the AR parameters obtained from the segments and the volume constant are used as inputs for the network. The classifiers operate on the respiration phases separately and a comparison between the results of the two phases indicates that expiration is more useful in diagnosis.

Keywords: Lung sounds, artificial neural networks, wavelet-based neural networks, multiresolution analysis.

SOLUNUM SESLERİNİN DALGACIK TABANLI SİNİR AĞLARI İLE SINIFLANDIRILMASI

ÖZET

Geçen yüzyılın ikinci yarısında, bilgisayar tabanlı sistemler tıbbın farklı alanlarında hastalık tanısında yaygın halde kullanılmıştır. Benzer çalışmalar, akciğer sesine dayanan tanıların da güvenilirliğini artırmaya yönelik olarak yapılmaya başlanmıştır.

Bu çalışmada, iki tip sınıflandırıcı kullanılmıştır. Bunlar dalgacık tabanlı sinir ağları ve yapay sinir ağlarıdır (YSA). Bu sınıflandırıcıların sağlıklı ve iki farklı sınıf patolojik akciğer seslerini sınılandırmadaki başarımları karşılaştırılmıştır. Bu sesler, hava akışıyla eşzamanlı olarak, sırtın iki tarafına yerleştirilen mikrofonlar kullanılarak alınmıştır. Sınıflandırıcıların girdileri 'çift-tek ayırımı' ve 'birini-dışarıda-bırakma' yöntemleri kullanılarak düzenlenmiştir.

İçsoluma ve dışsoluma evrelerine ait akciğer sesleri %25 örtüşme ile otuz bölüte ayrılmıştır. Dalgacık tabanlı sinir ağlarında, bu bölütlere ait sinyaller dalgacık dönüşümüyle sıklık uzayında beş seviyeye ayrıştırılmış ve her seviye için yeniden yapılandırılan sinyaller özbağlanım kaysayılarıyla ifade edilmiştir. Bu katsayılarla birlikte solunum döngüsünün alt evrelerinin (erken-orta-geç) ifadesi olan hacim katsayıları sınıflandırıcıda girdi olarak kullanılmıştır. Her oktava ait sinir ağının çıktısı, sınıflandırıcının sıklık aralıklarındaki başarımını ölçmek için biraraya getirilmiştir.

YSA'da ise, bölütlere ait sinyallerden elde edilen özbağlanım katsayılarıyla beraber hacim sabiti, sınıflandırıcının girdilerini oluşturmuştur. Sınıflandırıcı solunum döngüsünün iki evresine de uygulanmıştır. Sınıflandırıcının bu evrelere ait başarımları karşılaştırıldığında, dışsoluma seslerinin tanıda kullanılmasının daha uygun olduğunu görülmüştür.

Anahtar sözcükler: Akciğer sesleri, yapay sinir ağları, dalgacık tabanlı sinir ağları, çoklu çözünürlük analizi.

TABLE OF CONTENTS

Page

LIST OF FIGURES

LIST OF TABLES

1. INTRODUCTION

Auscultation is a simple, patient-friendly and non-invasive method used for the diagnosis of respiratory diseases. However it is considered of low diagnostic value due to the subjectivity in the evaluation of sounds by human auditory perception and the difficulty in relating qualitative assessments to other people. Moreover the frequency response of the stethoscope attenuates frequency components of lung sounds above about 120Hz [1] although it is shown that lung sounds have considerable frequency components up to 2000Hz [2].

Over the recent years, there has been increased research activity in computerized methods for recording and analysis of respiratory sounds [3-4]. By means of these methods,

- physicians can find the opportunity for interaction with their colleagues and experts in the diagnosis by means of internet or intranet although they may not work at the same location,
- the recordings can be stored for future reference and can be used in the detection of changes in pathological conditions of patients,
- a database can be built to use both in diagnosis of other patients and education of young physicians.

The spectral characteristics of two phases of respiratory cycle, namely inspiration and expiration, show variations according to the state and pathology of the lung, with the spectra of the pathological sounds containing higher frequency components. Moreover in the case of pathological subjects, lung sounds contain adventitious sounds which are either continuous (e.g. wheezes) or transient (e.g. crackles) in behavior. The presence of crackles and their characteristics (number, epochs of occurrence and pitch) are indicative of different diseases, however since their duration is usually less than 100 ms, they have insignificant influence on the total spectrum. In the analysis of such transients, multi-resolution analysis is preferable since flexible time-scale localization is possible [5].

In our laboratory, Lung Acoustics Laboratory (LAL), researchers have been working to construct the recording and analyzing system for about ten years. In this study, the aim is to improve a classification algorithm for the computer-based system, "Intelligent Stethoscope," to supply diagnostic aid for physicians using respiratory sounds.

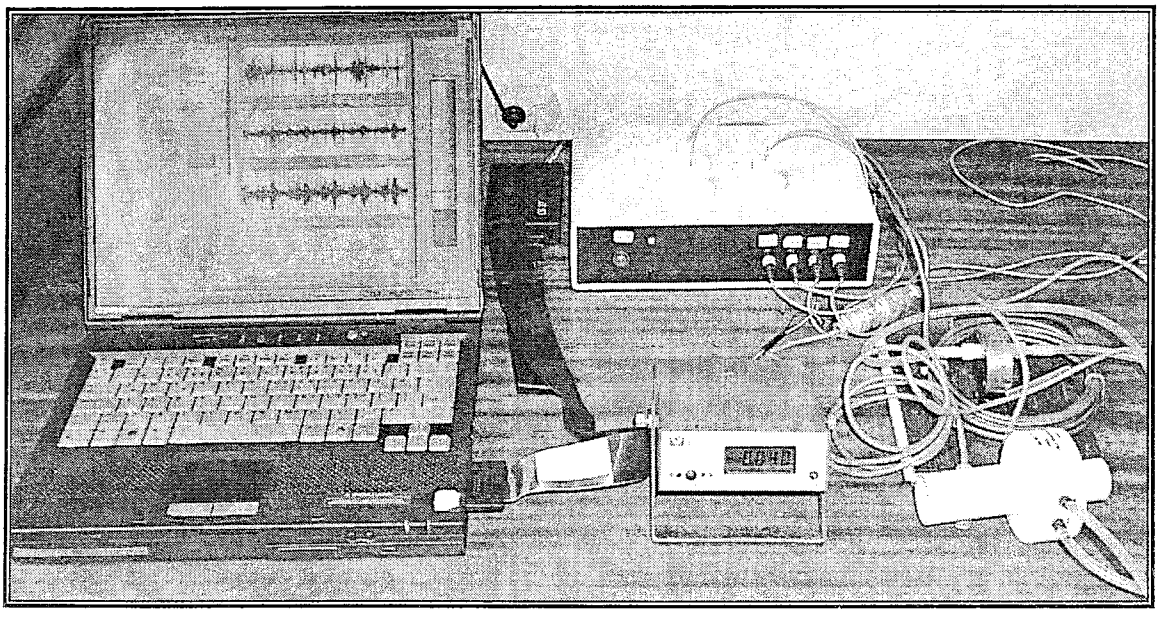

Figure 1.1 The components of the DAQ System

Our data acquisition (DAQ) system consists of

- a Fleish-type flowmeter (Validyne CD 379),
- three air-coupled microphones,
- a portable computer,
- analog signal conditioning card including amplifiers and filters,
- data acquisition card (NI-DAQCard500), and
- connectors.

Flow signal and respiratory sound signals are acquired simultaneously using the flowmeter and two microphones that are placed on the left and right posterior bases of the chest wall. The third microphone is used for measuring ambient noise. A low-noise preamplifier and a band-pass filter with flat frequency response at 80-2000 Hz are used in order to minimize frictional noise and heart sound interference and for an anti-aliasing cut-off frequency of 2 kHz. The amplified signals are digitized by the DAQ card at a 5 kHz

sampling rate and stored. For ordering and storing the sampled data, LabVIEW programming language is used.

The subjects form basically three classes, healthy and two main pathological classes of restrictive and obstructive diseases. The main cases of restrictive subjects are pneumonia, bronchopneumonia and fibrosing alveolitis whereas those of obstructive subjects are asthma, chronic bronchitis and emphysema. Three types of two-class based classification were processed in classifiers. They are

- Healthy-Restrictive,
- Healthy-Obstructive, and
- Healthy-Pathological.

Two types of classifiers, wavelet-based neural network and conventional artificial neural network (ANN), were used in classification. For conventional ANN, the respiratory sound signals belonging to inspiratory or expiratory phases were divided into thirty segments with 25% overlapping. The segments were modeled by autoregressive (AR) modeling. For each segment, four AR parameters that were acquired from modeling and a volume constant were used as inputs of classifier. The output of ANN determined the classifier performance.

In wavelet-based neural network, the 4^{th} level wavelet transform was applied to the each segment using 8^{th} order Daubechies' wavelet. After the application, four level wavelet coefficients and 4^{th} level scaling coefficients were acquired. By the reconstruction of these coefficients belonging to orthogonal five octaves, details and approximations were acquired. The inputs of classifiers were formed using the same approach as that of conventional ANN. However, details and approximations of segments were modeled in this classifier. The outputs of five networks belonging to five octaves were combined to determine the performance of classifier with respect to the frequency intervals.

The input matrices of classifiers were ordered two different ways, 'even-odd partitioning' and 'leave-one-out'. In the first method, input matrices of subjects were divided into testing and training input matrices with respect to their segment indexes. The

sets of odd indexed segments were used for training of classifiers whereas the set even ones were used for testing. In the second method, in each loop, the input matrix of one of the subjects from each class was used for testing of classifiers whereas those of other subjects were used for training of classifiers.

The organization of this thesis is as follows: Chapter 2 gives brief information about respiratory sounds and respiratory data acquisition. Chapter 3 consists of three topics that form the theoretical background of the algorithm used in our study, namely AR modeling using Yule-Walker equations, feed-forward back-propagation neural network and multiresolution analysis. In addition, the studies on respiratory sounds using the techniques of AR modeling and wavelet transforms are mentioned. In Chapter 4, our data acquisition system and classification algorithm are detailed. Chapter 5 contains the results and discussions about results. In Chapter 6, the classification algorithm and the ideas to improve the performance of the algorithm are discussed. In addition, recommendations for future studies are also included in this chapter. Appendix A contains the frequency responses of DAQ channels. Appendix B includes the diagrams of DAQ software while Appendix C presents patient profiles.

2. RESPIRATORY SOUNDS

2.1. Background

Respiratory sounds consist of all sounds related to respiration, e.g. breath sounds, adventitious sounds, cough sounds, snoring sounds, and sounds which stem from the respiratory muscles. Voiced sounds during breathing are not included in respiratory sounds [6].

Respiratory sounds can distinctively indicate the healthy and pathological conditions and they have been used for diagnosis since ancient times. Especially after the invention of the stethoscope by Laennec, the importance of auscultation in diagnosis has increased. He describes the breath sounds heard over the chest as "a distinct murmur corresponding to the flow of air into and out of air cells" [7]. However, the origin of the sounds is not completely certain and, probably, multiple mechanisms are involved [8].

The lung sounds cannot be generated by lung itself if there is no airflow. The turbulence of the air at the level of bronchi probably induces them. Because the gas velocity decreases and is less than critical level to induce turbulence, the airflow is silent in smaller bronchi [8].

The respiratory sounds of healthy subject heard over the chest are named as normal lung sounds. The peak frequency of normal lung sounds is usually below 100 Hz and it is very difficult to distinguish them from muscular and cardiovascular sounds. The energy of normal lung sounds decrease sharply between 100 and 200 Hz; however, they can still be detected at about 1000 Hz using sensitive microphones [3].

In pathological conditions, additional respiratory sounds (called as adventitious sounds) are superimposed over the normal lung sounds. They are divided into two main groups, namely transient and continuous adventitious sounds. The transient sounds, crackles, are explosive sounds heard mostly during inspiration rather than during expiration. It is assumed that crackles are originated from the acoustic energy generated by

pressure equalization or a change in elastic stress after a sudden opening of abnormally closed airways. As a result of segmental reopening of lung units, crackles may sometimes occur in healthy subject in deep inspiration [8]. Their duration is less than 20 ms and their frequency spectrum ranges from 100 Hz to 2 kHz or even higher.

Table 2.1

Major categories of respiratory sounds [3]

Respiratory Sound		Mechanisms	Origin	Acoustics	Relevance
Basic sounds	Normal lung sound	Turbulent flow vortices, unknown mechanisms	Central airways (expiration), lobar to segmental airway (inspiration)	Low-pass filtered noise (range <100 to >1,000 Hz)	Regional ventilation, airway caliber
	Normal tracheal sound	Turbulent flow, flow impinging on airway walls	Pharynx, larynx, trachea, large airways	Noise with resonances (range <100 to > 3,000 Hz)	Upper airway configuration
Adventitious sounds	Wheeze	Airway wall flutter, vortex shedding	Central and lower airways	Sinusoid (range ~100 to >1,000 Hz; duration, typically>80 ms)	Airway obstruction, flow limitation
	Rhonchus	Rupture of fluid films, airway wall vibrations	Larger airways	Series of rapidly dampened sinusoids (typically<300 Hz and duration>100 ms)	Secretions, abnormal airway collapsibility
	Crackle	Airway wall stress-relaxation	Central and lower airways	Rapidly dampened wave deflection (duration typically < 20 ms)	Airway closure, secretions

The continuous adventitious sounds, namely wheezing and rhonchus, are musical and sinusoidal sounds. Wheezes are produced by fluttering of the airways. When the airflow velocity reaches the critical level, the oscillations begin. The wheezes are always accompanied by flow limitation but each flow limitation is not necessarily accompanied by wheezes. The duration of wheezing is longer than 80 ms and its frequency components range between 100 Hz and to more than 1 kHz [3], [8]. In addition to the adventitious sounds mentioned above, another kind of sound, named as squawk, is a combination of crackles and wheezing. It is also called 'short wheezing'.

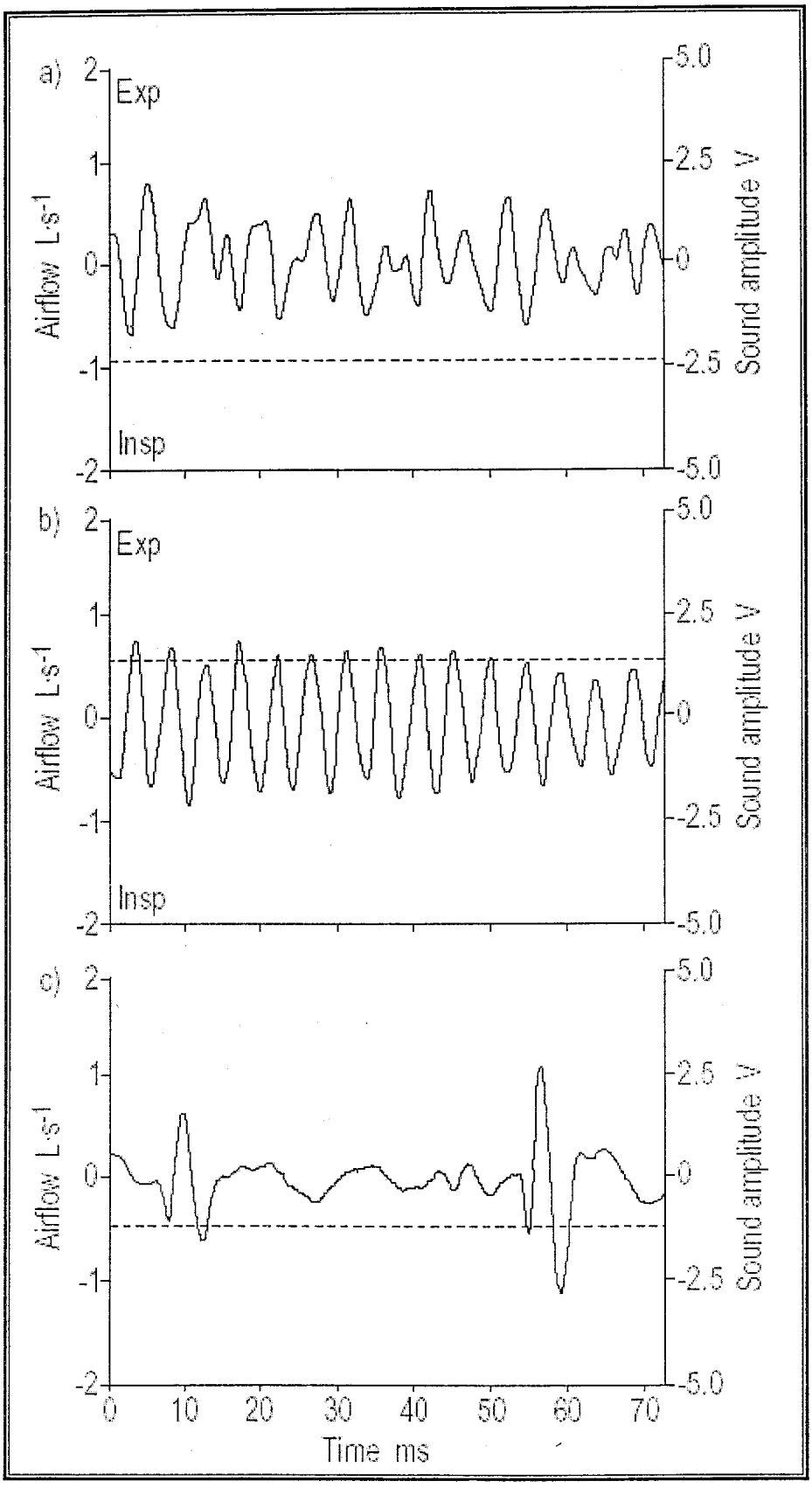

Figure 2.1 Examples of phonopneumograms of lung sounds in: a) a healthy subject; b) a patient with asthma with a wheezing sound; and c) a patient with alveolitis with crackles. —: sound amplitude; - - - : air-flow. Insp: Inspiration; Exp: Expiration [8].

In Table 2.1, a list of the main categories of respiratory sounds is shown with respect to mechanisms, origins, acoustical properties and relevance. In Figure 2.1, examples of normal lung sounds and pathological lung sounds with wheezing and crackles are depicted.

2.2. Obstructive and Restrictive Ventilatory Defects

The respiratory diseases stem from two main ventilatory defects, namely obstructive and restrictive defects. The former is a state that occurs generally in chronic obstructive diseases and asthma. During breathing, there is an airflow limitation in the lungs. Its characterizations are a decrease in the forced expiratory volume (FEV) more than any decrease in the vital capacity (VC) and low airflow at the mouth during forced breathing. The latter occurs commonly in diseases restricting lung expansion capability such as lung fibrosis, disorders of the pleural spaces, and chest wall neuromuscular diseases. It is characterized by a reduction in total volume capacity (TLC) [6].

2.3. Respiratory Data Acquisition and Preprocessing

The bandwidth used for respiratory sounds is between 60 to 100 Hz and 2 kHz when acquired on the chest wall whereas its upper limit is 4 kHz when recorded over trachea. The data acquisition (DAQ) system consists of sensors, amplifiers and filters, and an analog-digital (AD) converter [9]. High-pass filters eliminate low-frequency noise such as heart sounds, muscle sounds and frictional noise whereas low-pass-filters are used for anti-aliasing.

Two main types of sensors are used for respiratory recordings. The first type, "contact sensor," is coupled to the body surface and records surface movements directly. In the second type, "air-coupled sensor," the acoustic air pressure induced by body surface causes the movements of the diaphragm and the sensor record these movements. The air cavity between the chest wall and sensors is required to be closed since surface movements are so weak that the microphones cannot detect the pressure differences by free-field recordings or attachment to the chest wall [2],[9].

3. AUTOREGRESSIVE MODELING, NEURAL NETWORKS, MULTI-RESOLUTION ANALYSIS AND THEIR APPLICATIONS ON RESPIRATORY SOUNDS

The main methods used in our classifier involve autoregressive (AR) modeling using Yule-Walker equations, multilayer feed-forward neural networks, and multi-resolution analysis. Below is a discussion of these methods in conjunction with respiratory sounds.

3.1. Autoregressive Modeling

3.1.1. Stochastic Process and Modeling

Stochastic process is a time evolution of a statistical phenomenon according to probabilistic laws. The time evolution of phenomenon means that the process is a function of time, defined in a time interval. The statistical phenomenon means that, it is impossible to define the evolution of the process in time before conducting an experiment [10].

The idea of representation of a stochastic process by a model depends on Yule (1927). His idea is that a correlated time series that consist of highly correlated observations can be generated by applying a random process to a linear filter. The random process should have a Gaussian amplitude distribution and should be stable and time-invariant. The general time-domain description of the input-output relation for a stochastic model may be depicted in Figure 3.1. Autoregressive model is a popular type of linear stochastic models, where no past values of the model input are used [10].

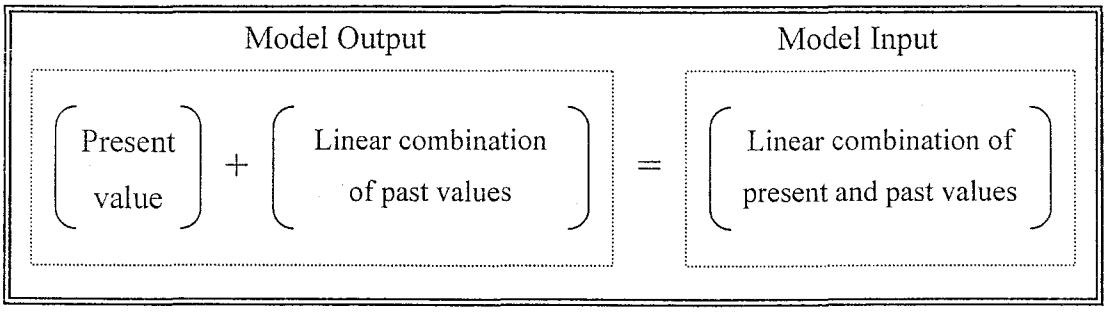

Figure 3.1 Description of the input-output relation of the stochastic model

3.1.2. Autoregressive Models and Yule-Walker Equations

The expression of present value of the process $y(n)$ by a finite linear combination of preceding p values and the error are shown by the equation

$$y(n) = l_1^* y(n-1) + ... + l_p^* y(n-p) + v(n) \tag{3.1}$$

where $l_1, l_2, ..., l_p$ are negative values of the set of AR parameters, $a_1, a_2, ..., a_p$, p is order of the model and $v(n)$ is white-noise process. The term $l_k^* y(n-k)$ is the scalar version of inner product of l_k and $y(n-k)$, where $k = 1,2,....., p$ [10].

For acquiring Yule-Walker equation, both sides of Eq. (3.1) are multiplied by $y^*(n-m)$ and expectation operator is applied to the equation. Because $E[y(n-k)y^*(n-m)]$ equals the autocorrelation function of process for a lag of $m-k$ and $E[v(n)y^*(n-m)]$ is zero for $m > 0$, the autocorrelation equation, Eq. (3.2), is acquired.

$$r(m) = l_1^* r(m-1) + l_2^* r(m-2) + ... + l_p^* r(m-p) \qquad \text{for } m > 0 \tag{3.2}$$

where $r(i)$ is the autocorrelation function of the process.

By calculating Eq. (3.2) for $m = 1,2,....., p$, we get a set of equations where the autocorrelation functions are known quantities whereas the AR parameters are the unknowns. This equation set can be expanded in matrix form, named as the Yule-Walker equations.

$$\begin{pmatrix} r(0) & r(1) & \cdots & r(p-1) \\ r^*(1) & r(0) & \cdots & r(p-2) \\ \vdots & \vdots & \ddots & \vdots \\ r^*(p-1) & r^*(p-2) & \cdots & r(0) \end{pmatrix} \begin{pmatrix} l_1 \\ l_2 \\ \vdots \\ l_p \end{pmatrix} = \begin{pmatrix} r^*(1) \\ r^*(2) \\ \vdots \\ r^*(p) \end{pmatrix} \tag{3.3}$$

3.1.3. Respiratory Sounds Application

In 1985, AR modeling was first used to estimate the characteristics of lung sounds by Cohen and Landsberg [2], [11]. Iyer and colleagues modeled the acoustic transmission through the lung parenchyma and chest wall as an all-pole filter [12]. With this approach, the source and transmission characteristics of lung sounds were estimated based on the lung sounds on the chest wall. The schematic diagram of their model is depicted in Figure 3.2. Cohen and Berstein designed an analyzing system for acoustic transmission of the respiratory system using two stochastic methods, namely AR and autoregressive moving average (ARMA) methods [13]. They used continuous speech utterance as acoustic stimulation.

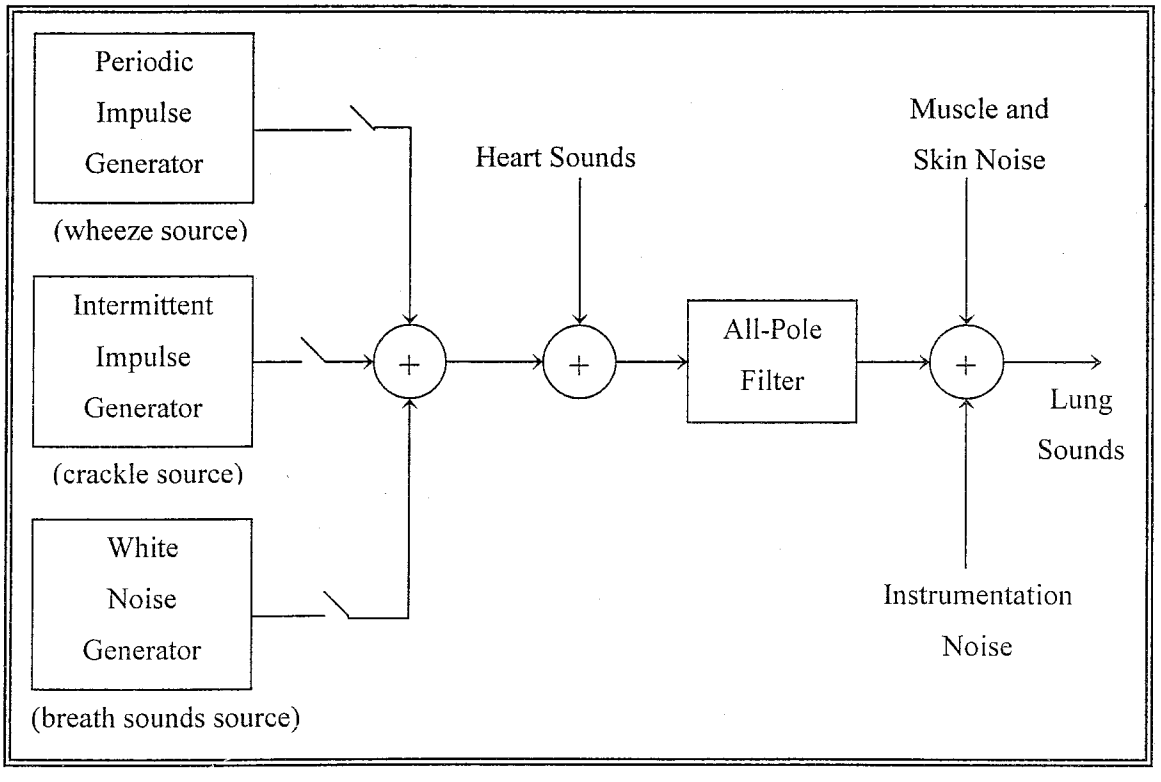

Figure 3.2 Iyer's schematic diagram of the AR model employed for lung sounds [11].

Vandershoot and coworkers demonstrated that AR model of lung sounds depends on flow and lung volume, and this model can de described by 3rd degree polynomials [14-16]. Using higher-order statistics, Hadjileontiadis and Panas design a similar AR model of source and transmission of lung sounds to Iyer's model [17]. Sankur and colleagues analyzed pathological and healthy respiratory sound data using AR vectors in two

classifiers in order to construct a diagnostic aid [18]. They also modeled transient sounds, crackles, using stochastic modeling, and classified lung sounds using crackle parameter-based classifiers [19-20]. In addition, they made statistical and spectral analysis in different studies using AR modeling [21-22].

3.2. Multilayer Feed-Forward Networks

3.2.1. Introduction

Generally, neural network is designed as a machine to model the way the human brain performs a particular task through a process of learning. Through this learning process, the network acquires knowledge, and stores it in interneuron connection known as weights. By the way of the adaptation and training of the weights, it can be used successfully in communications, control, biomedical engineering, and other diverse fields.

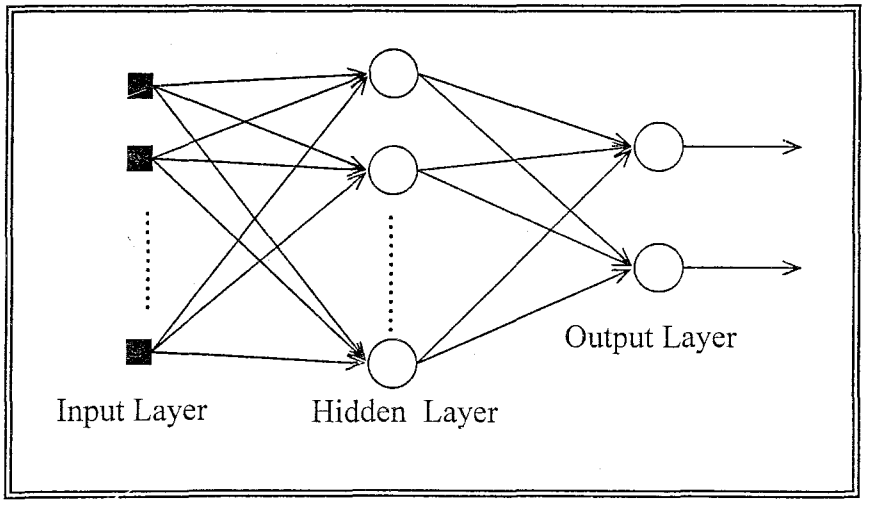

Figure 3.3 Architectural graph of multilayer network with one hidden layer.

Multilayer feed-forward network is an important type of neural networks. The network consists of an input layer of sensory nodes, one or more hidden layers and output layer constituted by computation nodes (Figure 3.3). This type of network has three distinctive characteristics. Firstly, there is a nonlinear function at the output of each node. This function is differentiable everywhere. Secondly, the network has hidden neurons

between input and output layers. By this way, it may extract more meaningful features from inputs to solve difficult problems. Thirdly, by the multiple layers, there is high degree of connectivity. It generally uses back-propagation algorithm in a supervised manner to solve complex problems [23-24].

3.2.2. Back-propagation Algorithm and Learning

In the network using back-propagation algorithm, there are two paths for process through layers of the network, namely forward and backward. During forward process, the effects of input vectors propagate layer by layer and, finally, produce the actual response of the network in the output layer. The weights are fixed during this process.

On the other hand, in the backward process, the actual response of the network is subtracted from the desired response to acquire error signal. The error signal is then propagated backward through the network. Consequently, the weights are adjusted in order to eliminate the error signal and, therefore, decrease the difference between actual and desired response of the network. The graph of the three-layer feed-forward network and its back-propagation signals are shown in Figure 3.4.

When adapting the weight connecting node i to node j, the correction $\Delta w_{ji}(n)$ should be calculated by means of,

$$\begin{pmatrix}\text{Weight}\\ \text{Correction}\\ \Delta w_{ji}(n)\end{pmatrix} = \begin{pmatrix}\text{Learning-rate}\\ \text{parameter}\\ \eta\end{pmatrix} \text{x} \begin{pmatrix}\text{Local}\\ \text{gradient}\\ \delta_j(n)\end{pmatrix} \text{x} \begin{pmatrix}\text{Input signal}\\ \text{of neuron } j\\ y_j(n)\end{pmatrix} \qquad (3.4)$$

The local gradient $\delta_j(n)$ formulas, (3.5) and (3.6), differ with respect to whether the neuron is an output or a hidden node [23].

$$\delta_j(n) = e_j(n)\varphi_j'(v_j(n)) \qquad \text{if neuron } j \text{ is output node} \quad (3.5)$$

where $e_j(n)$ is the error signal, and $\varphi_j'(v_j(n))$ is derivative of activation function, whereas,

$$\delta_j(n) = \varphi_j'(v_j(n)) \sum_k \delta_k(n) w_{kj}(n) \qquad \text{if neuron } j \text{ is hidden node} \qquad (3.6)$$

where $\sum_k \delta_k(n) w_{kj}(n)$ is the weighted sum of the local gradients computed for the nodes in the next layer.

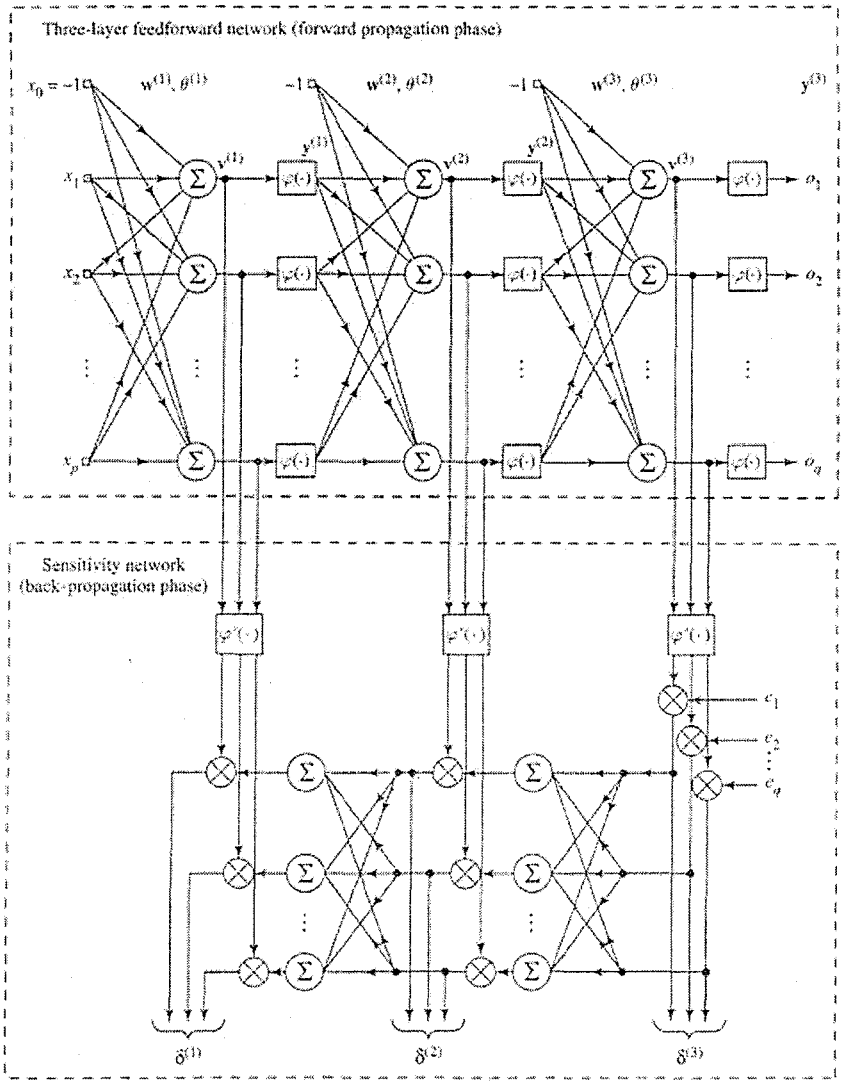

Figure 3.4 The graph of three-layer feed-forward network with its associated sensitivity network. $w^{(l)}$ = weight vector of a neuron in layer l. $\theta^{(l)}$ = threshold of a neuron in layer l. $v^{(l)}$ = vector of a net internal activity levels of neurons in layer l. $y^{(l)}$ = vector of function signals of neurons in layer l [23].

3.3. Wavelet Transforms and Multi-resolution Analysis

3.3.1. Wavelet and Wavelet Expansion Systems

In contrast to the concept of "wave" that is used in Fourier transform, wavelet, namely "small wave," is a finite-energy function (Figure 3.5). By means of its localization properties, it can be used efficiently in the analysis of nonstationary, transient signals. In other words, only a small finite number of coefficients are needed to represent these signals.

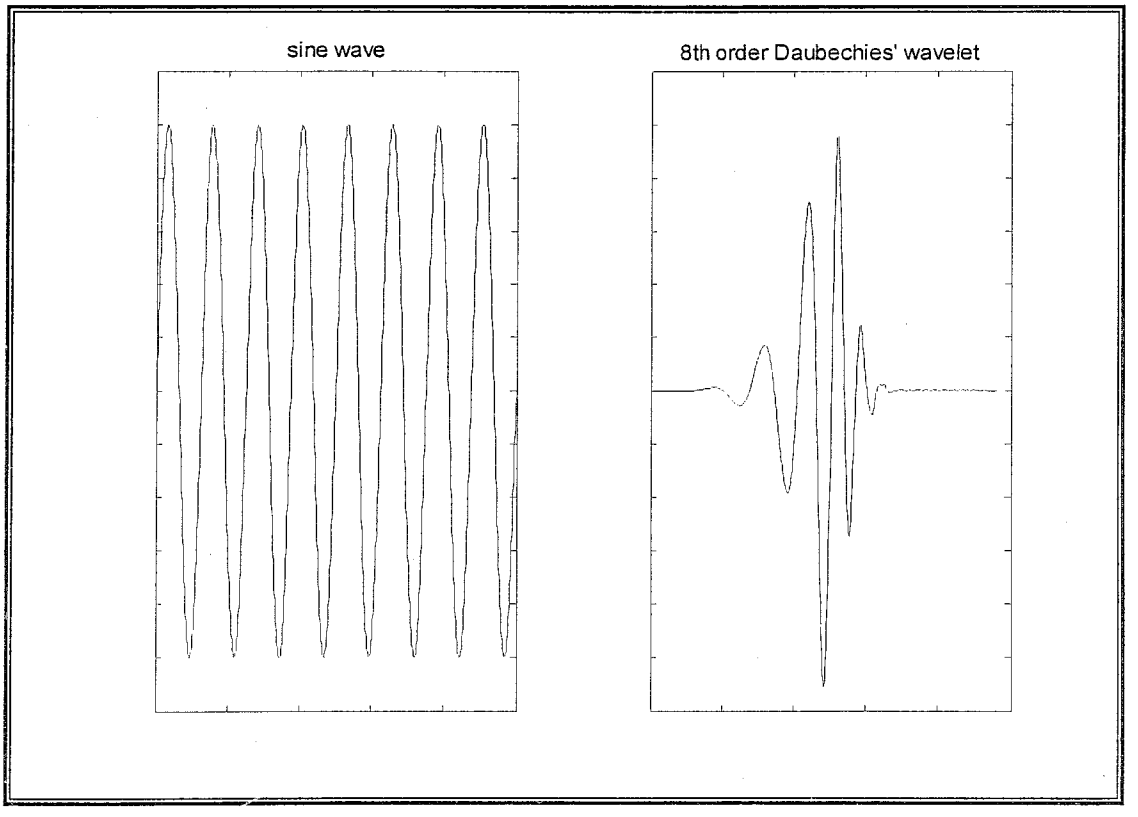

Figure 3.5 Wave and wavelet examples

For most expansions of a signal, the goal is to find the expansion coefficients that will give more descriptive information about the signal than can be directly observed from the signal itself. A second goal is to have most of the coefficients that are zero or very small. This is very important in diverse areas, such as statistical estimation and detection, data compression, nonlinear noise reduction, and fast algorithms.

The wavelet expansion system may be expressed by

$$f(t) = \sum_j \sum_k a_{jk} \psi_{jk}(t) \tag{3.7}$$

where $\psi_{jk}(t)$ are wavelet expansion functions, both j and k are integer indices, and a_{jk} are the discrete wavelet transform coefficients of the signal, $f(t)$.

A wavelet system has six characteristics that may be divided into two main groups, namely general and more distinctive ones [25-26].

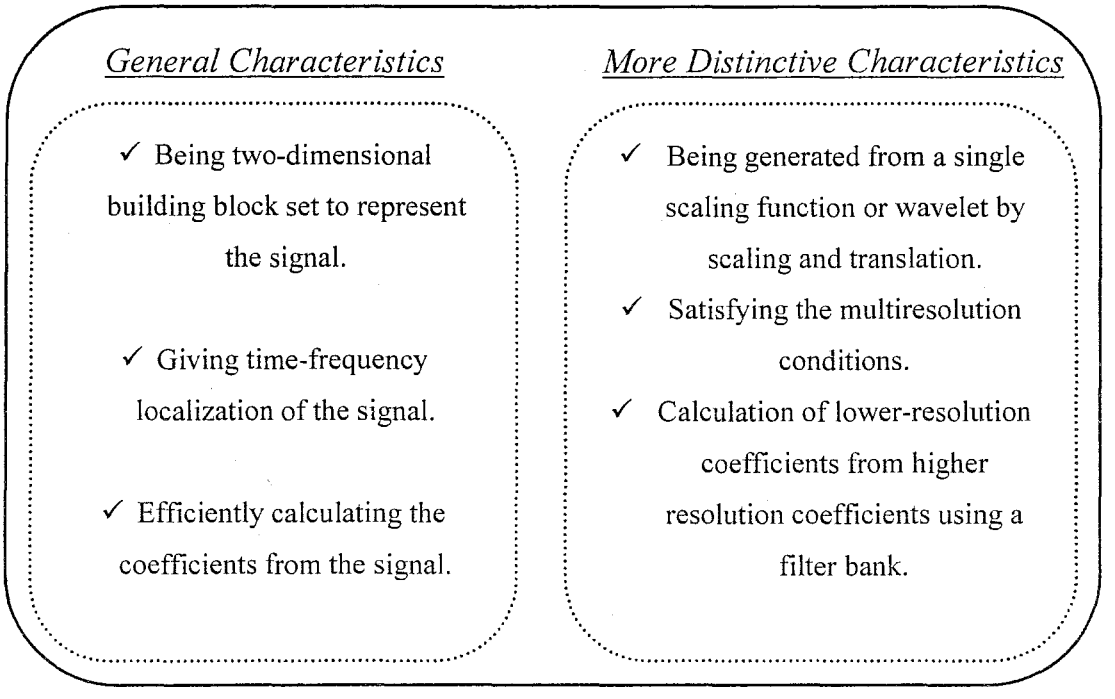

Figure 3.6 Characteristics of a wavelet system

As the first distinctive characteristic, the mother wavelet (3.8) parameterizes two dimensions, namely time or space location and the frequency or scale.

$$\psi_{jk}(t) = 2^{j/2} \psi(2^j t - k) \qquad j,k \in \mathbb{Z} \tag{3.8}$$

where $\mathbb{Z}$ is the set of all integers.

By changing the index k, the location of the wavelet moves horizontally. Thus, the expansion can represent the location of the events in time or space. By changing the index j, the shape of the wavelet changes in scale. This change affects the resolution and allows expansion to represent the detail. The larger j is, the finer the scale is and the smaller the steps become in time [25]. This translation and scaling property of wavelet may be depicted in Figure 3.7.

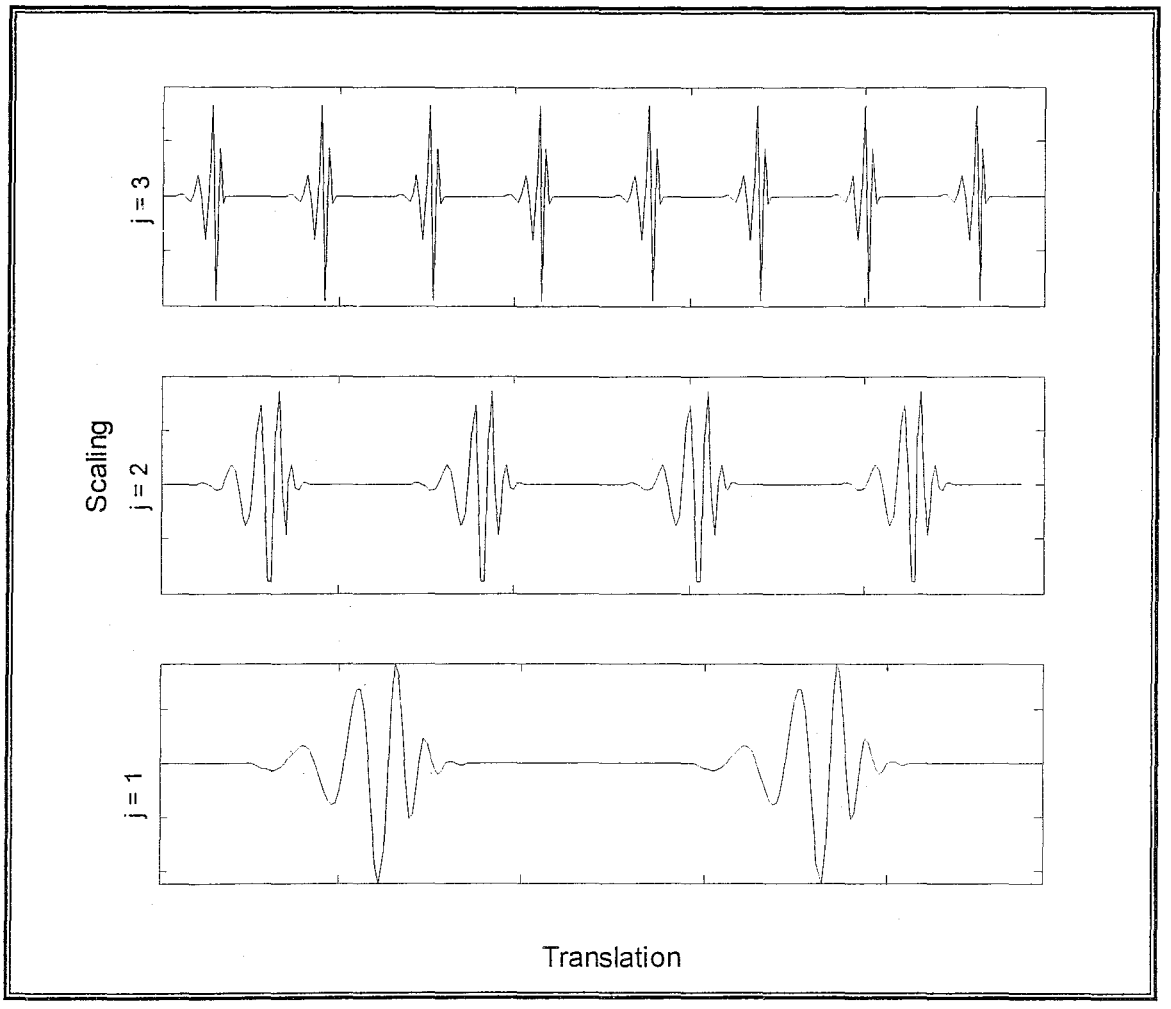

Figure 3.7 Translation and scaling of 8th order Daubechies' wavelet. For preventing cluttering, only selected terms in translation are shown.

3.3.2. Multi-resolution Analysis, Scaling and Wavelet Functions

For achieving multi-resolution analysis (MRA), there should be a sequence $\{V_j\}_{j\in\mathbb{Z}}$ of closed subspaces of the space $L^2(\mathbb{R})$ such that

$$V_j \subset V_{j+1} \quad \text{for all } j \in \mathbb{Z} \tag{3.9}$$

$$V_{-\infty} = \{0\} \quad \text{and} \quad V_{\infty} = L^2 \tag{3.10}$$

$$f(t) \in V_j \Leftrightarrow f(2t) \in V_{j+1} \tag{3.11}$$

where "L" signifies a Lebesque integral, "2" denotes the integral of the square of the modulus of the function [25-27]. The nested subspaces may be depicted in Figure 3.8.

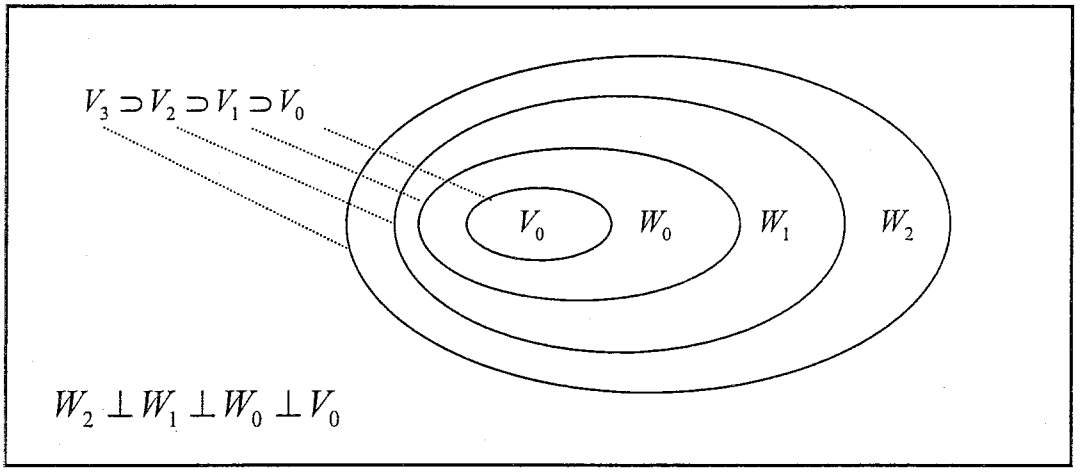

Figure 3.8 Scaling function and wavelet vector spaces [25].

In this stage of MRA, the concepts of scaling function $\varphi_{jk}(t)$ (3.12) and vector subspaces are correlated to each other. By definition, the vector spaces are spanned by scaling function (3.13) and the space that contains higher resolution signal will also contain lower resolution ones. If V_0 contains scaling function $\varphi(t)$, then V_1 will contain $\varphi(t)$ and, therefore, $\varphi(2t)$ that spans the bases of V_1 will also span $\varphi(t)$ (3.14).

$$\varphi_{jk}(t) = 2^{j/2}\varphi(2^j t - k) \tag{3.12}$$

$$f(t) = \sum_k a_k \varphi(2^j t + k) \qquad f(t) \in V_j \tag{3.13}$$

$$\varphi(t) = \sum_n h(n)\sqrt{2}\varphi(2t - n) \tag{3.14}$$

where h(n) is scaling function coefficients and $\sqrt{2}$ is the norm of the scaling function [25].

The need for a wavelet function $\psi_{jk}(t)$ stems from the idea of defining a new set of functions that spans the differences of the spaces that are spanned by the scaling function. Therefore, the better description and parameterization of the features of signals are aimed. The wavelet functions and scaling functions are defined orthogonal to each other. Consequently, the energy of the signal can be partitioned in the wavelet transform domain by means of Parseval's theorem (Appendix C). W_j is defined as orthogonal complementary space of V_j in V_{j+1}.This may be described in (3.15), (3.16) and Figure 3.8.

$$L^2 = V_j \oplus W_j \oplus W_{j+1} \oplus W_{j+2} \ldots\ldots \tag{3.15}$$

$$V_j = W_{j-1} \oplus W_{j-2} \oplus W_{j-3} \ldots\ldots \tag{3.16}$$

Because a wavelet vector space, e.g. W_0, is contained by the next scaling space V_1, the wavelet function can be represented by the scaling function (3.17) for the set of coefficients $h_1(n)$ (3.18) and the prototype or mother wavelet (3.19) can be generated from (3.17) [25].

$$\psi(t) = \sum_n h_1(n)\sqrt{2}\varphi(2t-n), \qquad \text{for } n \in \mathbb{Z} \tag{3.17}$$

$$h_1(n) = (-1)^n h(1-n) \tag{3.18}$$

$$\psi_{jk}(t) = 2^{j/2}\psi(2^j t - k) \tag{3.19}$$

By (3.15) for $j = j_0$ and (3.19), the discrete wavelet transform (DWT) of a signal $f(t)$ can be represented by the form

$$f(t) = \sum_k c_{j_0}(k)2^{j_0/2}\varphi(2^{j_0}t-k) + \sum_k \sum_{j=j_0}^{\infty} d_j(k)2^{j/2}\psi(2^j t-k) \tag{3.20}$$

where $c(k)$ is defined as approximation or scaling coefficients and $d_j(k)$ is defined as detail or wavelet coefficients.

3.3.3. Multiple-level Decomposition and Reconstruction

For representing a signal in multiple-level scales or frequency bands, we will use the wavelet and scaling coefficients that are mentioned in equation (3.20). To use these expansion coefficients efficiently, they should be formulized in terms of each other. In the decomposition process, coefficients at a lower scale level are interpreted in terms of those at a higher scale. The equations (3.20) and (3.21) show the relationships [25]. To formulize these expansion coefficients, we may use the orthogonality of spaces and wavelet and scaling functions.

$$c_j(k) = \sum_m h(m-2k)c_{j+1}(k) \tag{3.20}$$

$$d_j(k) = \sum_m h_1(m-2k)c_{j+1}(m) \tag{3.21}$$

where $c_j(k)$ represents scaling coefficients, $d_j(k)$ represents wavelet coefficients.

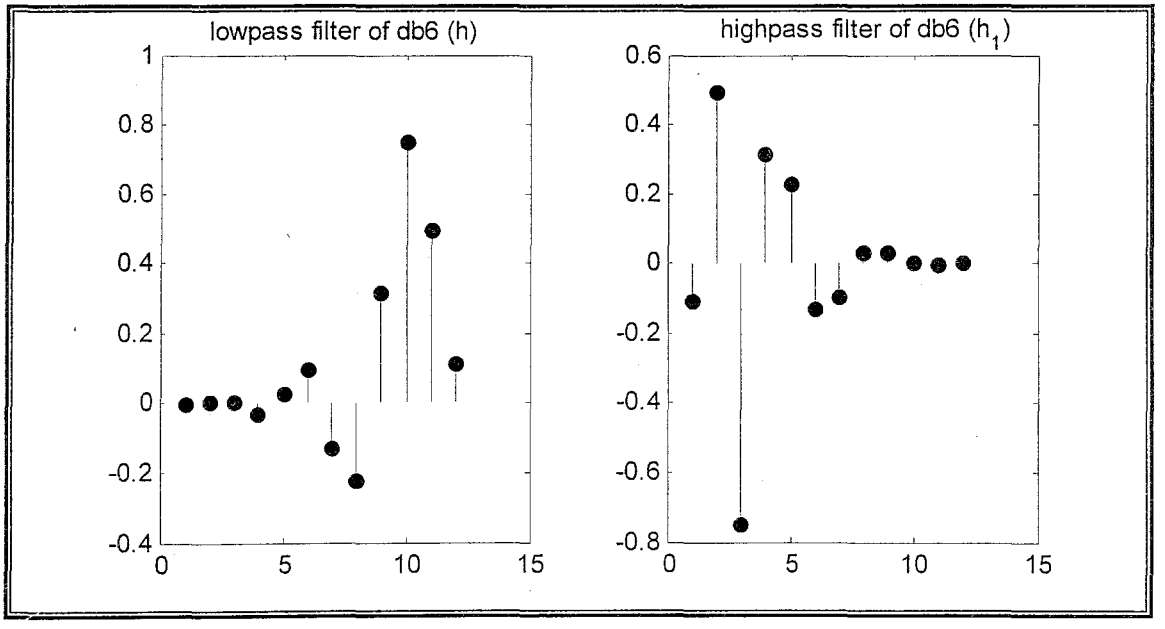

Figure 3.9 The low-pass and high-pass filter of 6th order Daubechies' wavelet.

$h(m-2k)$ and $h_1(m-2k)$ are called wavelet decomposition filters. When decomposing a signal, the low-pass filter $h(m-2k)$ yields scaling coefficients (3.20)

whereas the high-pass filter $h_1(m-2k)$ yields wavelet coefficients (3.21). As shown in Figure 3.9, the relationship between them is

$$h_1(n) = (-1)^n h(1-n). \tag{3.22}$$

In multiple-level decomposition, this two-band analysis is repeated on the scaling coefficients. The process $\downarrow 2$ that is shown in the figure is called down-sampling (decimating). While processing the analysis, the total number of samples is doubled by two filters, then down-sampling halves it to the original number. Consequently, in first stage, the sample number of each coefficient set will be $N/2$ and, in the nth stage, the number will be reduced to $N/2^n$.In Figure 3.10, two-level decomposition is depicted. Whereas the sample number of original signal is 1024, those of 3rd level coefficients is $1024 / 2^2$, namely 256.

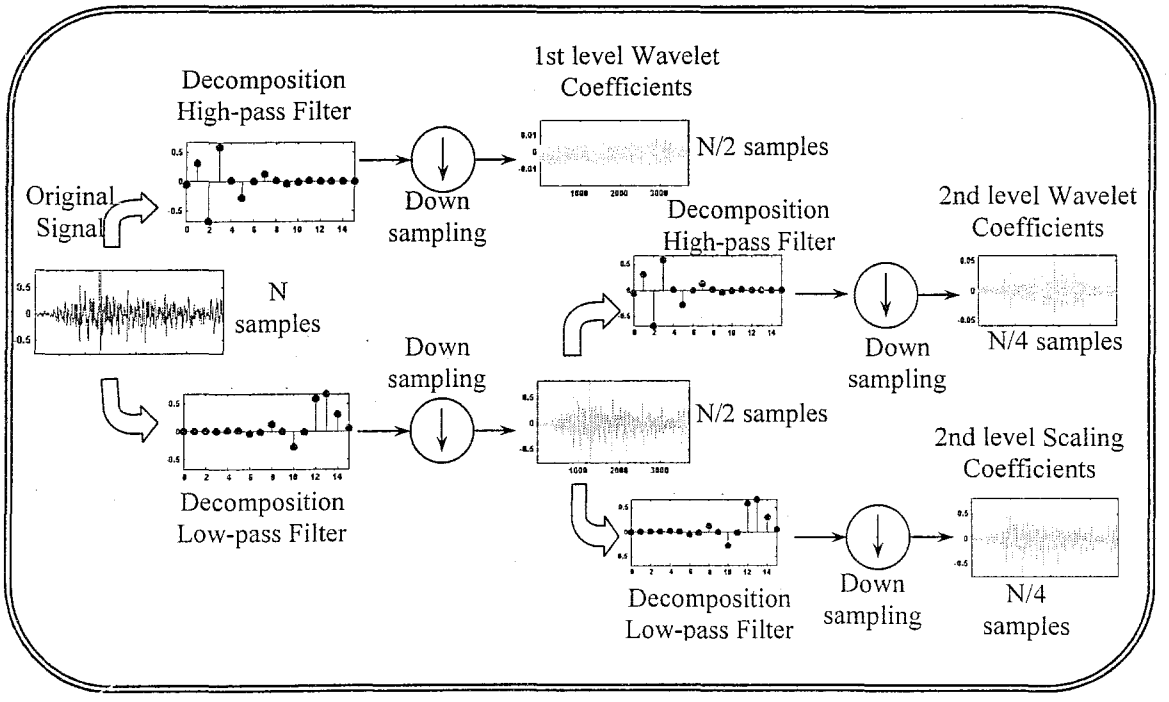

Figure 3.10 Two-level two-band decomposition.

As the reverse process of the decomposition, in the reconstruction, the scaling coefficients at a finer resolution will emerge from the coarser-level scaling and wavelet coefficients (3.23).

$$c_{j+1}(k) = \sum_m c_j(m)h(k-2m) + \sum_m d_j(m)h_1(k-2m) \tag{3.23}$$

In this synthesis, for reaching the required sample number of the upper-level coefficients, zeros are inserted between each term of the input before filtering (Figure 3.11).

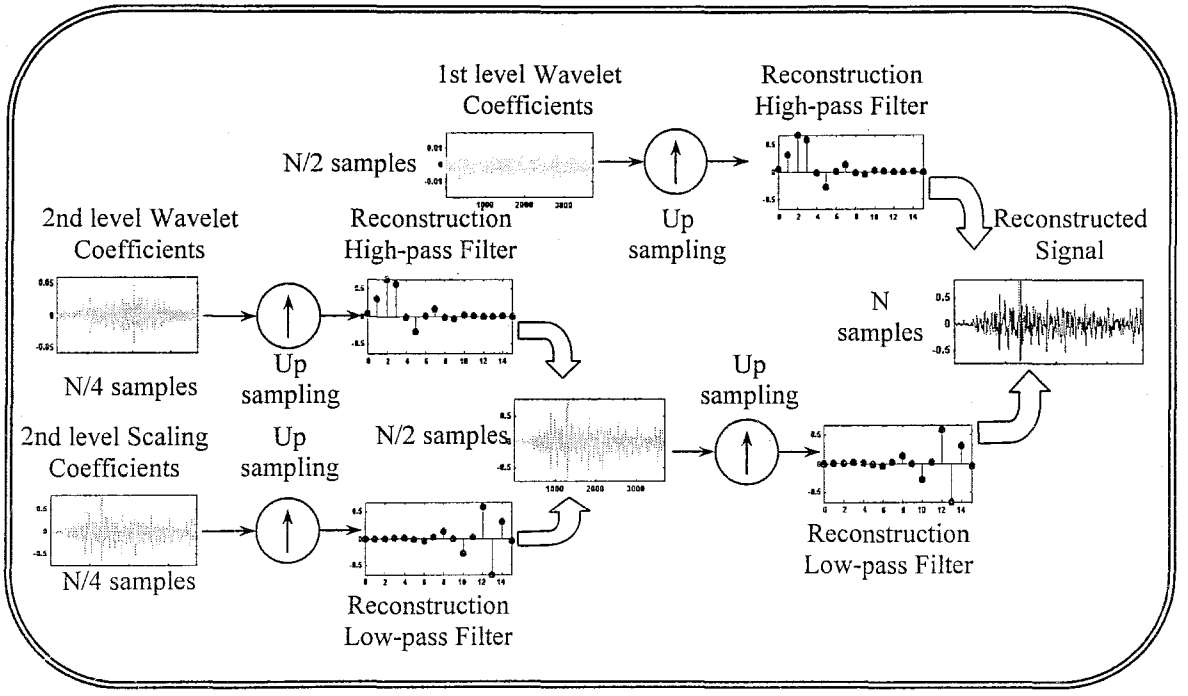

Figure 3.11 Two-level two-band reconstruction.

3.3.4 Respiratory Sound Applications

As mentioned above, adventitious sounds, such as crackles and wheezes, are superimposed over the normal lung sounds in pathological conditions. Their characteristics, such as number and pitch, supply descriptive information about the pulmonary or health condition of subjects. However adventitious sounds, especially crackles, may have no detectable influence on the frequency spectrum since their duration is very short. The high performance of MRA in transient analysis may be effective for applying wavelet analysis in modeling lung sounds. On the other hand, under some conditions, the time-scale approach can be important to analyze sub-bands of signal. The

aims of the studies may be classified into three groups, namely detection of adventitious sounds, feature extraction and noise cancellation.

1. Pesu and colleagues [28] used wavelet packet decomposition method for detecting abnormal respiratory sounds and, consequently, classifying respiratory sound signal segments as containing crackles, wheezes or normal lung sounds. However, their results are not good enough for using in routine clinical application. Hadjileontiadis and Panas combined MRA with hard threshold in order to separate pathological discontinuous adventitious sounds (crackles) from vesicular sounds [29]. Due and coworkers used continuous WT for crackle detection and classification [30]. Yerer also designed an online auto crackle detector instrument that uses DWT and IDWT [31].

2. Sankur and colleagues proposed a method for classification of respiratory sound signals into healthy and pathological classes. For this purpose, they used multiresolution decomposition analysis and extracted feature vectors for classifiers from each octave band [32]. Pittner and Kamarthi dealt with the assessment of process parameters using features extracted from wavelet coefficients of process signal. They applied a preprocessing routine on the coefficients that computes robust features using Euclidean norms [33].

3. Charleston and coworkers studied on the cancellation of heart sounds from respiratory sounds using joint time-delay and signal estimation procedure. They applied this procedure to each sub-band of the signal acquired by using DWT [34]. Bahoura and colleagues proposed a technique for denoising respiratory sounds using Donoho's method. They applied thresholding operation to acquired wavelet packet decomposition coefficients [35].

The above mentioned studies have indicated that using wavelet analysis is an efficient method to characterize lung sound signals containing adventitious sounds.

4. A RESPIRATORY SOUNDS CLASSIFICATION SYSTEM USING WAVELET-BASED NEURAL NETWORK

4.1. Data Acquisition (DAQ)

4.1.1. Method

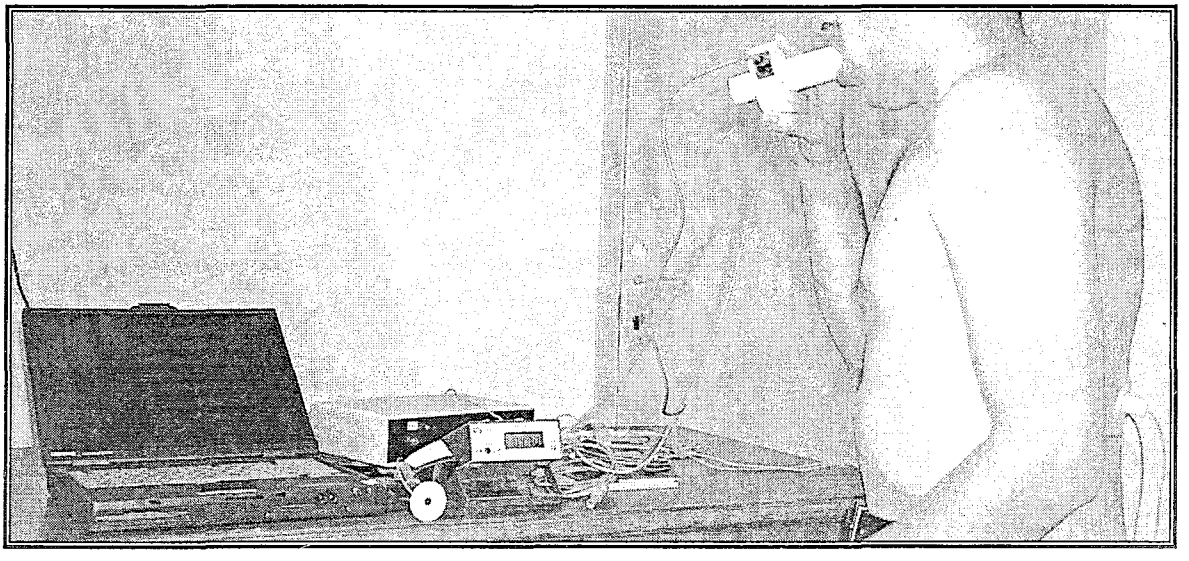

Figure 4.1 The simultaneous acquisition of respiratory sound signal and flow signal

Flow signal and pulmonary sound signal were acquired simultaneously, using a Fleisch-type flowmeter (Validyne CD379) and two air-coupled electret microphones in order to synchronize on the inspiration-expiration phases (Figure 4.1). The microphones were placed on the left and right posterior bases of the lungs (Figure 4.2), and the subjects were monitored with the aid of a volume tank on the computer screen to breathe at flow rates above 1L/s for optimum lung sound intensity. A third microphone was used for measuring ambient noise.

A low-noise preamplifier, a 8^{th} order Butterworth low-pass filter with 2 kHz cut-off frequency and an 4^{th} order Bessel high-pass filter with 80 Hz cut-off frequency were used in order to minimize frictional noise and heart sound interference and for an anti-aliasing cut-off frequency of 2 kHz. The frequency responses of the three channels used to acquire respiratory sound signals are flat between 100 Hz and around 2000 Hz whereas the

frequency response of the channel used to acquire flow signal is flat at 0–50 Hz (Appendix A). The preprocessed signals were digitized by a 12-bit ADC Card (NI-DAQ500) at a 5 kHz sampling rate and stored. The block diagram of the DAQ system is depicted in Figure 4.3.

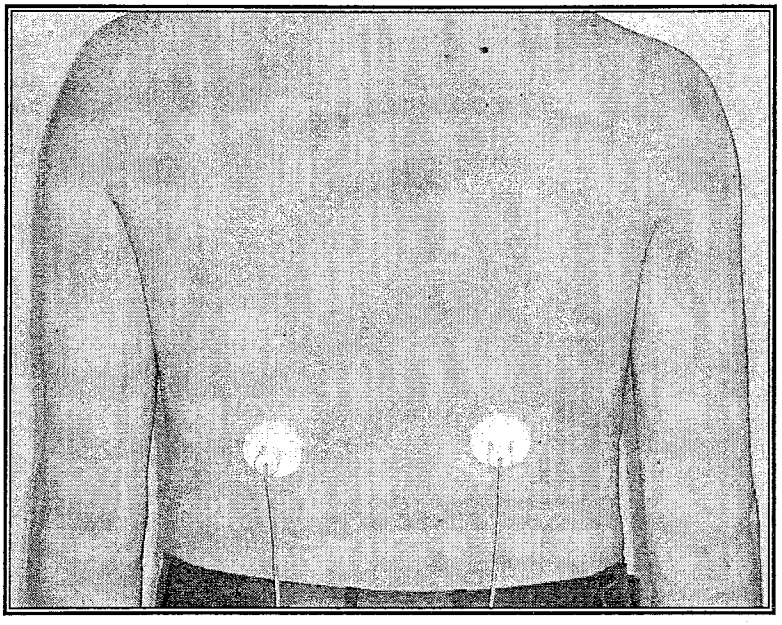

Figure 4.2 The microphones which are placed on the left and right posterior bases of the lungs.

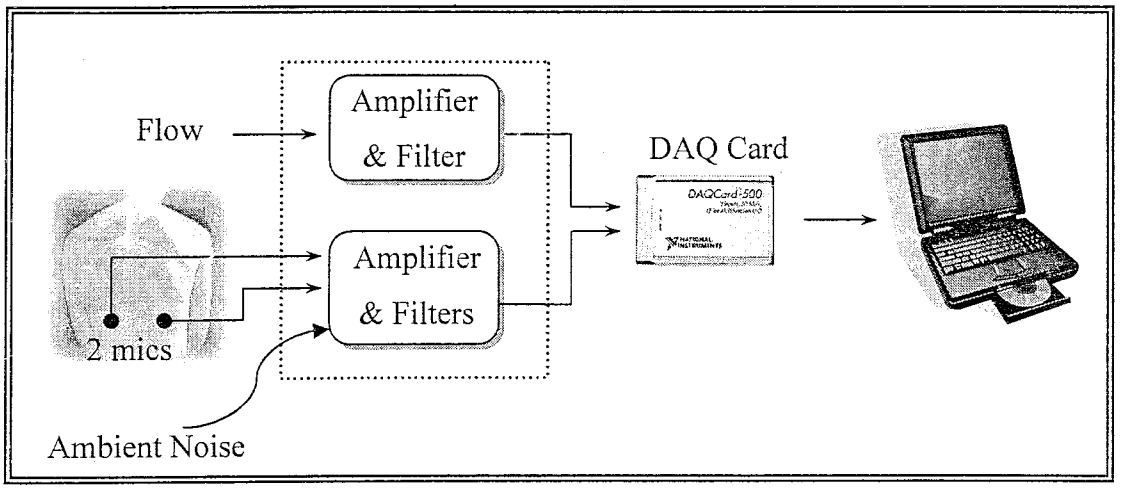

Figure 4.3 Block diagram of simultaneous acquisition of signals of respiratory sounds and flow.

4.1.2. The Data Acquisition Software

To establish a user interface for acquisition of signals of respiratory sound and flow, LabVIEW programming language was used (Figure 4.4). Several controls and indicators were placed on the left-hand side of the front panel. By means of controls, the channel for real-time representation, the order of channels, total time of data acquisition and scan rate were controlled. In addition, to supply the option of continuous or limited duration acquisition for user and to interrupt the process manually, two control buttons were placed.

Four charts are placed in the middle of interface. The chart at the top is used to present flow and selected microphone in real-time. Other three charts are used for synchronized presentation of flow and three microphone channels, mic1, mic2 and ambient channels, respectively. They display the data at the end of acquisition. On the right-hand side, a volume tank is placed to indicate flow rate. Volume tank is used to monitor subjects to breathe at flow rates above 1L/s. The diagram window of software is presented in Appendix B.

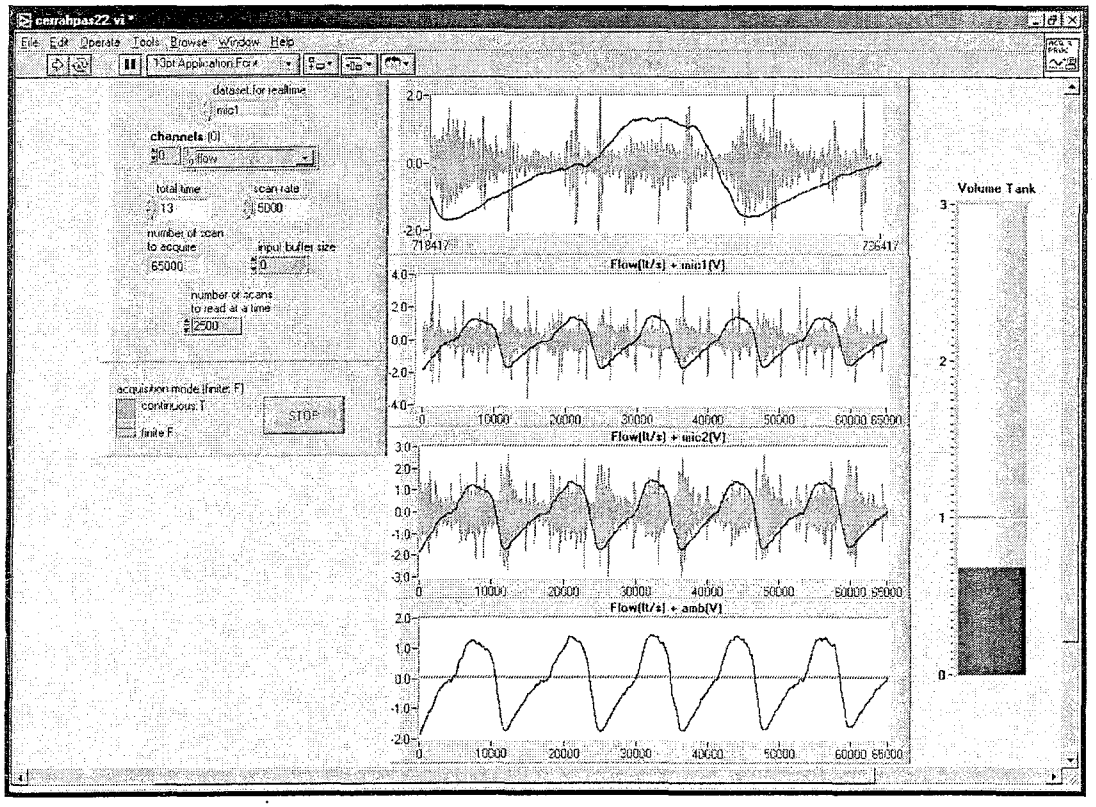

Figure 4.4 User interface of software (Front panel)

4.1.3 Microphone Capsules

For the first part of our study, microphone capsule having air cavity suggested by Charbonneau [36] in 1983 was used (Figure 4.5) [37]. In 1995, Kraman and his colleagues [38] studied and compared different shaped microphone capsules. In our experiments, it was seen that new suggested capsules are more sensitive to the transients. In Figure 4.6, the new model of air couplers is depicted.

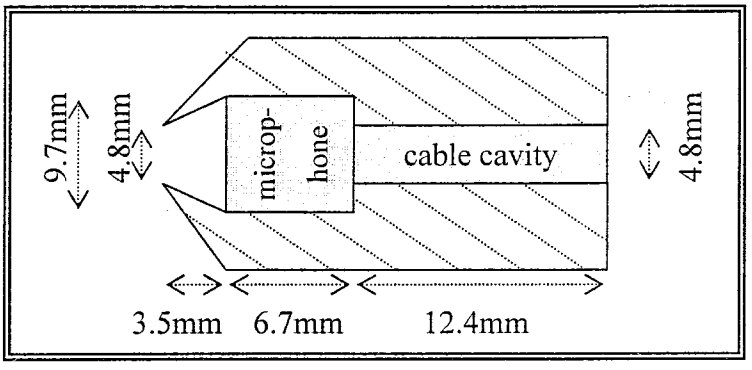

Figure 4.5 Charbonneau's microphone capsule model

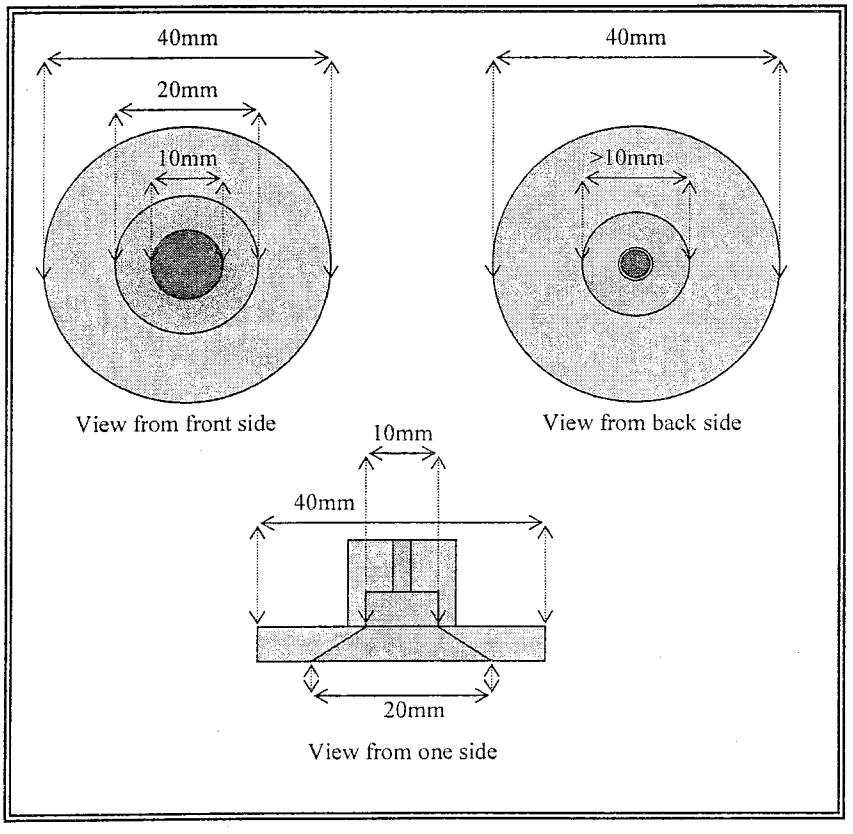

Figure 4.6 Kraman's microphone capsule model

4.2. Determination of the Network Features

4.2.1. Segmentation and Wavelet Transform

The respiratory sound signals acquired from each subject were divided in accordance with the flow phases, namely expiration and inspiration. Selected expiratory or inspiratory sound signals were divided into thirty segments with 25% overlapping (Figure 4.7). The 4^{th} degree WT using 8^{th} order Daubechies' wavelet (Figure 4.8) was applied to each segment. Since each component of the signal is a measure of the correlation between the signal and the corresponding element of the wavelet family, wavelet transform analysis of a signal can be interpreted as a special type matched filtering.

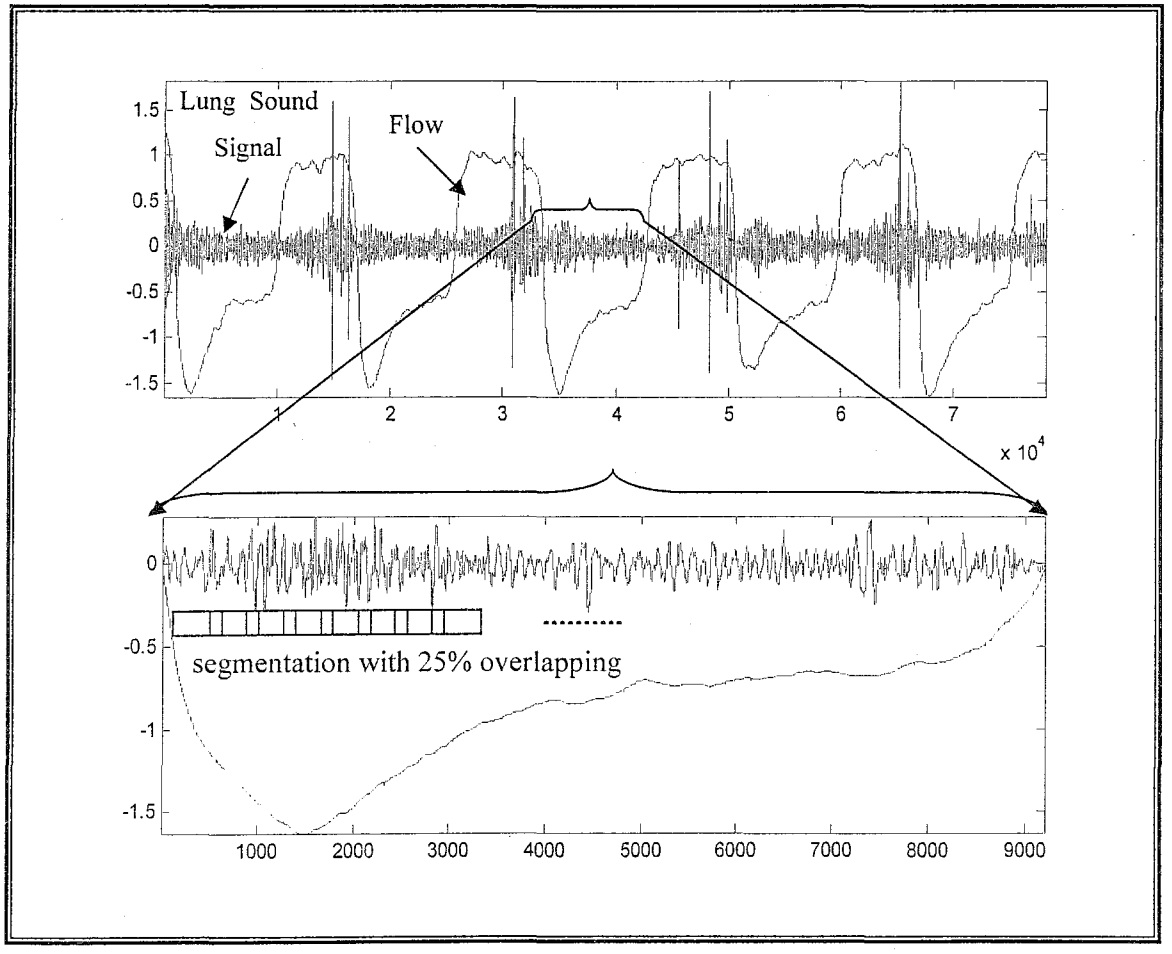

Figure 4.7 Respiratory sound waveforms with superimposed flow signal (above). Expiratory sound signal with its flow signal selected from the total recorded signal (below).

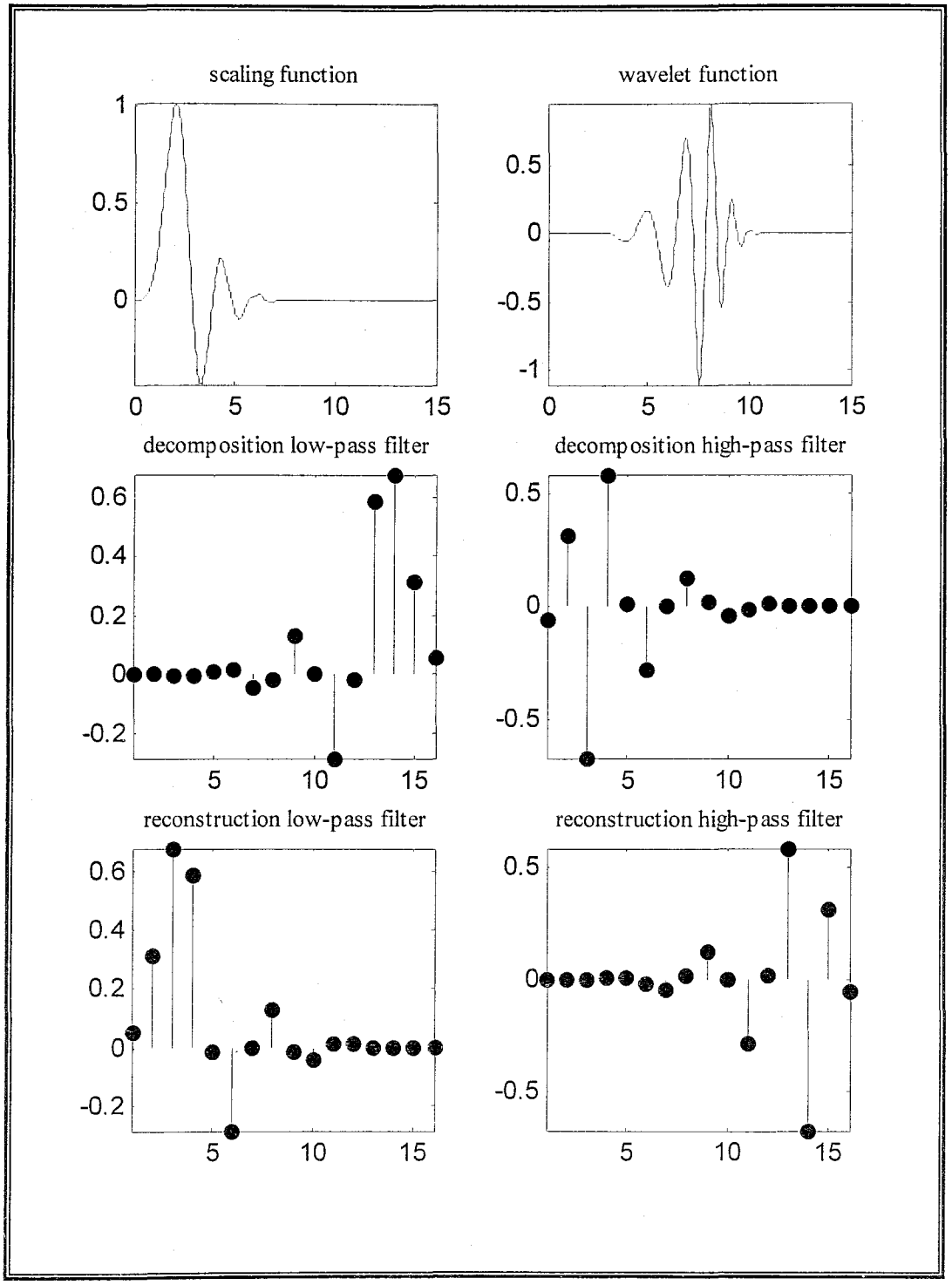

Figure 4.8 Scaling function, wavelet fuction and filters of 8th order Deubechies' wavelet.

Wavelet filters, resembling crackles in the respiratory sound signal, increase the correlation between short duration transients and the wavelet waveforms, therefore, enhance their bearing on the decomposed signal component. Daubechies' wavelets have been used in an earlier study in the detection of crackles due to their resemblance to crackles [5].

Two quadrature mirror filters (QMFs) were used in WT to divide the frequency space of input signal into two equal and orthonormal sub-spaces which can be termed as detail and approximation spaces. This process was applied to the approximation signal four times to get a dyadic structure of five sub-spaces of the original signal representing the following five octaves: 2500-1250 Hz, 1250-625 Hz, 625–312.5 Hz, 312.5–156.25 Hz, 156.25–0 Hz (~80 due to low-pass filter). The 4th level decomposition of a sample of lung sound was depicted in Figure 4.9. In the analysis, the first four octave bands stem from wavelet coefficients whereas the fifth is constructed from approximation (scaling) coefficients. Since each signal has five wavelet components, the total number of segments representing each subject's signal is 150(= 30 * 5). In Figure 4.10, 4.11 and 4.12, the wavelet and scaling coefficients of 4th level decomposition of expiratory sound signals were depicted. The signals belong to three subjects from different classes, namely obstructive, restrictive and healthy.

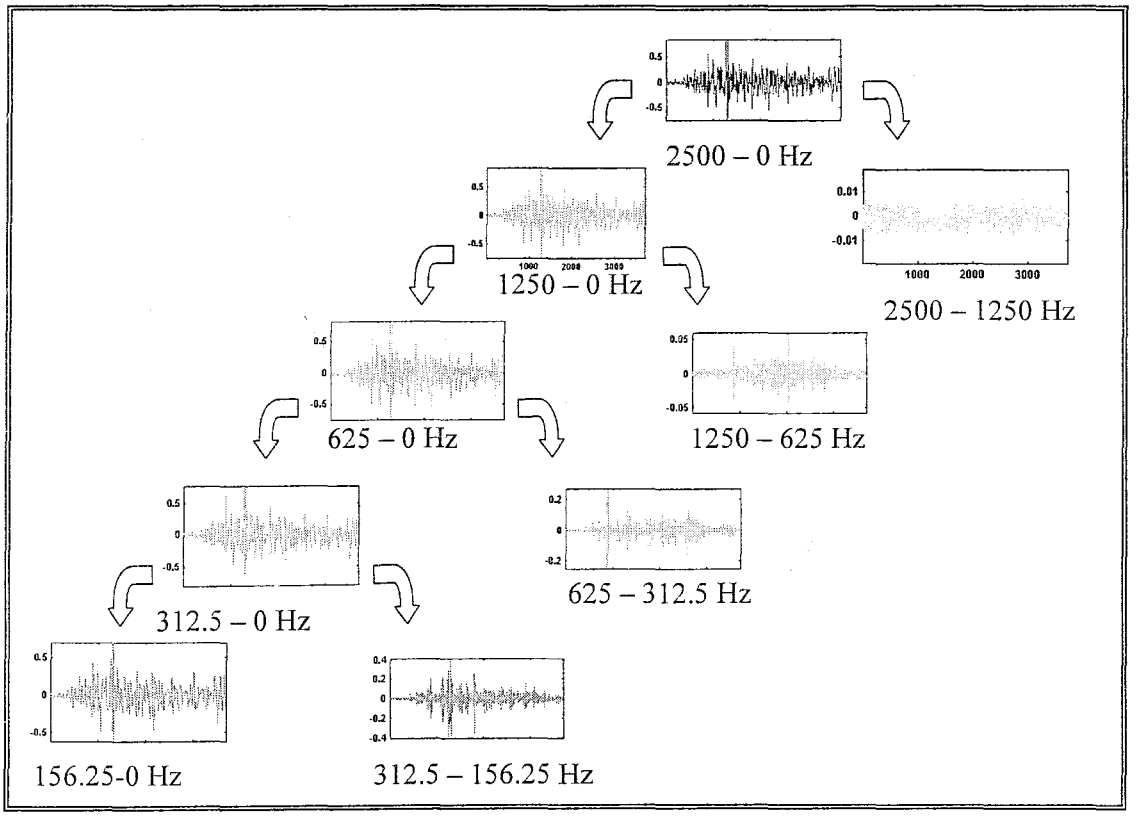

Figure 4.9 The 4th level decomposition of a respiratory signal sample and the octaves representing scales of wavelet and scaling coefficients of each level.

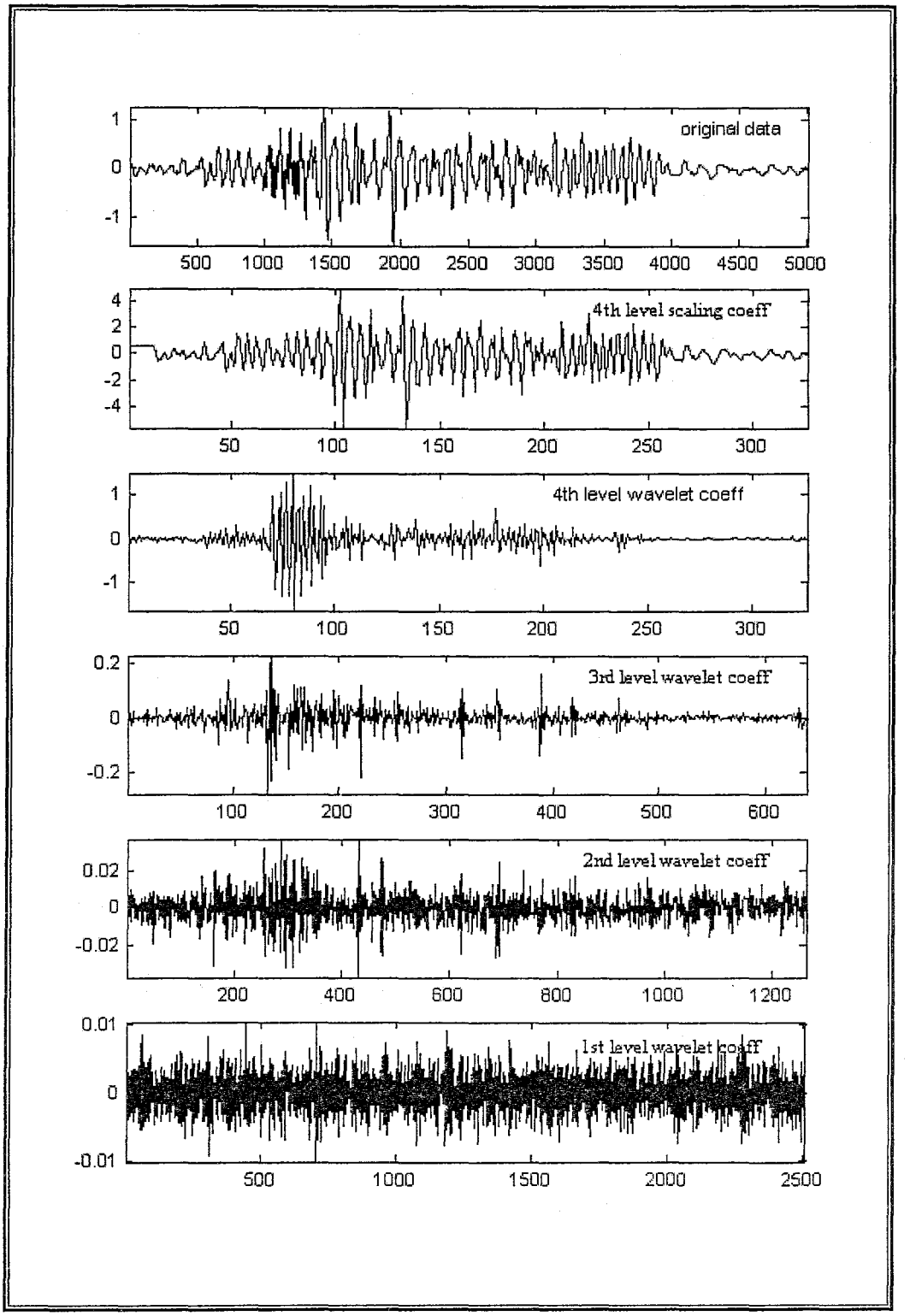

Figure 4.10 Scaling and wavelet coefficients of the 4th level decomposition of respiratory sound signal of restrictive subject's expiration phase.

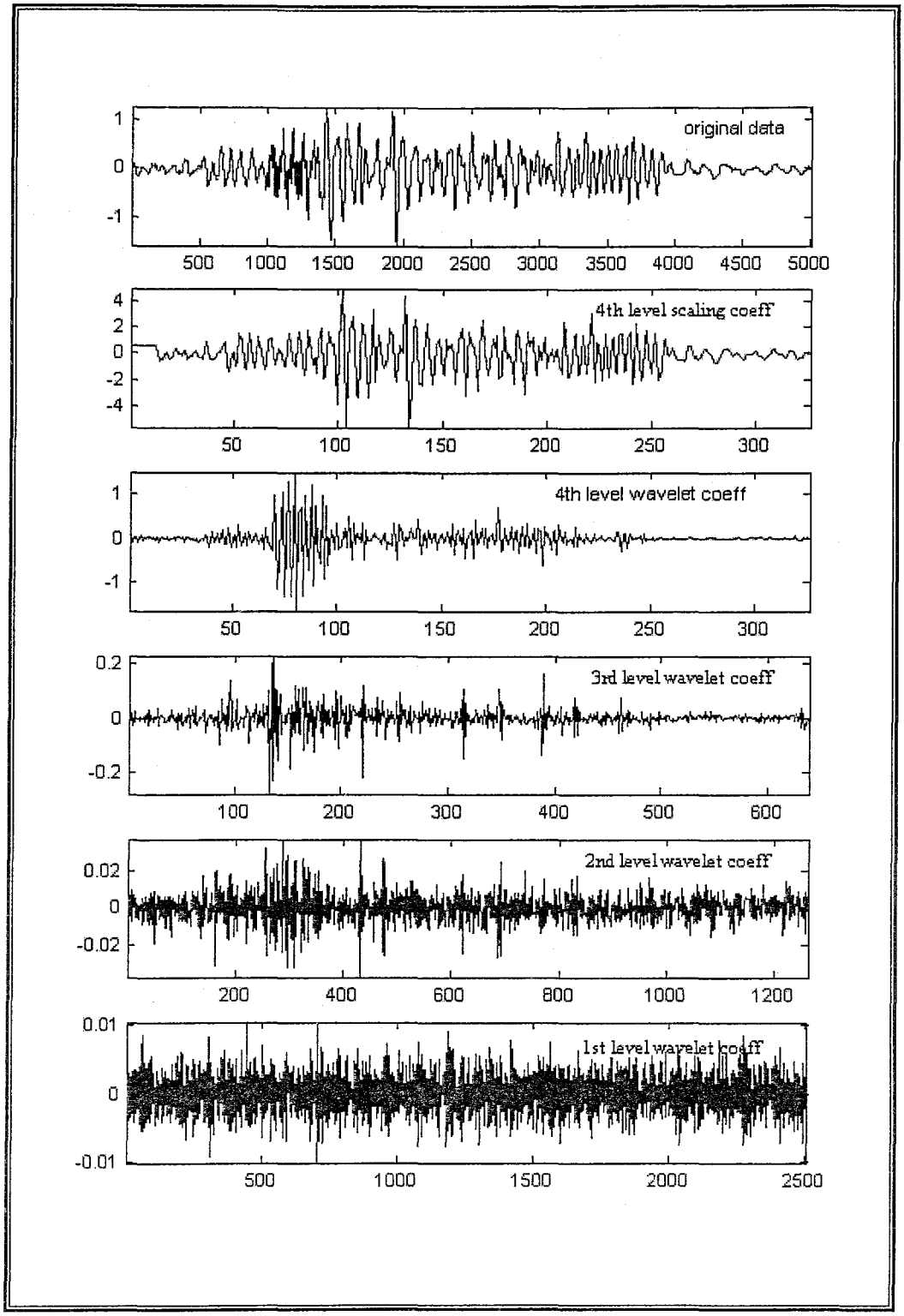

Figure 4.11 Scaling and wavelet coefficients of 4th level decomposition of respiratory sound signal of obstructive subject's expiration phase

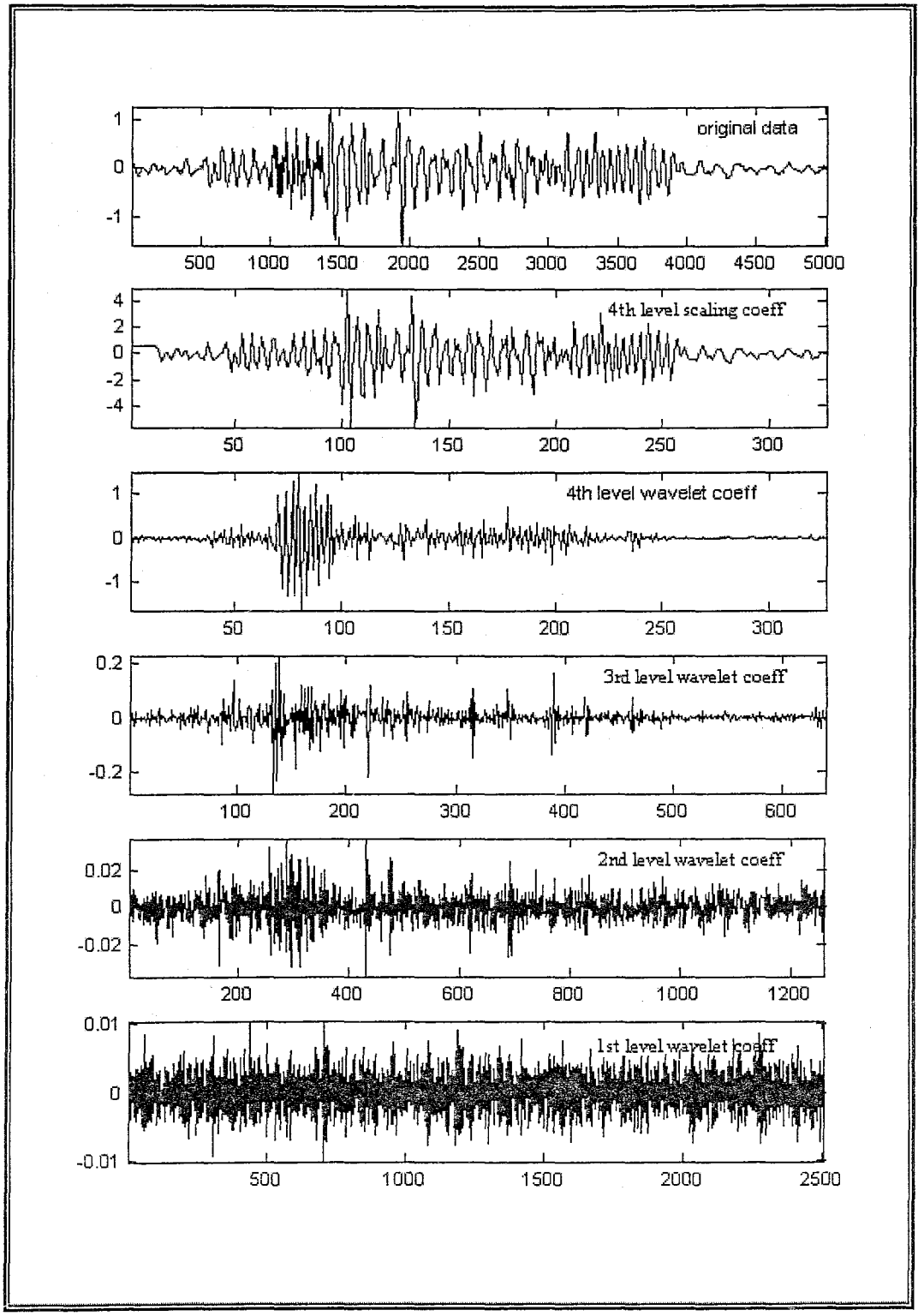

Figure 4.12 Scaling and wavelet coefficients of 4th level decomposition of respiratory sound signal of healthy subject's expiration phase.

At this stage, we have $N/2^n$ coefficients for each level of decomposition where N is the number of samples of original signal and n is the level number. For reconstructing approximations and details themselves from their coefficients, the same process that is used to reconstruct the original signal is applied to the coefficients vectors. However, instead of the same level detail or approximation coefficients, vectors of zeros whose lengths are the same of the coefficients are combined with these vectors. In Figure 4.13, the reconstruction of the second level wavelet coefficients is depicted.

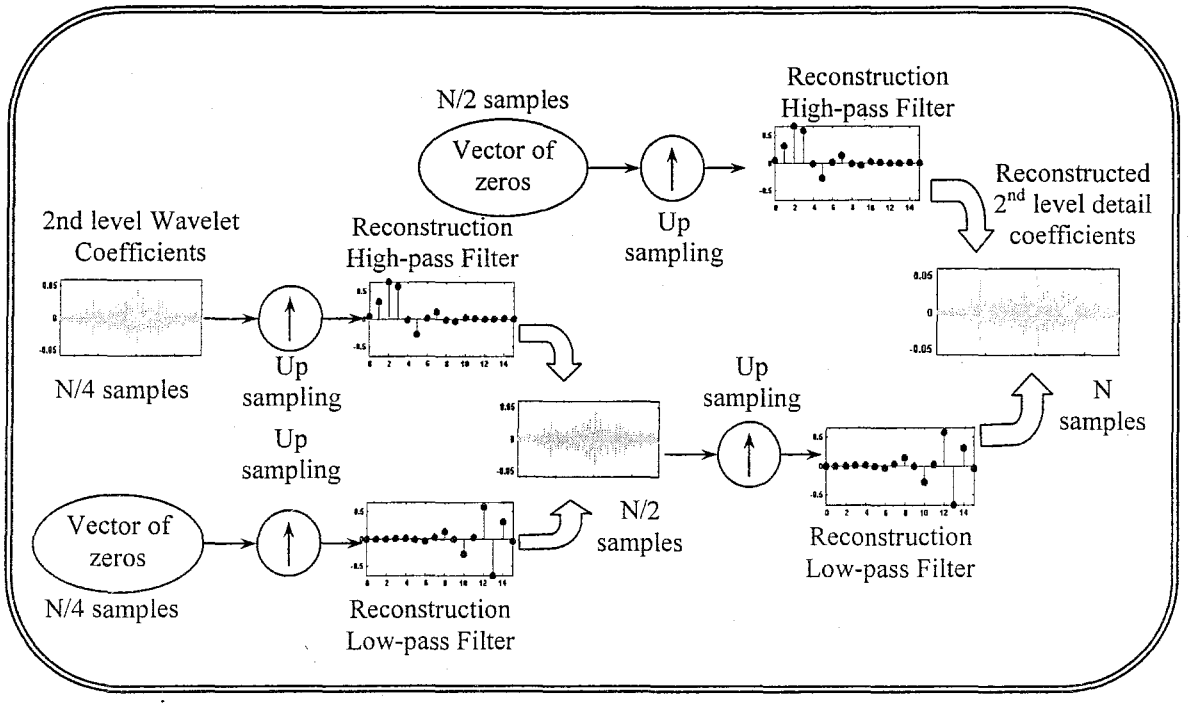

Figure 4.13 Reconstruction of 2nd level wavelet coefficients.

4.2.2. AR Modeling and Volume Constant

A fourth order AR model is used to represent reconstructed coefficients vector at each level. The parameters calculated by means of Yule-Walker method constitute the first four feature inputs of the ANN. The 5th feature input is a volume constant corresponding to the average of the fraction of tidal volume of the lung during early, mid, late expiration, namely 0.85 for the first ten segments, 0.50 for the second segments and 0.15 for the last ten segments. This feature contains phase information about expiration cycle, which is in

accordance with the terminology used by physicians. The final three dimensional input matrix for each subject has 5 (4 AR parameters + volume constant) * 30 (segments) * 5 (octaves) elements. Equation 4.1 shows mother input matrix acquired from each subject.

$$A = \begin{pmatrix} a_{1,1,k} & a_{1,2,k} & \cdots & a_{1,29,k} & a_{1,30,k} \\ a_{2,1,k} & \ddots & \cdots & \cdots & a_{2,30,k} \\ a_{3,1,k} & \vdots & \ddots & \cdots & \vdots \\ a_{4,1,k} & \vdots & \vdots & \ddots & \vdots \\ vc_{1,k} & \cdots & \cdots & v_{29,k} & vc_{30,k} \end{pmatrix} \qquad k \in \mathbb{Z} \tag{4.1}$$

$$Tr = \begin{pmatrix} a_{1,1,k} & a_{1,3,k} & \cdots & a_{1,27,k} & a_{1,29,k} \\ a_{2,1,k} & \ddots & \cdots & \cdots & \vdots \\ a_{3,1,k} & \vdots & \ddots & \cdots & \vdots \\ a_{4,1,k} & \vdots & \vdots & \ddots & \vdots \\ v_{1,k} & v_{3,k} & \cdots & v_{27,k} & v_{29,k} \end{pmatrix} \tag{4.2}$$

$$Tr(i, j+1, k) = A(i, 2j+1, k) \tag{4.3}$$

$$Ts = \begin{pmatrix} a_{1,2,k} & a_{1,4,k} & \cdots & a_{1,28,k} & a_{1,30,k} \\ a_{2,2,k} & \ddots & \cdots & \cdots & \vdots \\ a_{3,2,k} & \vdots & \ddots & \cdots & \vdots \\ a_{4,2,k} & \vdots & \vdots & \ddots & \vdots \\ v_{2,k} & v_{4,k} & \cdots & v_{28,k} & v_{30,k} \end{pmatrix} \tag{4.4}$$

$$Ts(i, j+1, k) = A(i, 2j+2, k) \tag{4.5}$$

where column number implies selected segment number, k implies the octave number which ranges from 1 to 5. Tr is training input matrix and Ts is testing input matrix. They are selected from mother input matrix.

4.3. Neural Network Analysis

A feed-forward back-propagation network with five input nodes, five hidden layer nodes and one output node was used in classification (Figure 4.14). The performance function and activation function of the network were mean-squared error and hyperbolic tangent sigmoid function, respectively. In Figure 4.14, 'n' implies number of nodes of hidden layer whereas 'm' implies those of output layer.

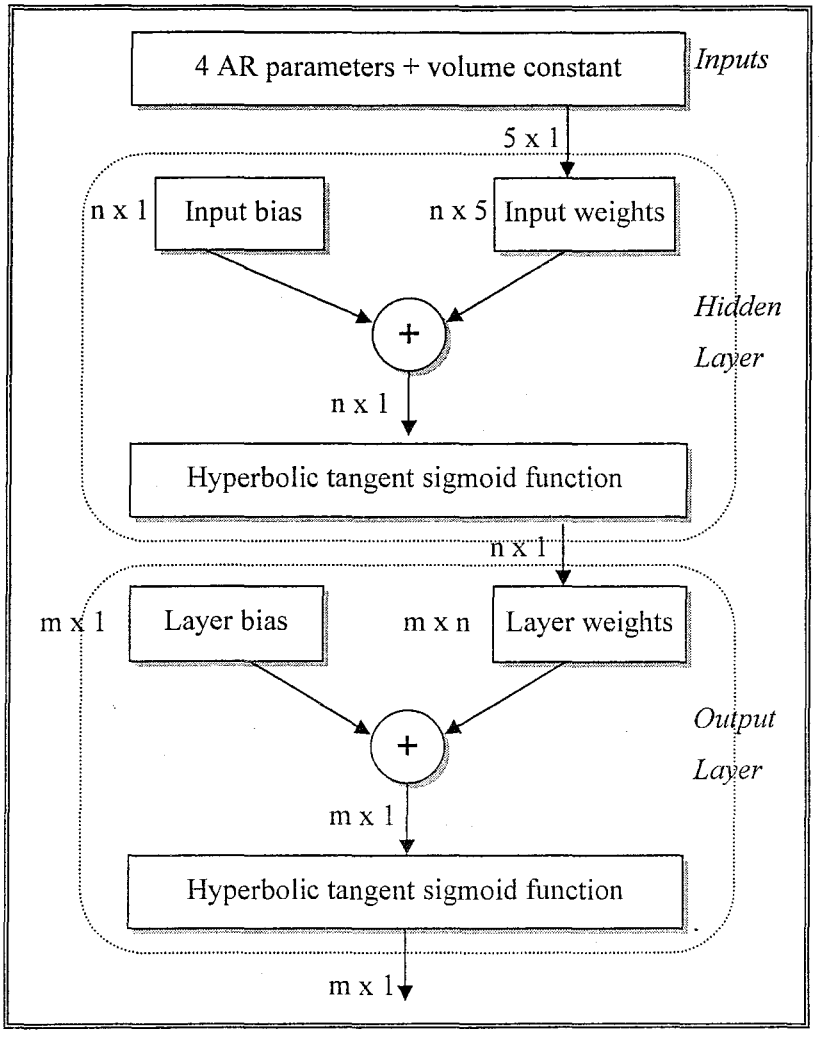

Figure 4.14 The block diagram of the used ANN.

At the first stage of the study, the input dataset was divided into two sub-sets. As mentioned in AR parameter section as matrix form, odd-indexed segments of thirty total segments for each octave were used as training data set whereas even indexed segments were used as testing data set (Figure 4.15). The performance of the classifier was based on

the outcome of the classification of the training and testing set. In the second stage, leave-one-out method was used for classification. In this method, while training, one subject was excluded for each class. They were used as testing set for classifiers. This method was used for each subject for reaching total performance of classifiers.

To compare with the performances of wavelet-based networks, conventional ANN was used as a classifier in the first step of studies. The block diagram of classification algorithm of the wavelet-based neural network may be depicted in Figure 4.16.

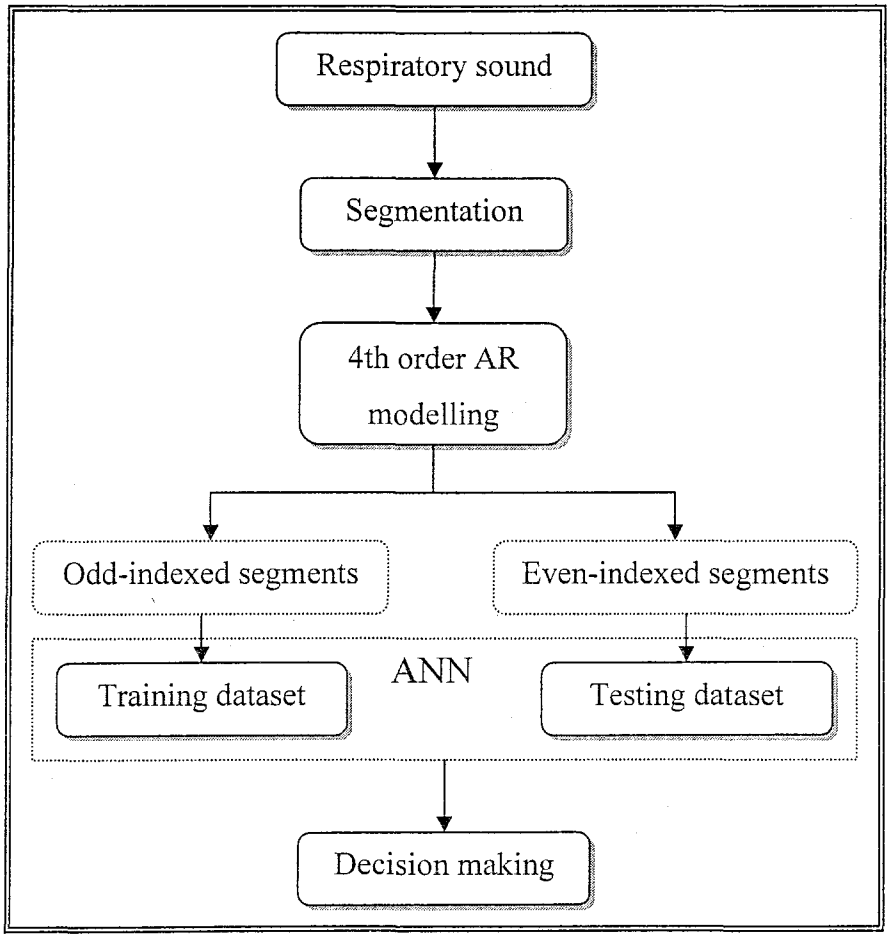

Figure 4.15 The block diagram of first-style dataset selection and classification (even-odd partitioning).

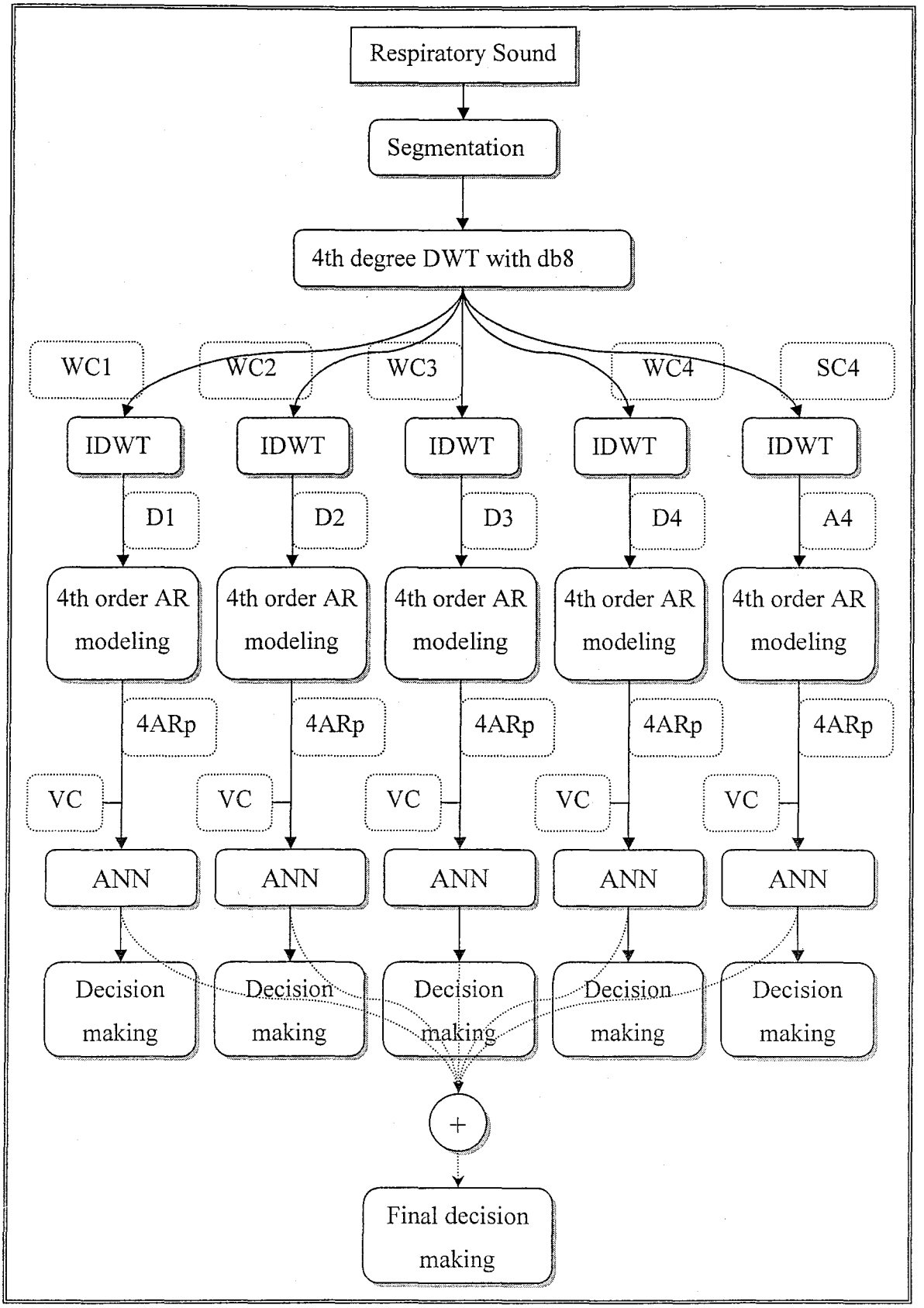

Figure 4.16 The block diagram of classification algorithm of the wavelet-based ANN. WC: Wavelet Coefficients, SC: Scaling Coefficients, D: Detail, A: Approximation, 4ARp: 4 AR parameters, VC: Volume Constant.

5. RESULTS AND DISCUSSIONS

The results are presented according to the methods of construction of training and testing dataset, 'even-odd partitioning' and 'leave-one-out' methods. In addition, the results of each method are separated into two sub-groups, again with respect to the type of classifiers, namely 'conventional ANN' and 'wavelet-based neural network'. The figures in this chapter are labeled according to pathological names of classes, 'healthy', 'obstructive' and 'restrictive'.

5.1. Results

5.1.1. Results of Even-Odd Partitioning Method

5.1.1.1. Results of Conventional ANN

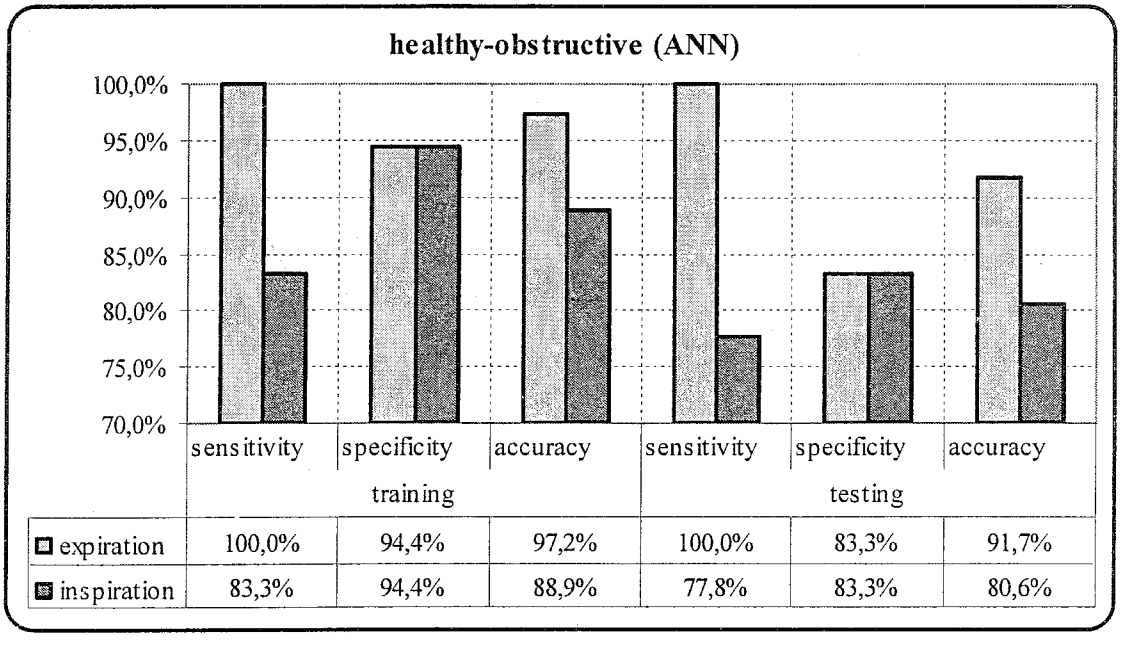

	training			testing		
expiration	100,0%	94,4%	97,2%	100,0%	83,3%	91,7%
inspiration	83,3%	94,4%	88,9%	77,8%	83,3%	80,6%

Figure 5.1 For two classes, healthy and obstructive, comparison of the results of conventional ANN classifier with respect to two phases, expiration and inspiration.

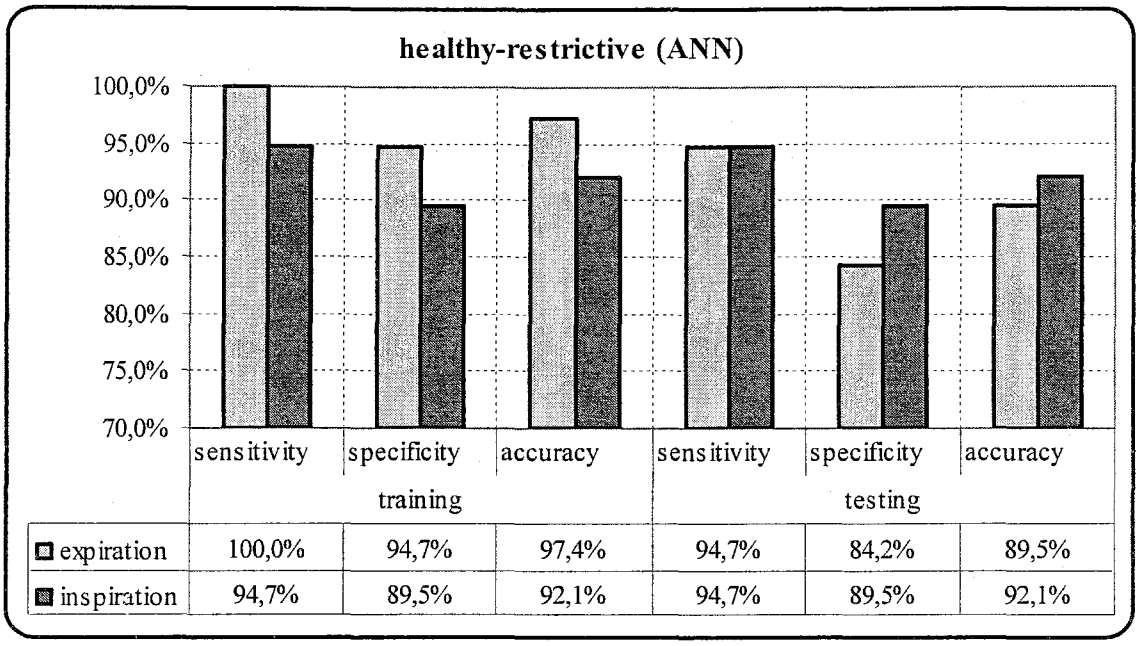

	sensitivity	specificity	accuracy	sensitivity	specificity	accuracy
	training			testing		
expiration	100,0%	94,7%	97,4%	94,7%	84,2%	89,5%
inspiration	94,7%	89,5%	92,1%	94,7%	89,5%	92,1%

Figure 5.2 For two classes, healthy and restrictive, comparison of the results of conventional ANN classifier with respect to two phases, expiration and inspiration.

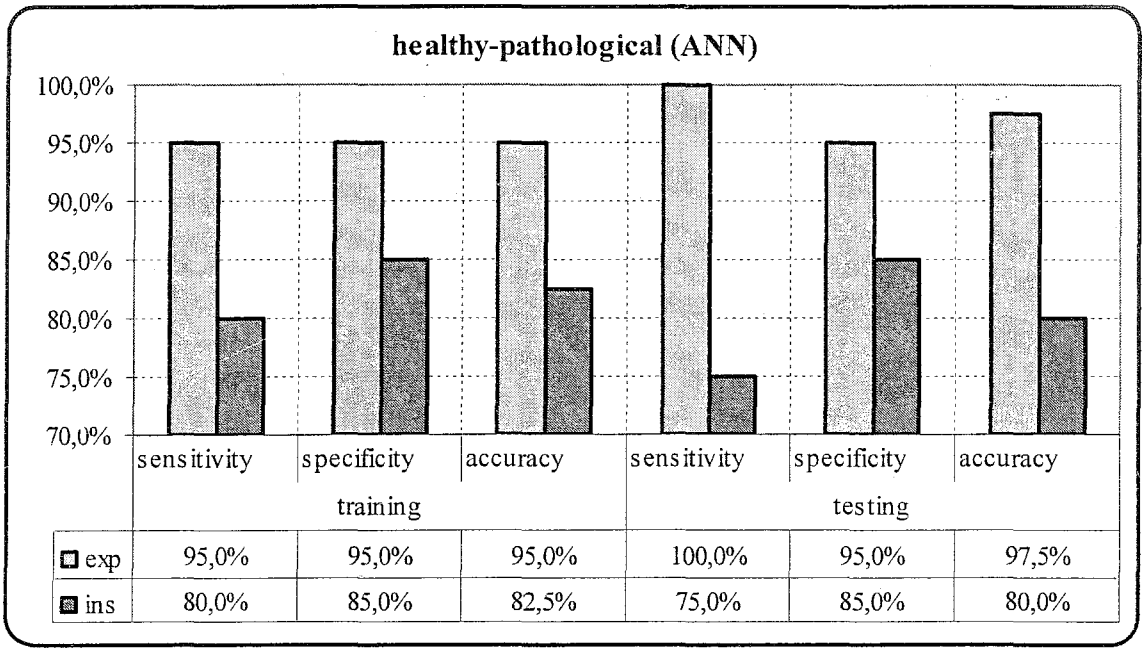

	sensitivity	specificity	accuracy	sensitivity	specificity	accuracy
	training			testing		
exp	95,0%	95,0%	95,0%	100,0%	95,0%	97,5%
ins	80,0%	85,0%	82,5%	75,0%	85,0%	80,0%

Figure 5.3 For two classes, healthy and pathological, comparison of the results of conventional ANN classifier with respect to two phases, expiration and inspiration

5.1.1.2. Results of Wavelet-based Neural Networks

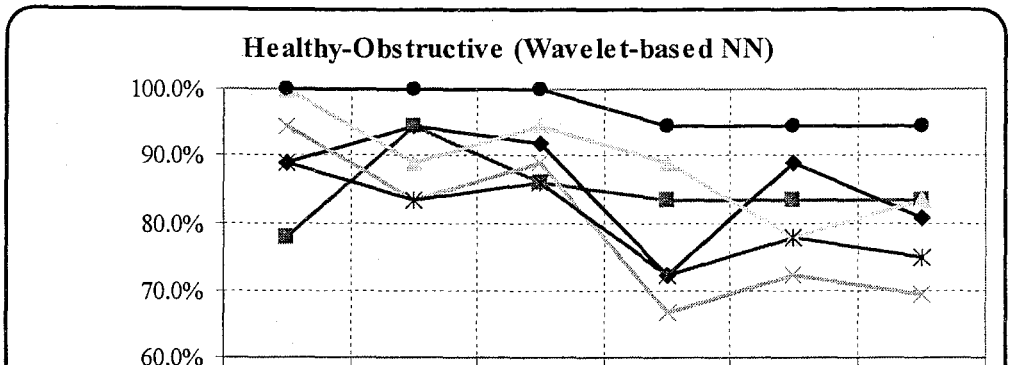

	Sensitivity	Specificity	Accuracy	Sensitivity	Specificity	Accuracy
	training			testing		
2500-1250	88.90%	94.40%	91.70%	72.20%	88.90%	80.60%
1250-625	77.80%	94.40%	86.10%	83.30%	83.30%	83.30%
625-312.5	100.00%	88.90%	94.40%	88.90%	77.80%	83.30%
312.5-156.3	94.40%	83.30%	88.90%	66.70%	72.20%	69.40%
156.3-0	88.90%	83.30%	86.10%	72.20%	77.80%	75.00%
FINAL	100.00%	100.00%	100.00%	94.40%	94.40%	94.40%

Figure 5.4 For two classes, healthy and obstructive, the results of wavelet-based NN classifier with respect to five complementary octaves.

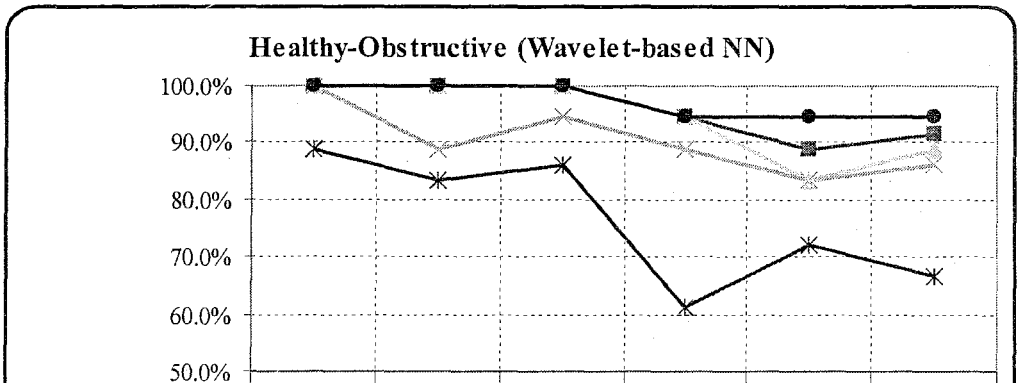

	sensitivity	specificity	accuracy	sensitivity	specificity	accuracy
	training			testing		
2500-156,25Hz	100.0%	100.0%	100.0%	94.4%	88.9%	91.7%
2500-312,5Hz	100.0%	100.0%	100.0%	94.4%	88.9%	91.7%
2500-625Hz	100.0%	100.0%	100.0%	94.4%	83.3%	88.9%
625-0Hz	100.0%	88.9%	94.4%	88.9%	83.3%	86.1%
312,5-0Hz	88.9%	83.3%	86.1%	61.1%	72.2%	66.7%
2500-0 Hz	100.0%	100.0%	100.0%	94.4%	94.4%	94.4%

Figure 5.5 For two classes, healthy and obstructive, the results of wavelet-based NN classifier with respect to six frequency intervals.

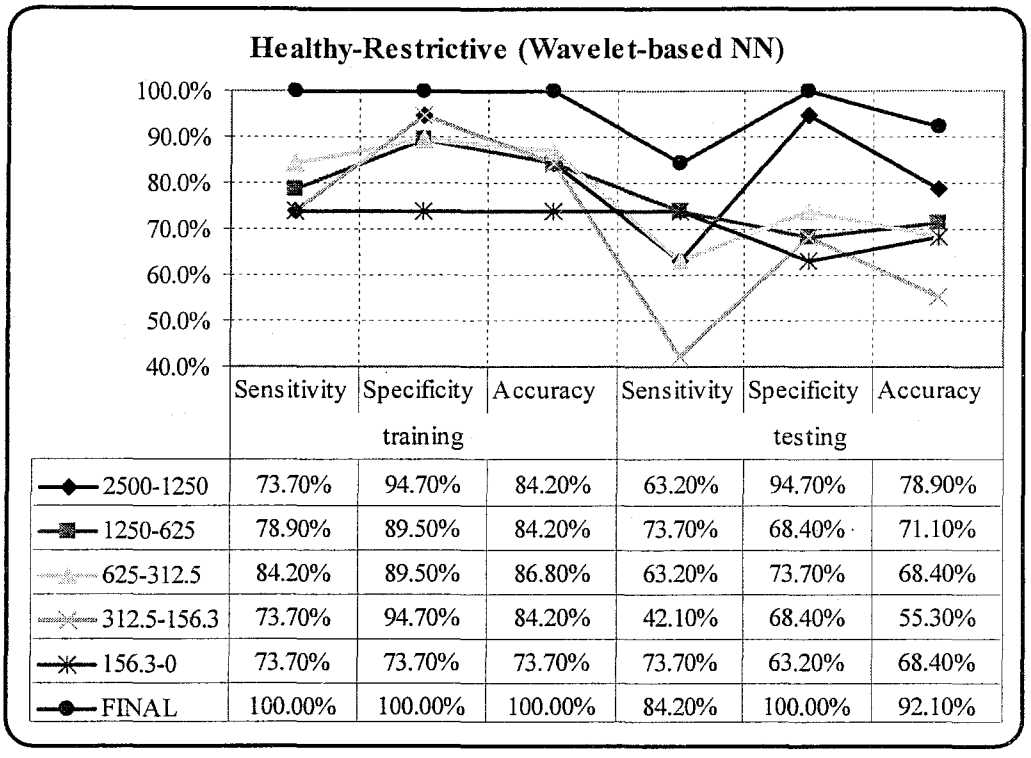

	Sensitivity	Specificity	Accuracy	Sensitivity	Specificity	Accuracy
	training			testing		
2500-1250	73.70%	94.70%	84.20%	63.20%	94.70%	78.90%
1250-625	78.90%	89.50%	84.20%	73.70%	68.40%	71.10%
625-312.5	84.20%	89.50%	86.80%	63.20%	73.70%	68.40%
312.5-156.3	73.70%	94.70%	84.20%	42.10%	68.40%	55.30%
156.3-0	73.70%	73.70%	73.70%	73.70%	63.20%	68.40%
FINAL	100.00%	100.00%	100.00%	84.20%	100.00%	92.10%

Figure 5.6 For two classes, healthy and restrictive, the results of wavelet-based NN classifier with respect to five complementary octaves.

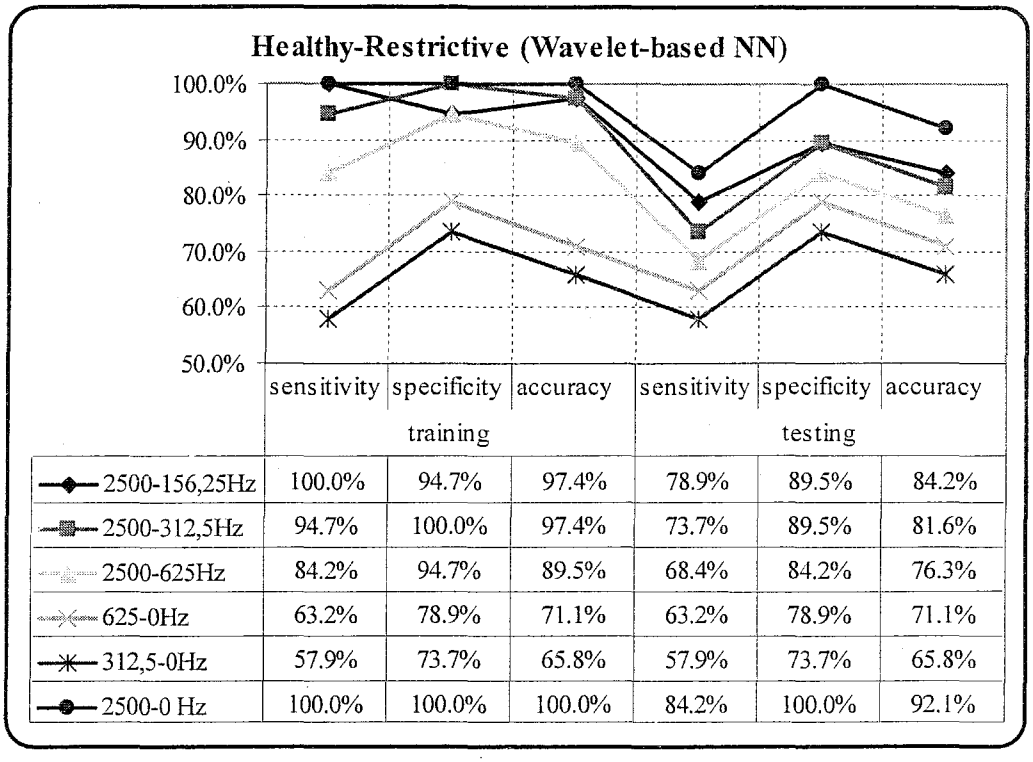

	sensitivity	specificity	accuracy	sensitivity	specificity	accuracy
	training			testing		
2500-156,25Hz	100.0%	94.7%	97.4%	78.9%	89.5%	84.2%
2500-312,5Hz	94.7%	100.0%	97.4%	73.7%	89.5%	81.6%
2500-625Hz	84.2%	94.7%	89.5%	68.4%	84.2%	76.3%
625-0Hz	63.2%	78.9%	71.1%	63.2%	78.9%	71.1%
312,5-0Hz	57.9%	73.7%	65.8%	57.9%	73.7%	65.8%
2500-0 Hz	100.0%	100.0%	100.0%	84.2%	100.0%	92.1%

Figure 5.7 For two classes, healthy and obstructive, the results of wavelet-based NN classifier with respect to six frequency intervals.

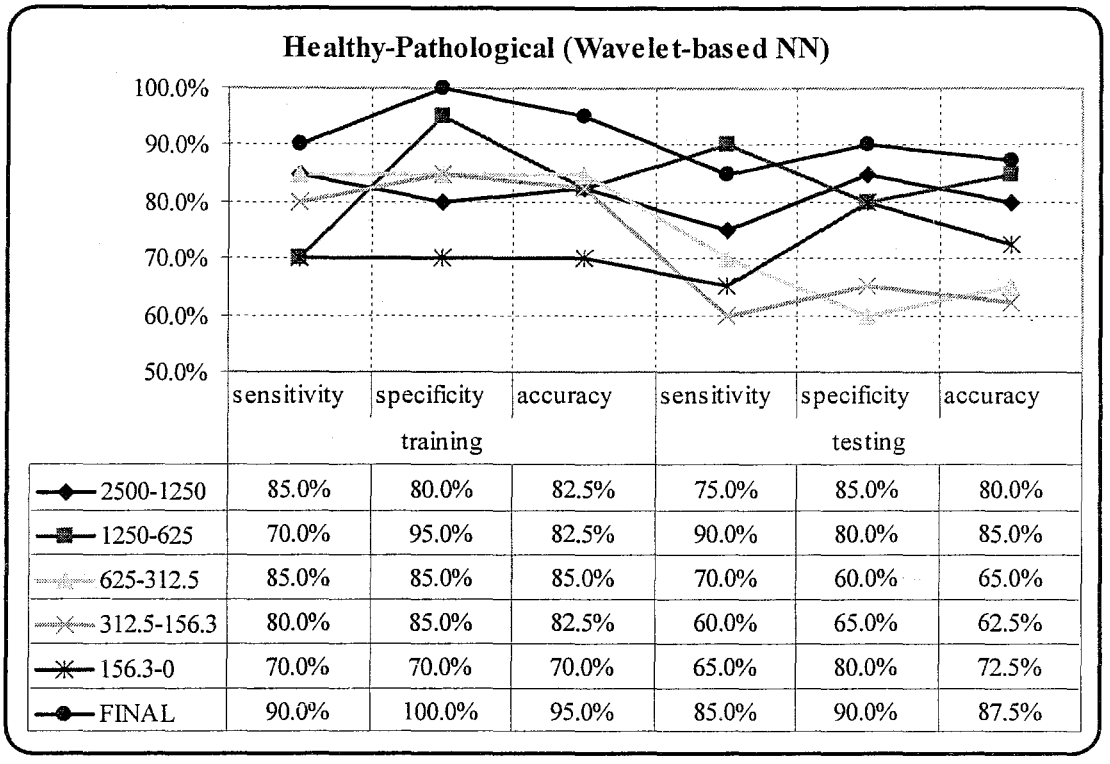

	sensitivity	specificity	accuracy	sensitivity	specificity	accuracy
	training			testing		
2500-1250	85.0%	80.0%	82.5%	75.0%	85.0%	80.0%
1250-625	70.0%	95.0%	82.5%	90.0%	80.0%	85.0%
625-312.5	85.0%	85.0%	85.0%	70.0%	60.0%	65.0%
312.5-156.3	80.0%	85.0%	82.5%	60.0%	65.0%	62.5%
156.3-0	70.0%	70.0%	70.0%	65.0%	80.0%	72.5%
FINAL	90.0%	100.0%	95.0%	85.0%	90.0%	87.5%

Figure 5.8 For two classes, healthy and pathological, the results of wavelet-based NN classifier with respect to five complementary octaves.

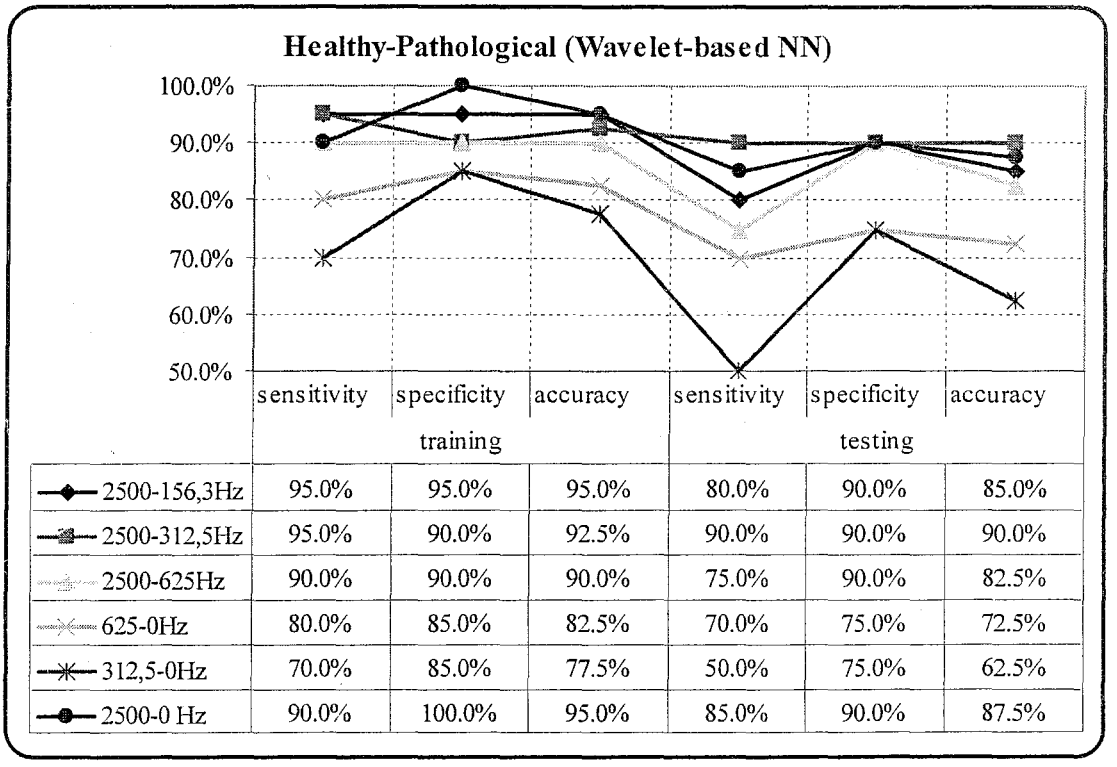

	sensitivity	specificity	accuracy	sensitivity	specificity	accuracy
	training			testing		
2500-156,3Hz	95.0%	95.0%	95.0%	80.0%	90.0%	85.0%
2500-312,5Hz	95.0%	90.0%	92.5%	90.0%	90.0%	90.0%
2500-625Hz	90.0%	90.0%	90.0%	75.0%	90.0%	82.5%
625-0Hz	80.0%	85.0%	82.5%	70.0%	75.0%	72.5%
312,5-0Hz	70.0%	85.0%	77.5%	50.0%	75.0%	62.5%
2500-0 Hz	90.0%	100.0%	95.0%	85.0%	90.0%	87.5%

Figure 5.9 For two classes, healthy and pathological, the results of wavelet-based NN classifier with respect to six frequency intervals.

5.1.1.3. Comparison of the Results of Two Types of Classifiers

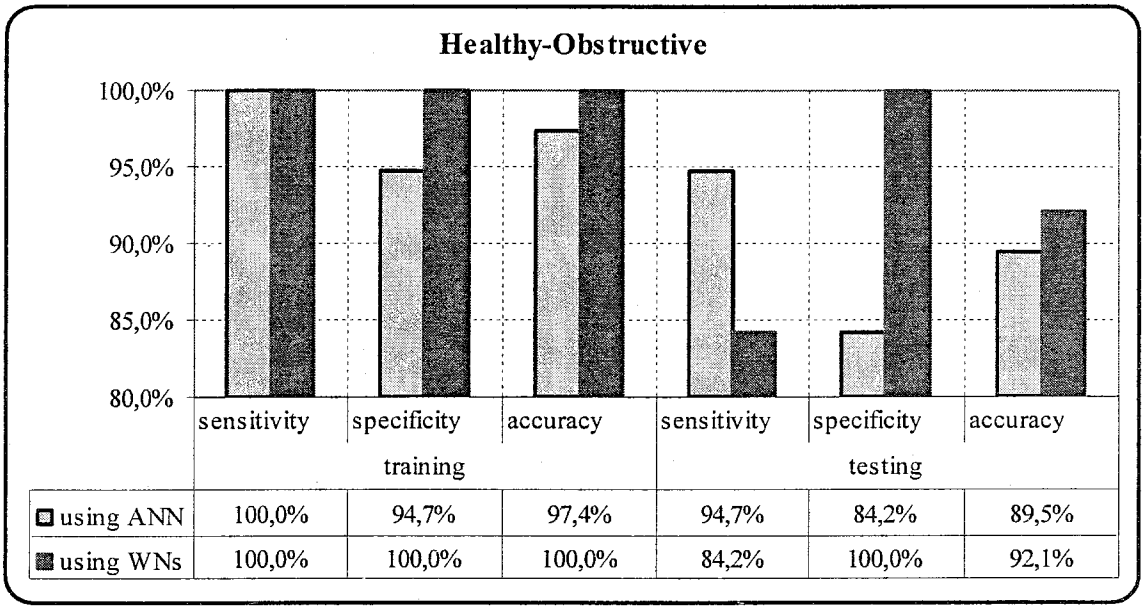

	training			testing		
using ANN	100,0%	94,7%	97,4%	94,7%	84,2%	89,5%
using WNs	100,0%	100,0%	100,0%	84,2%	100,0%	92,1%

Figure 5.10 For two classes, healthy and obstructive, comparison of the results of conventional ANN classifier and wavelet-based NN classifier.

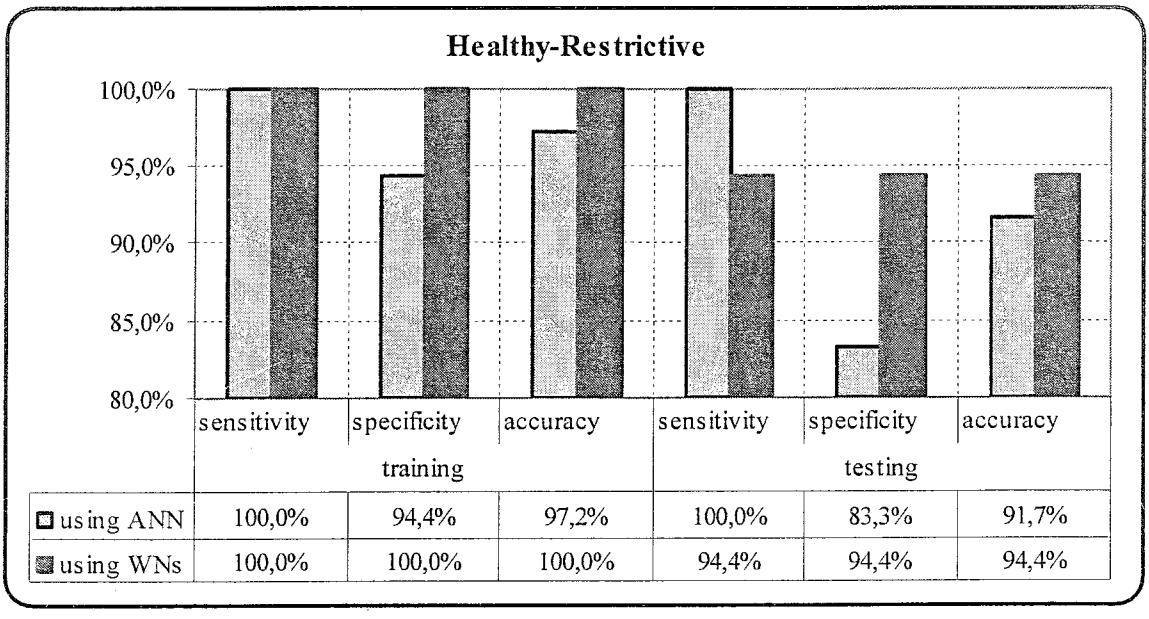

	training			testing		
using ANN	100,0%	94,4%	97,2%	100,0%	83,3%	91,7%
using WNs	100,0%	100,0%	100,0%	94,4%	94,4%	94,4%

Figure 5.11 For two classes, healthy and restrictive, comparison of the results of conventional ANN classifier and wavelet-based NN classifier.

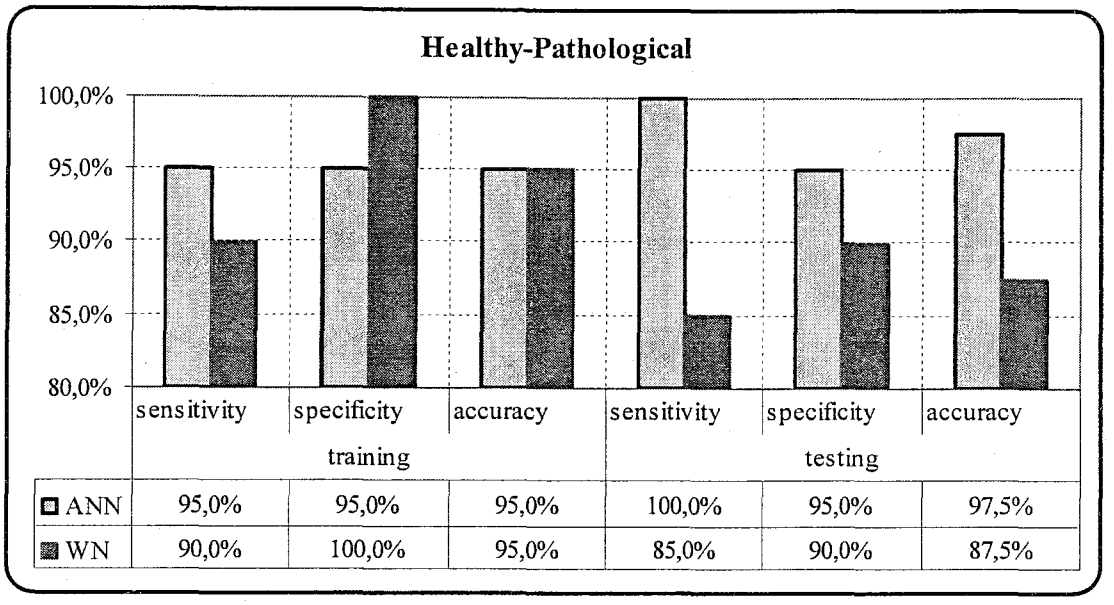

Figure 5.12 For two classes, healthy and pathological, comparison of the results of conventional ANN classifier and wavelet-based NN classifier.

5.1.2. Results of Leave-one-out Method

5.1.2.1. Results of Conventional ANN

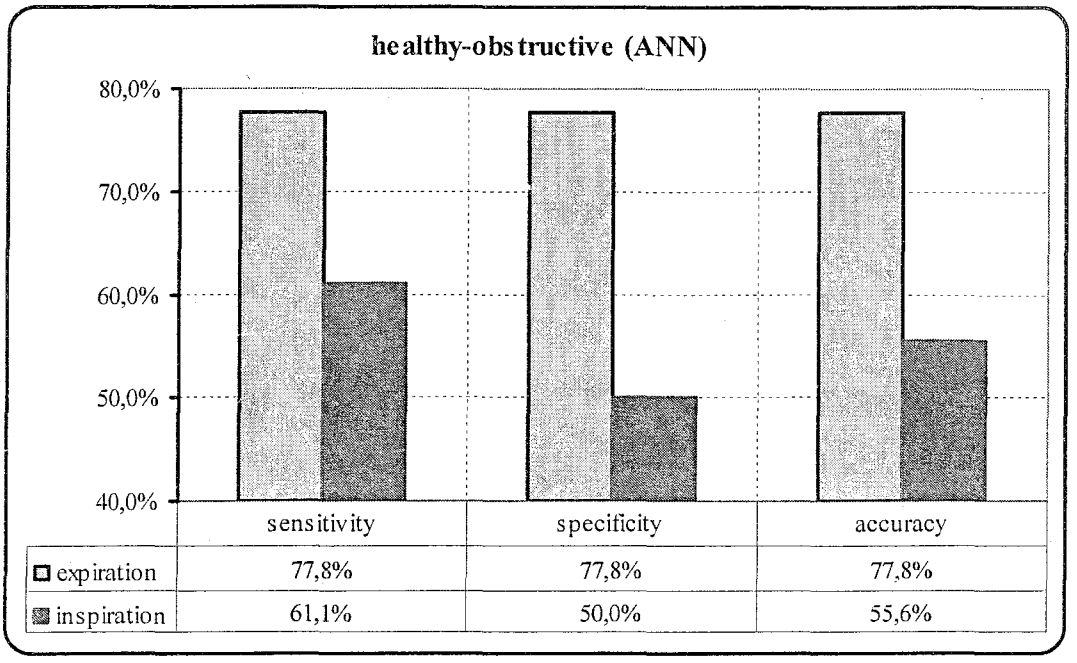

Figure 5.13 For two classes, healthy and obstructive, comparison of the results of conventional ANN classifier with respect to two phases, expiration and inspiration.

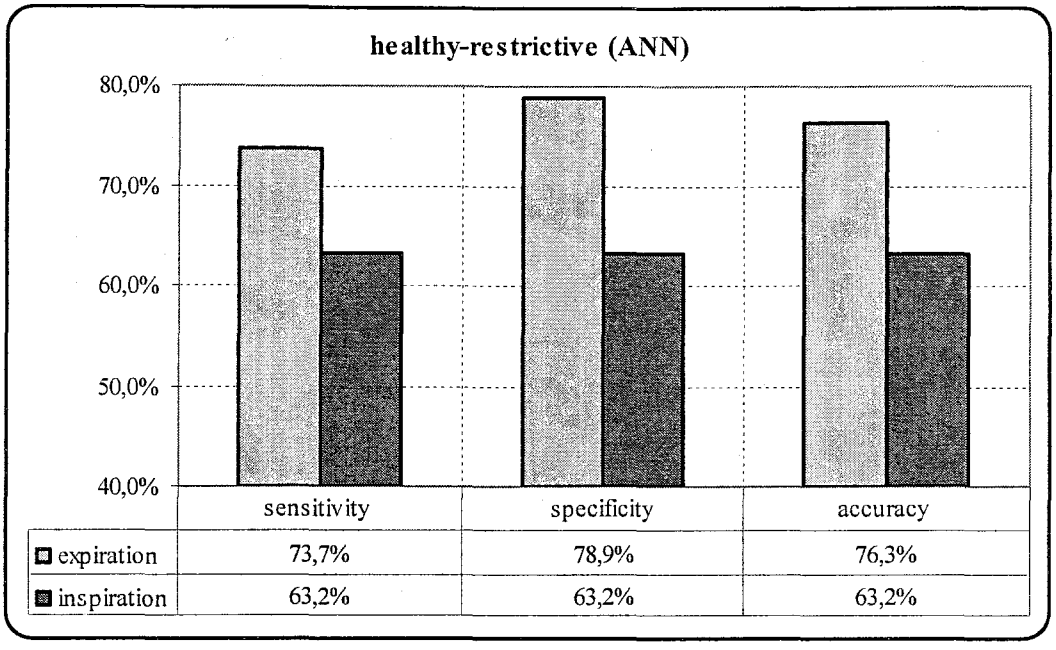

Figure 5.14 For two classes, healthy and restrictive, comparison of the results of conventional ANN classifier with respect to two phases, expiration and inspiration.

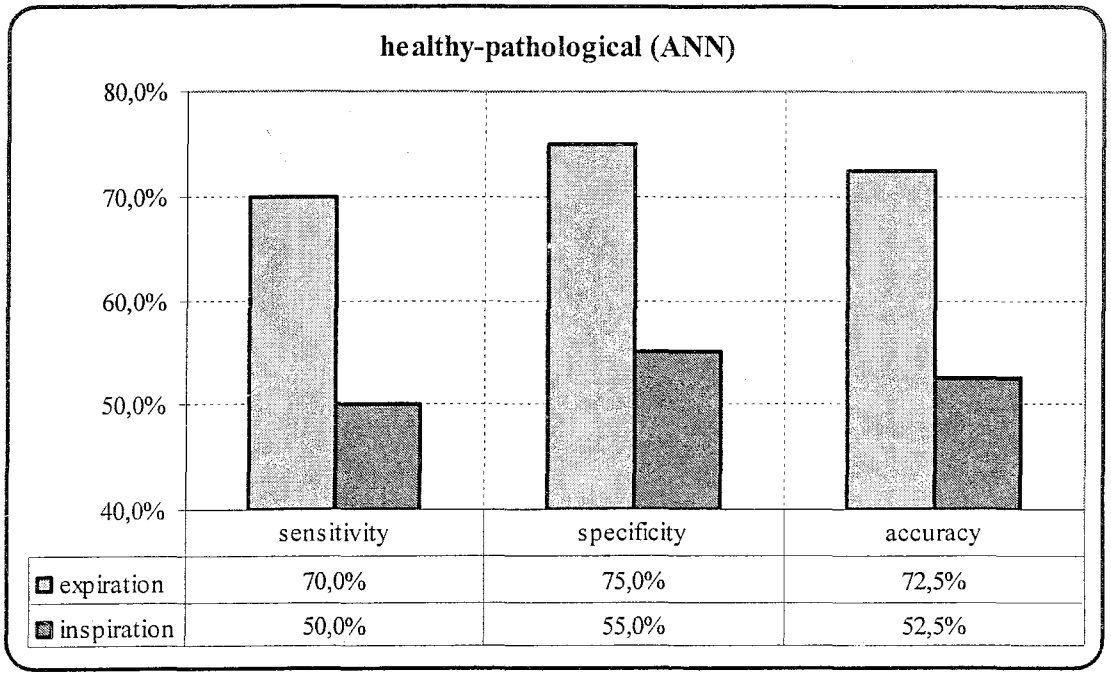

Figure 5.15 For two classes, healthy and pathological, comparison of the results of conventional ANN classifier with respect to two phases, expiration and inspiration.

5.1.2.2. Results of Wavelet-based Neural Networks

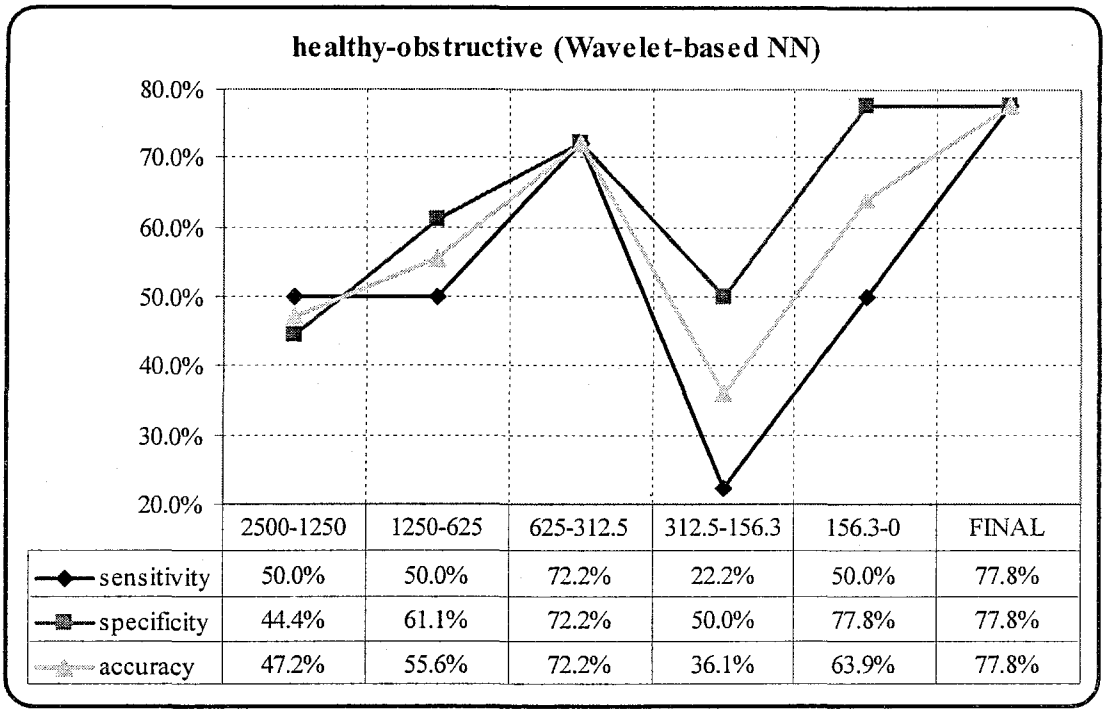

	2500-1250	1250-625	625-312.5	312.5-156.3	156.3-0	FINAL
sensitivity	50.0%	50.0%	72.2%	22.2%	50.0%	77.8%
specificity	44.4%	61.1%	72.2%	50.0%	77.8%	77.8%
accuracy	47.2%	55.6%	72.2%	36.1%	63.9%	77.8%

Figure 5.16 For two classes, healthy and obstructive, the results of wavelet-based NN classifier with respect to five complementary octaves.

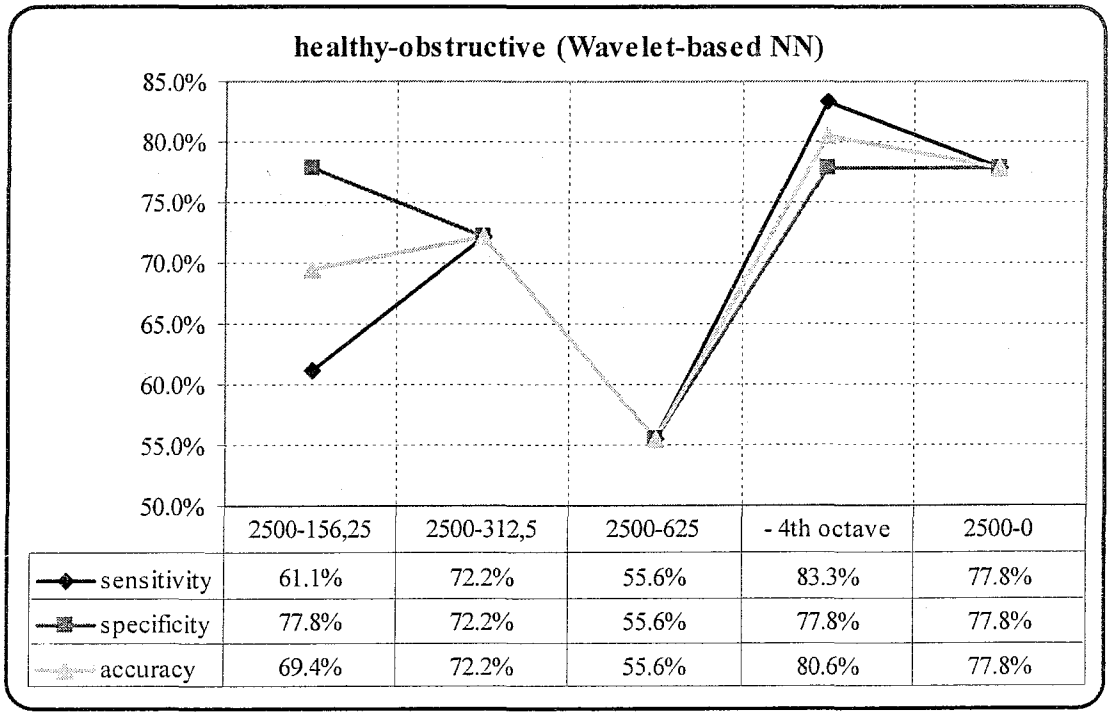

	2500-156,25	2500-312,5	2500-625	- 4th octave	2500-0
sensitivity	61.1%	72.2%	55.6%	83.3%	77.8%
specificity	77.8%	72.2%	55.6%	77.8%	77.8%
accuracy	69.4%	72.2%	55.6%	80.6%	77.8%

Figure 5.17 For two classes, healthy and obstructive, the results of wavelet-based NN classifier with respect to five frequency intervals.

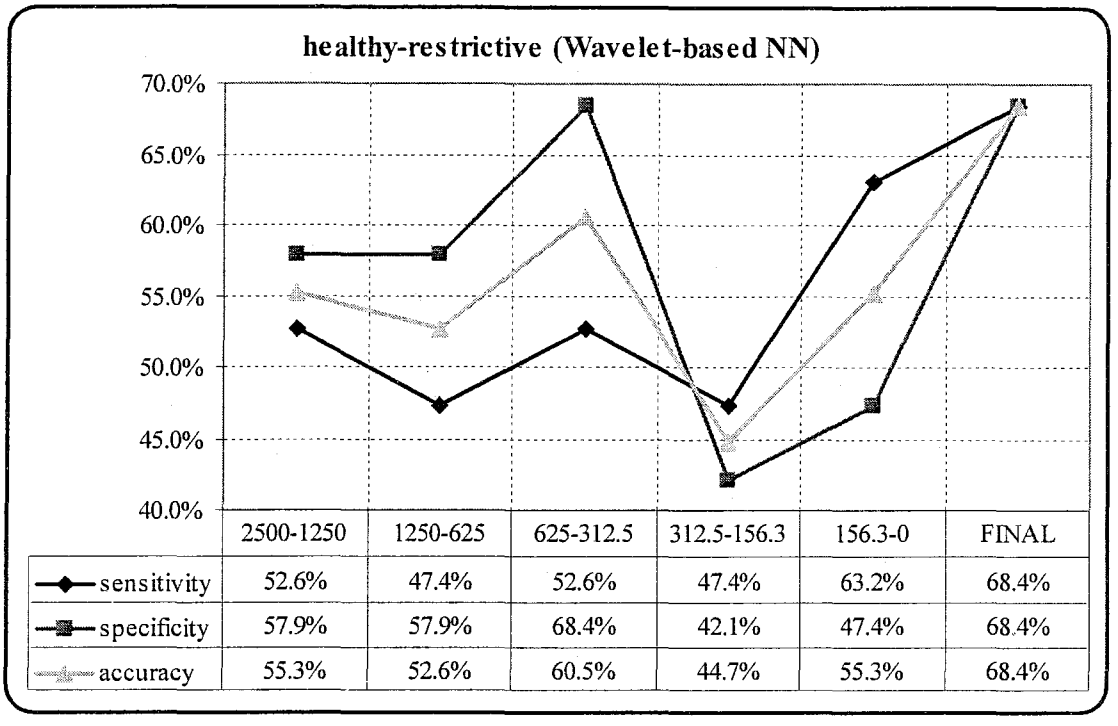

	2500-1250	1250-625	625-312.5	312.5-156.3	156.3-0	FINAL
sensitivity	52.6%	47.4%	52.6%	47.4%	63.2%	68.4%
specificity	57.9%	57.9%	68.4%	42.1%	47.4%	68.4%
accuracy	55.3%	52.6%	60.5%	44.7%	55.3%	68.4%

Figure 5.18 For two classes, healthy and restrictive, the results of wavelet-based NN classifier with respect to five complementary octaves.

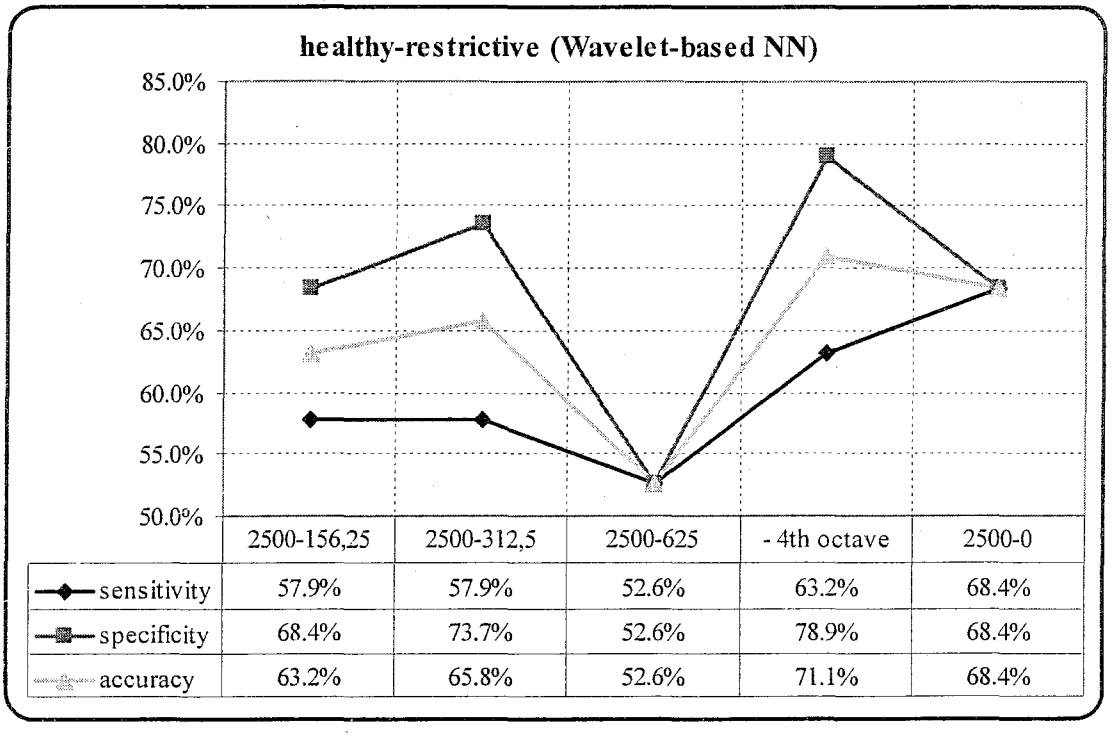

	2500-156,25	2500-312,5	2500-625	- 4th octave	2500-0
sensitivity	57.9%	57.9%	52.6%	63.2%	68.4%
specificity	68.4%	73.7%	52.6%	78.9%	68.4%
accuracy	63.2%	65.8%	52.6%	71.1%	68.4%

Figure 5.19 For two classes, healthy and obstructive, the results of wavelet-based NN classifier with respect to five frequency intervals.

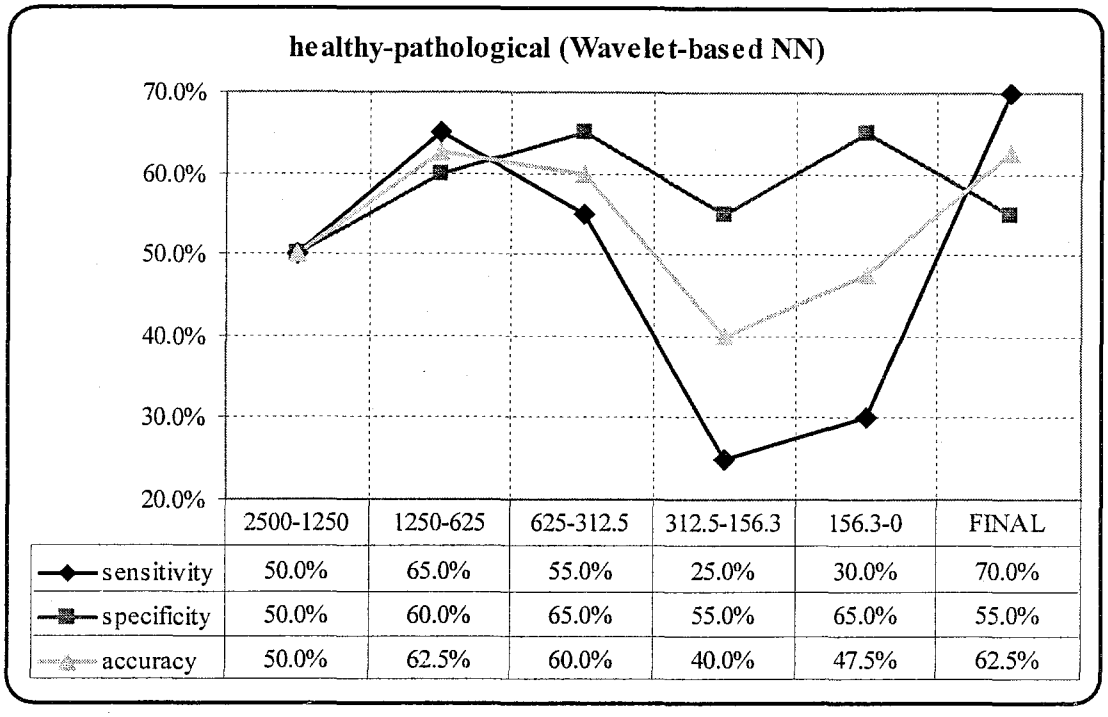

	2500-1250	1250-625	625-312.5	312.5-156.3	156.3-0	FINAL
sensitivity	50.0%	65.0%	55.0%	25.0%	30.0%	70.0%
specificity	50.0%	60.0%	65.0%	55.0%	65.0%	55.0%
accuracy	50.0%	62.5%	60.0%	40.0%	47.5%	62.5%

Figure 5.20 For two classes, healthy and pathological, the results of wavelet-based NN classifier with respect to five complementary octaves.

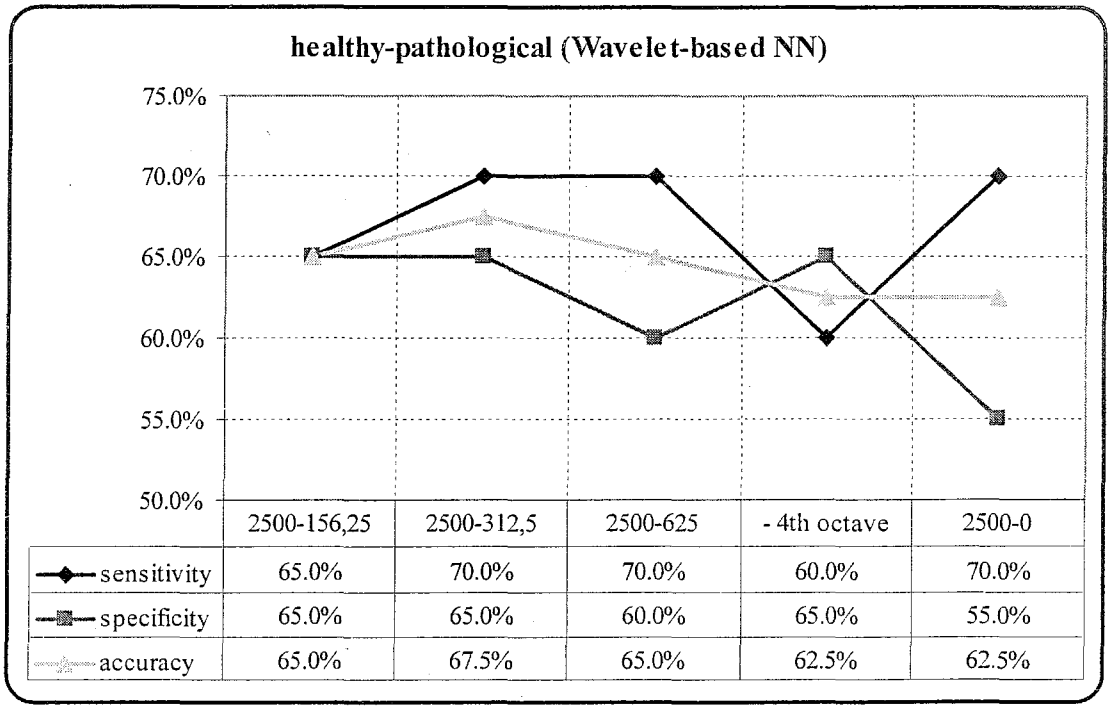

	2500-156,25	2500-312,5	2500-625	- 4th octave	2500-0
sensitivity	65.0%	70.0%	70.0%	60.0%	70.0%
specificity	65.0%	65.0%	60.0%	65.0%	55.0%
accuracy	65.0%	67.5%	65.0%	62.5%	62.5%

Figure 5.21 For two classes, healthy and pathological, the results of wavelet-based NN classifier with respect to five frequency intervals.

5.1.2.3. Comparison of the Results of Two Types of Classifiers

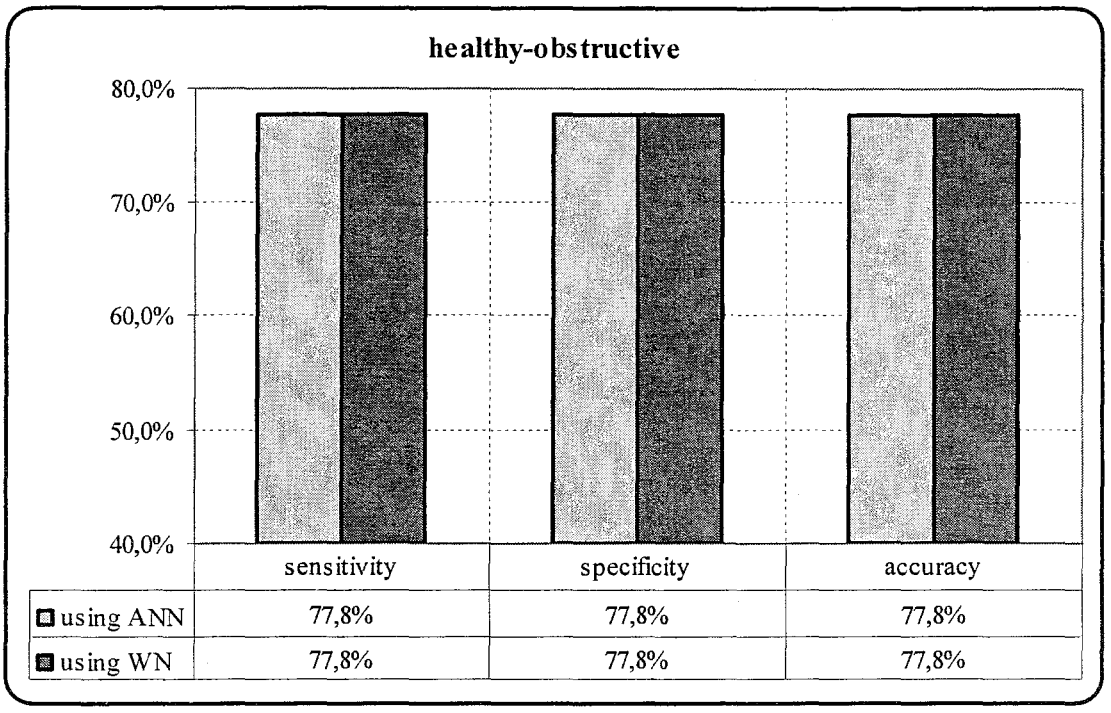

	sensitivity	specificity	accuracy
using ANN	77,8%	77,8%	77,8%
using WN	77,8%	77,8%	77,8%

Figure 5.22 For two classes, healthy and obstructive, comparison of the results of conventional ANN classifier and wavelet-based NN classifier.

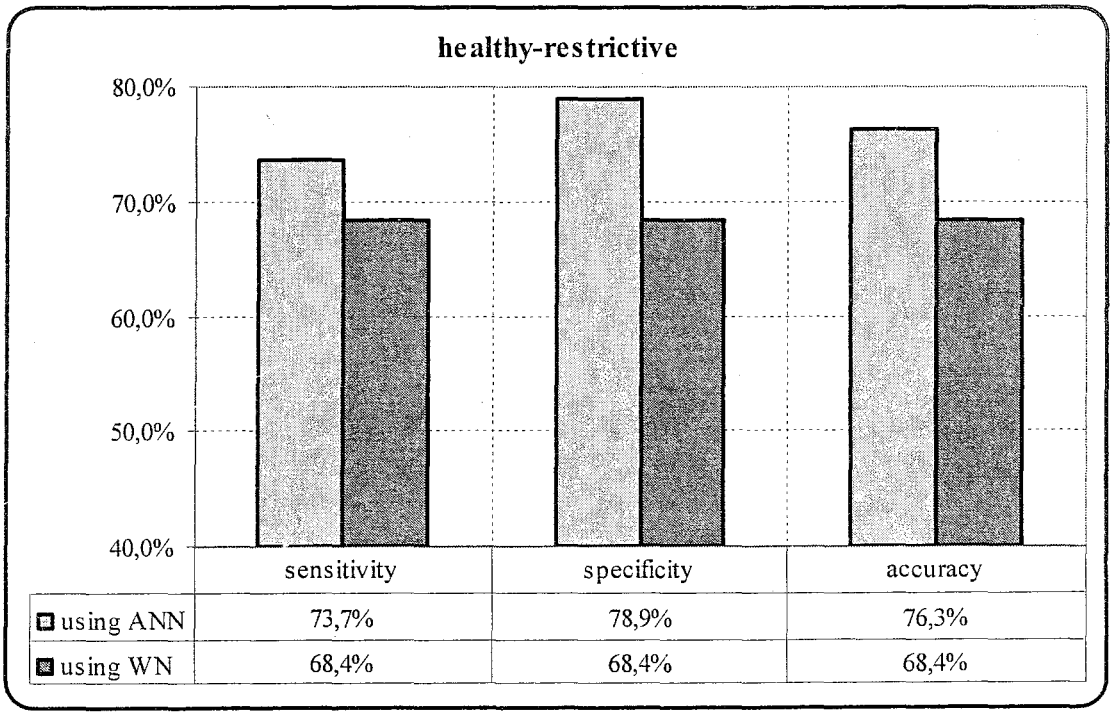

	sensitivity	specificity	accuracy
using ANN	73,7%	78,9%	76,3%
using WN	68,4%	68,4%	68,4%

Figure 5.23 For two classes, healthy and restrictive, comparison of the results of conventional ANN classifier and wavelet-based NN classifier.

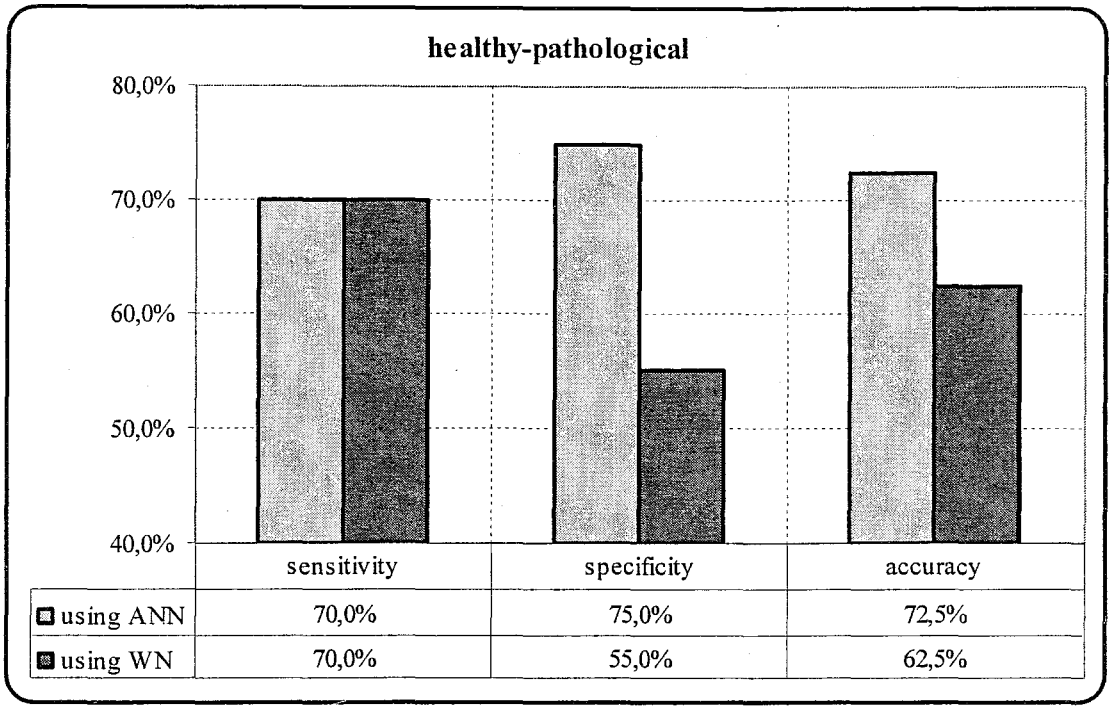

Figure 5.24 For two classes, healthy and pathological, comparison of the results of conventional ANN classifier and wavelet-based NN classifier.

5.2. Discussions

The database consists of respiratory sounds from 20 healthy subjects, 19 patients with restrictive lung disease and 18 patients with obstructive lung disease (The patient profiles are shown in Appendix C). Three types of two-class based classification were processed in classifiers (Table 5.1).

Table 5.1

The number of subjects used in each classification.

Type of Classification	Class		
	Healthy	Obstructive	Restrictive
Healthy-Obstructive	18	18	-
Healthy-Restrictive	19	-	19
Healthy-Pathological	20	10	10

The performances of the classifiers were determined by means of the following statistical parameters:

Sensitivity: number of pathological subjects classified correctly / total number of pathological subjects;

Specificity: number of healthy subjects classified correctly /total number of healthy subjects;

Accuracy: number of subjects correctly classified / total number of subjects.

Table 5.2

The numbers of segment results used for decision in ANN and wavelet-based network.

				# of segments
Even-odd Partitioning	for ANN			15
	for Wavelet based NN	for each octave		15
		for frequency intervals	2500-0 (Final Result)	75
			2500-156,25	60
			2500-312,5	45
			2500-625	30
			625-0	45
			312,5-0	30
Leave-one-out	for ANN			30
	for Wavelet based NN	for each octave		30
		for frequency intervals	2500-0 (Final Result)	150
			2500-156,25	120
			2500-312,5	90
			2500-625	60
			-4th octave	120

Because of the type of activation function, network outputs for each segment ranged from –1 to 1. To optimize the results, sigmoid function was applied to the segmental outputs. The sum of fifteen segmental outputs gave us the results for each subject. The decisions were made with respect to the signs of the results. In ANN, these decisions were final decisions for each subject whereas, in wavelet-based NN, they were the decisions for each octave. The combination of the octave results gave us the results of frequency

intervals (Table 5.1). For instance, to find the result for the frequency interval of 2500-312.5 Hz, the results of three octaves, 2500-1250 Hz, 1250-625 Hz and 625-312.5 Hz, were summed. Therefore, when thirty segments were used for the octave decision, ninety segments were used for this frequency interval. In Table 5.1, "-4th octave" means that the result of 4th octave was not used in final decision, however those of all other four octaves were used in decision making.

For 'even-odd partitioning' method, to be able to evaluate the performance of wavelet-based NN and to decide which phase of respiratory cycle should be used in classification, conventional ANN was applied to the inspiratory and expiratory phases of subjects separately, as an initial step. The performances of ANN are shown in Figures 5.1, 5.2 and 5.3. In healthy-obstructive and healthy-pathological classification, accuracies of classifiers for expiration were 91.7% and 97.5% whereas those for inspiration are 80.6% and 80.0% for inspiration. The accuracy for inspiration is better than that for expiration in only healthy-restrictive classification, therefore, respiratory sound signals belonging to expiration phase were used in the wavelet-based NN according to the results of the other two kinds of classifications and the previous study [18].

Table 5.3

The frequency bands of octaves

Octave No	1	2	3	4	5
Freq. Band (Hz)	2500-1250	1250-625	625-312.5	312.5-156.3	156.3-0

The performances of wavelet-based NN are shown in Figures 5.4 and 5.5 for healthy-obstructive classification, in Figures 5.6 and 5.7 for healthy-restrictive classification and in Figures 5.8 and 5.9 for healthy-pathological classification. In healthy-obstructive classification, the accuracies of performances of octaves range from 69.40% for the 4th octave to 83.30% for the 2nd and 3rd octaves. By combining various octaves, the performances of frequency intervals differ between 66.7% for the interval of 312.5-0 Hz and 94.40% for the interval of 2500-0 Hz. In healthy-restrictive classification, the accuracies of octaves differ from 55.30% for the 4th octave to 78.90% for the 1st octave. The performances of frequency intervals range between 65.8% for the interval of 312.5-0 Hz and 92.10% for the interval of 2500-0 Hz. In healthy-pathological classification,

performances of octaves differ from 62.5% for the 4th octave to 85.0% for the 2nd octave. The performances of frequency intervals range from 62.5% for the interval of 312.5-0 Hz to 87.50% for the interval of 2500-0 Hz.

It is clear that the performances of the classifications in the 4th octave are the lowest and those in the 5th octave are 2nd, 2nd and 3rd worst in respective classifications. This result is to be expected since the spectral characteristics of healthy and pathological sounds may overlap at lower frequency bands. However, the contribution of the distinctive octaves is greater in the final result due to the action of the neural network.

Figures 5.10, 5.11 and 5.12 show the comparisons of performances of classifiers. For classifications of healthy-obstructive, healthy-restrictive and healthy-pathological, final results of wavelet-based NN are 92.1%, 94.4% and 87.5%, respectively, whereas results of ANN are 89.5%, 91.7% and 97.5%, respectively. For the first two classifications, results of wavelet-based NN are better than those of ANN, however, for the third classification, the results of ANN are superior.

For the 'leave-one-out' method, conventional ANN was similarly applied to two phases of respiratory cycles separately, as an initial step. Figures 5.13, 5.14 and 5.15 show the results of ANN. For the three two-class classifications, the results of classifiers for expiration are better than those for inspiration. They are 77.8%, 76.3% and 72.5% for expiration whereas 55.6%, 63.2% and 52.5% for inspiration respectively. Therefore, in the 'leave-one-out' method, respiratory sounds from expiration phase were also used in classifiers using wavelet-based NN.

The performances of wavelet-based NN are shown in Figures 5.16, 5.18 and 5.20 with respect to octaves, and in Figures 5.17 and 5.19 and 5.21 for five frequency intervals. In healthy-obstructive classifications, the accuracies of classifiers with respect to octaves differ from 36.1% for the 4th octave to 72.2% for the 3rd octave. The performances of frequency intervals range between 55.6% for the interval of 2500-625 Hz and 80.6% for the interval that does not contain 4th octave, namely '-4th octave'. In healthy-restrictive classification, the accuracies of octaves differ from 44.7% for the 4th octave to 60.5% for the 3rd octave. The performances of frequency intervals are between 52.6% for the interval

of 2500-625 Hz and 71.1% for '-4th octave'. In healthy-pathological classification, performances of octaves differ from 40.0% for the 4th octave to 62.5% for the 2nd octave. The performances of frequency intervals range from 62.5% for '-4th octave' and intervals of 2500-0 Hz to 67.5% for the interval of 2500-312.5 Hz.

The classification of lung sounds belonging to the 4th octave likewise gives again the worst results. This means that for two-class pathological and healthy subjects, this interval has similar properties and their AR modeling overlap.

Finally, comparing the two classifiers, the accuracies are 77.8%, 76.3% and 72.5% for ANN where those are 77.8%, 68.4% and 62.5 for wavelet-based NN.

6. CONCLUSIONS

In this study, an algorithm for classification of respiratory sounds is presented. This algorithm is based on three approaches, autoregressive (AR) modeling using Yule-Walker equations, multilayer feed-forward neural networks, and multi-resolution analysis. We compare the performance of our classifier, wavelet-based network, with a conventional ANN. For comparison, two different methods are employed, "even-odd partitioning" and "leave-one-out".

This study shows us that the components of respiratory sounds at high frequencies carry more specific information about the subjects' pathological conditions whereas the spectral characteristics of healthy and pathological sounds may overlap at lower frequencies.

At this level of research, the performance of wavelet-based network is not sufficiently accurate for use in routine clinical applications. Additional studies that need to be carried out to improve the performance of the classifier may be listed as follows:

- The output of neural networks belonging to five octaves may be used as inputs of a second ANN. The distinctive components of respiratory sounds at higher frequency bands may have more effect in decision making as the results of different octaves dictate.

- With the addition of the acquired new respiratory sounds, the database may be enlarged with time. Using this large database, the classifier can be trained more accurately.

- In this study, the features of the network are extracted from AR modeling of details and approximation that are the reconstructed forms of the coefficients. A different approach of modeling the wavelet and scaling coefficients directly may be used.

Studies recommended as future work are as follows:

- By using multi-resolution analysis and the ambient noise acquired using a third microphone, the noise in respiratory sounds may be reduced. With noise reduction, the performance of the analysis may be improved.

- With a larger database, a three-class based classification, namely restrictive, obstructive and healthy, may be achieved. In addition, some studies on the classification of specific pathological conditions, such as pneumonia or asthma, may be attempted. Based on these studies, diagnosis systems for each disease may be built.

- With the application of the classification algorithm together with the DAQ system, an automatic classification system can be built. In our system, this can be achieved by the adaptation of the algorithm to LabVIEW programming language (or MATLAB may run on LabVIEW but it will be required to run two programs at the same time and the process will be slower). The addition of a biotelemetry system for data acquisition would make this system more versatile.

APPENDIX A: FREQUENCY RESPONSES OF THE CHANNELS

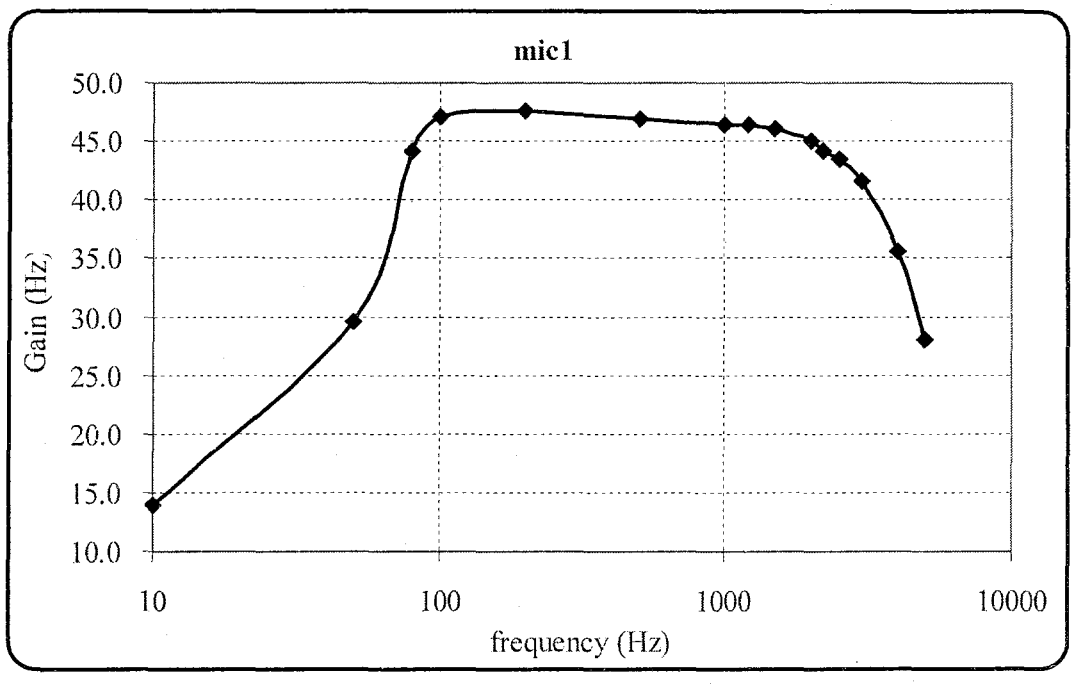

Figure A.1a Chart of the frequency response of channel 1.

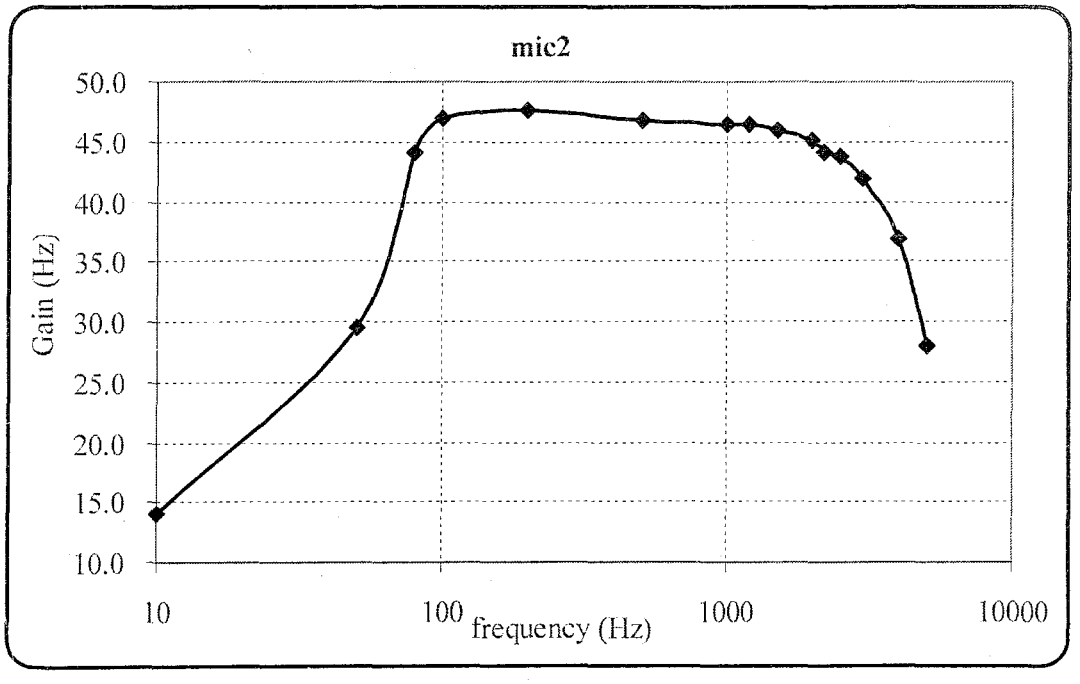

Figure A.1b Chart of the frequency response of channel 2.

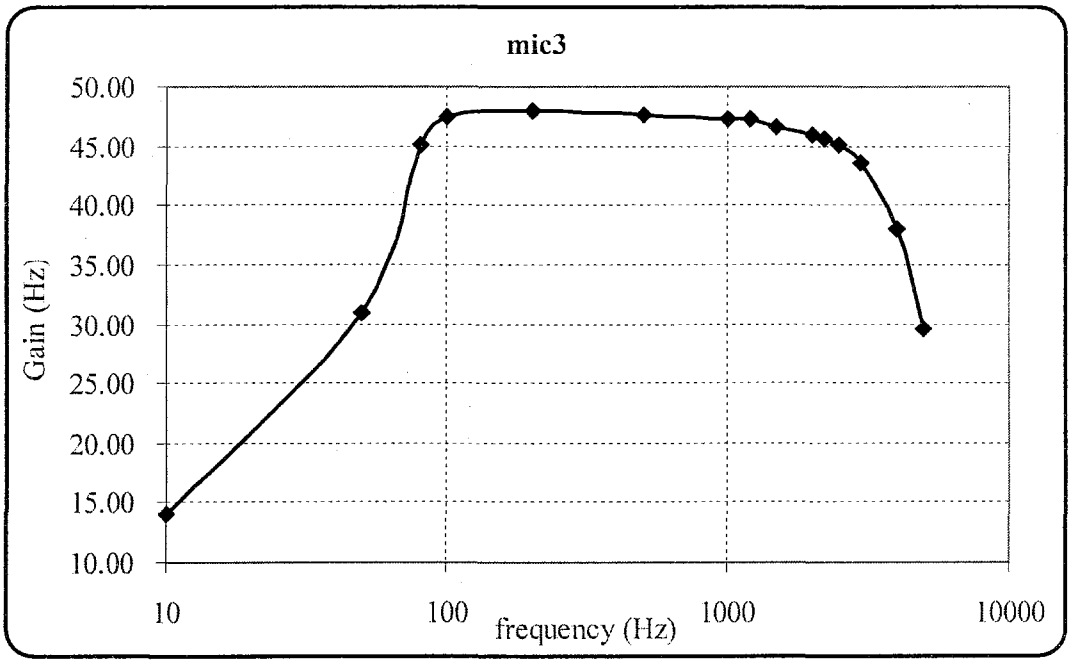

Figure A.1c Chart of the frequency response of channel 3.

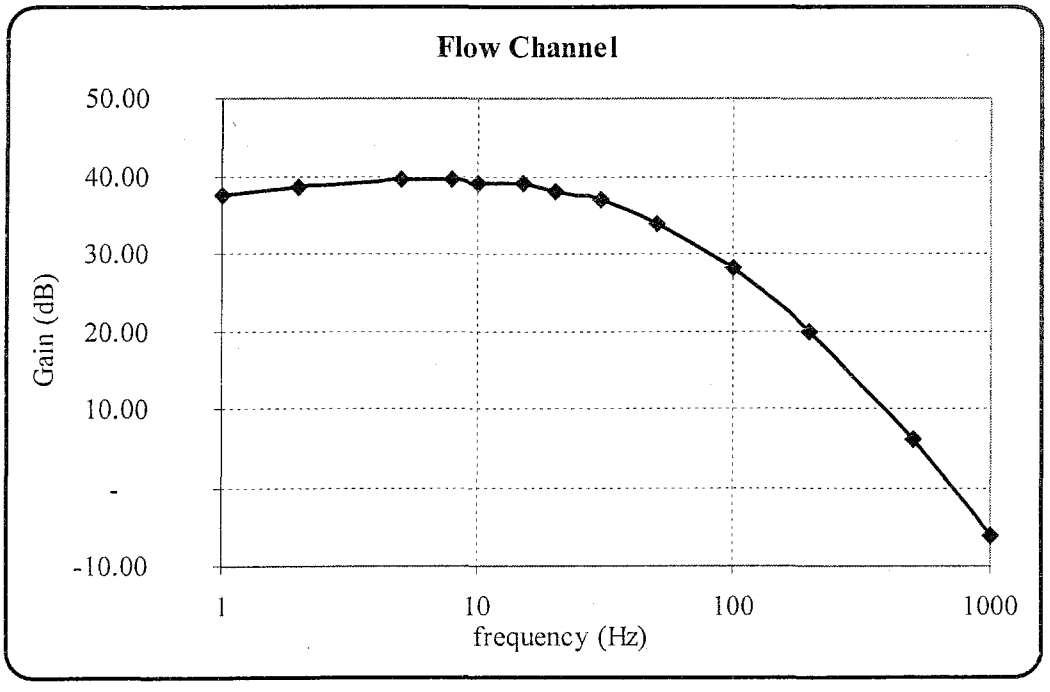

Figure A.1d Chart of the frequency response of the flow channel.

APPENDIX B: DIAGRAM WINDOW OF DAQ SOFTWARE

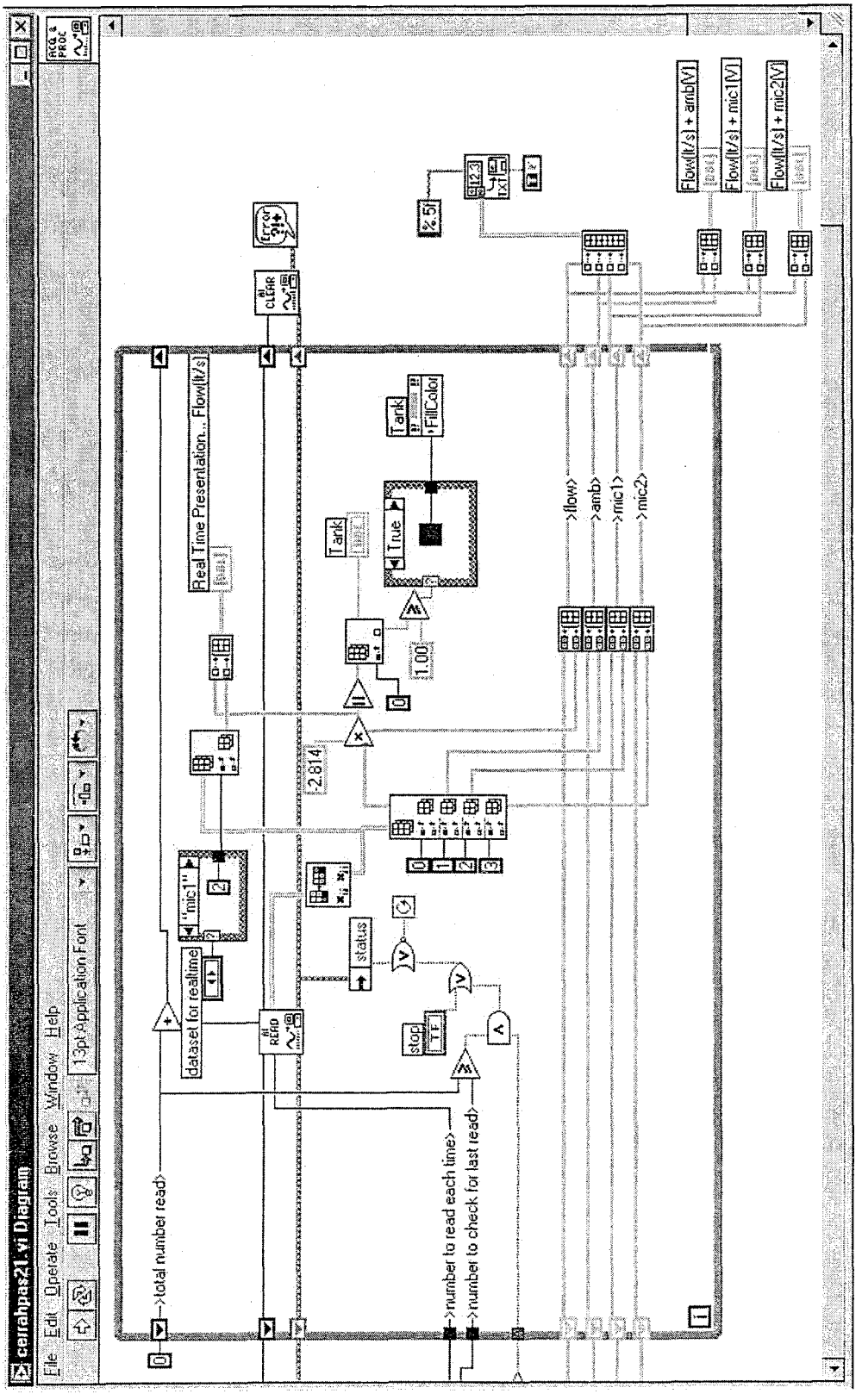

Figure B.1a While loop and data storing part of the process

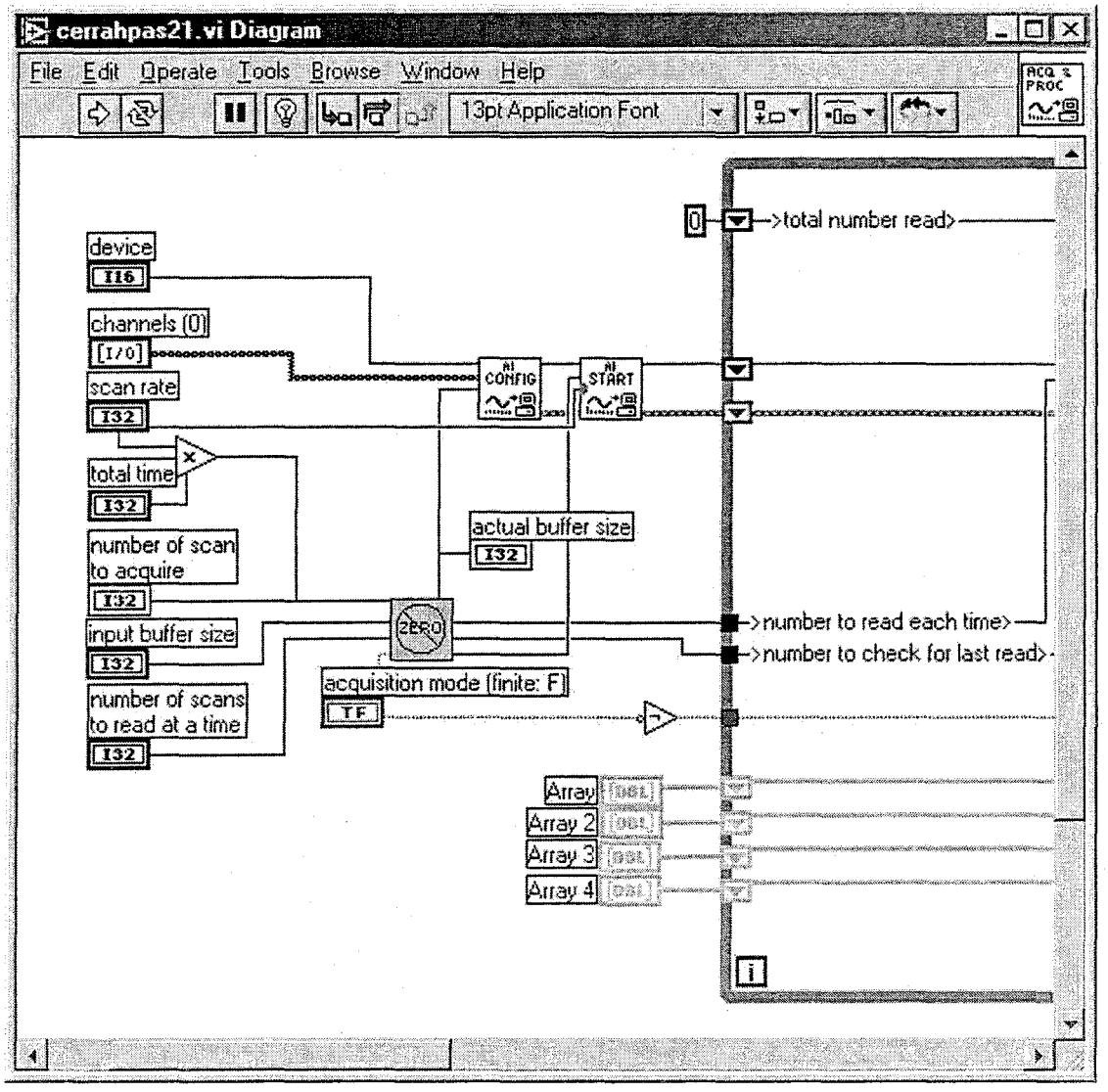

Figure B. 1b The first part of the diagram (the controls of the process)

APPENDIX C: PATIENT PROFILES

Table C.1
Patient profile used in the classification. M: male, F: female, Obs: obstructive, Res: restrictive, Hlt: healthy [30].

No	M/F	Class	Pathology	Age	No	M/F	Class	Pathology	Age
1	F	Obs	asthma	46	30	M	Res	pleuresy	33
2	F	Obs	asthma	17	31	M	Res	pl. effusion	49
3	F	Obs	asthma	35	32	M	Res	b. pneumonia	8
4	F	Obs	asthma	10	33	M	Res	b. pneumonia	13
5	F	Obs	asthma	34	34	F	Res	f.alveolitis	51
6	F	Obs	asthma	40	35	F	Res	f.alveolitis	56
7	F	Obs	asthma	33	36	F	Res	f.alveolitis	59
8	F	Obs	chr. bronch.	15	37	F	Res	f.alveolitis	70
9	M	Obs	chr. bronch.	60	38	M	Hlt	healthy	24
10	M	Obs	chr. bronch.	64	39	M	Hlt	healthy	24
11	M	Obs	chr. bronch.	54	40	M	Hlt	healthy	25
12	M	Obs	chr. bronch.	67	41	M	Hlt	healthy	26
13	F	Obs	chr. bronch.	46	42	M	Hlt	healthy	24
14	F	Obs	chr. bronch.	42	43	M	Hlt	healthy	24
15	F	Obs	chr. bronch.	47	44	M	Hlt	healthy	24
16	M	Obs	emphysema	55	45	M	Hlt	healthy	26
17	M	Obs	emphysema	61	46	M	Hlt	healthy	26
18	M	Obs	emphysema	64	47	M	Hlt	healthy	28
19	M	Res	pneumonia	63	48	M	Hlt	healthy	30
20	F	Res	pneumonia	63	49	M	Hlt	healthy	32
21	F	Res	pneumonia	9	50	M	Hlt	healthy	33
22	M	Res	pneumonia	9	51	F	Hlt	healthy	24
23	F	Res	pneumonia	8	52	F	Hlt	healthy	26
24	F	Res	pneumonia	7	53	F	Hlt	healthy	26
25	F	Res	pneumonia	18	54	M	Hlt	healthy	8
26	M	Res	pneumonia	60	55	M	Hlt	healthy	12
27	M	Res	pneumonia	65	56	F	Hlt	healthy	8
28	M	Res	pneumonia	67	57	F	Hlt	healthy	8
29	M	Res	pneumonia	67					

REFERENCES

1. Gavriely, N., D.W. Cugell, *Breath Sound Methodology*, CRC Press, Florida, 1995.

2. Abella, M., J. Formolo, and D.G. Penny, "Comparison of Acoustic Properties of Six Popular Stethoscopes," *Journal of the Acoustical Society of America*, Vol. 91, pp. 2224-2228, 1992.

3. Pasterkamp, H., S.S. Kraman, and G.R. Wodicka, "Respiratory Sounds, Advances Beyond the Stethoscope," *American Journal of Respiratory and Critical Care Medicine*, Vol. 156, pp. 974–987, 1997.

4. Sovijärvi, A.R.A, J. Vanderschoot, J.E. Earis, "Computerized Respiratory Sound Analysis (CORSA): recommended standards for terms and techniques," *European Respiratory Review,* Vol. 10, pp. 585-649, 2000.

5. Sankur, B., E.C. Guler, and Y.P. Kahya, "Multiresolution Biological Transient Extraction Applied to Respiratory Crackles," *Computers in Biology and Medicine,* Vol. 26, pp. 25-39, 1996.

6. Sovijärvi, A.R.A., F. Dalmasso, J. Vanderschoot, L.P. Malmberg, G. Righini, and S.A.T. Stoneman, "Definition of Terms for Applications of Respiratory Sounds," *European Respiratory Review,* Vol. 10, no. 77, pp. 597–610, 2000.

7. Laennec, R.T.H., *A treatise on diseases of the chest, in which they are described according to their anatomical characters, and their diagnosis established on a new principle by means of acoustics instruments*, Translation form the French by John Forbes, London, 1821.

8. Sovijärvi, A.R.A., L.P. Malmberg, G. Charbonneau, J. Vanderschoot, F. Dalmasso, C. Sacco, M. Rossi, and J.E. Earis, "Characteristics of Breath Sounds and Adventitious Respiratory Sounds," *European Respiratory Review,* Vol. 10, pp. 591–596, 2000.

9. Vannuccini, L., J.E. Earis, P. Helistö, B.M.G. Cheetham, M. Rossi, A.R.A. Sovijärvi, and J. Vanderschoot, "Capturing and Preprocessing of Respiratory Sounds," *European Respiratory Review,* Vol. 10, no. 77, pp. 616–620, 2000.

10. Box, G.P., and G.M. Jenkins, *The Time Series Analysis, Forecasting and Control,* Holden-Day, California, 1976.

11. Cohen, A. and D. Landsberg, "Analysis and Automatic Classification of Breath Sounds," *IEEE Transactions on Biomedical Engineering*, Vol. 31, pp. 585-590, 1985.

12. Iyer, V.K., A. Ramamorthy, and Y. Ploysongsang, "Autoregressive Modeling of Lung Sounds: Characterization of Source and Transmission," *IEEE Transactions on Biomedical Engineering*, Vol. 36, pp. 1133-1137, 1989.

13. Cohen, A., and A.D. Berstein, "Acoustic Transmission of the Respiratory System Using Speech Stimulation," *IEEE Transactions on Biomedical Engineering,* Vol. 38, pp. 126-132, 1991.

14. Vanderschoot, J., and H.J.W. Schreur, "Flow and Volume Related AR-modeling Of Lung Sounds," *Engineering in Medicine and Biology Society, Proceedings of the Annual International Conference of the IEEE*, Vol. 13, pp. 385-386, 1991.

15. Vanderschoot, J., N.G.J. Coppello, and H.J.W. Schreur, "AR Model Orders of Lung Sounds," *Engineering in Medicine and Biology Society, Proceedings of the Annual International Conference of the IEEE*, Vol. 14, pp. 2531-2532, 1992.

16. Vanderschoot, J., and H.J.W. Schreur, "Selection of regressors for AR (q, v) modeling of normal lung sounds," *Engineering in Medicine and Biology Society, Proceedings of the15th Annual International Conference of the IEEE*, pp. 371-372, 1993.

17. Hadjileontiadis, L.J., and Panas S.M., "Autoregressive Modeling of Lung Sounds using Higher-Order Statistics: Estimation of Source and Transmission," *Higher-Order Statistics, Proceedings of the IEEE Signal Processing Workshop on,* pp. 4-8, 1997.

18. Sankur, B., Y.P. Kahya, and E.Ç. Guler "Comparison of AR-based Algorithms for Respiratory Sounds Classification," *Computers in Biology and Medicine,* Vol. 21, pp. 67-76, 1994.

19. Kahya, Y.P., C. Guler, E., B. Sankur, and S. Raudys, "Hierarchical classification of respiratory sounds," *Engineering in Medicine and Biology Society, Proceedings of the 20th Annual International Conference of the IEEE* , pp1598-1601, 1998.

20. Kahya, Y.P., E.C. Guler, C. Ozcan, and E. Sankur, "Classification of respiratory sounds using crackle parameters," Engineering in Medicine and Biology Society, Bridging Disciplines for Biomedicine, 18th Annual International Conference of the IEEE, pp. 952-953, 1996.

21. Kahya, Y.P., E.C. Guler, and B. Sankur, "Statistical analysis of lung sound data," *BMES/EMBS Conference, Proceedings of the First Joint*, pp. 1015, 1999.

22. Guler, E.C., T. Engin; B. Sankur, and Y.P. Kahya, "Spectral analysis of respiratory sounds in healthy and pathological subjects," *Proceedings of the International Biomedical Engineering Days,* pp. 70 -74, 1992.

23. Haykin, S., *Neural Networks*, A Comprehensive Foundation, Macmillan, New Jersey, 1994.

24. Lippmann, R.P., "An Introduction to Computing with Neural Nets," *IEEE Acoustics, Speech and Signal Processing Magazine*, pp. 4-22, April, 1987.

25. Burrus, C.S., R.A. Gopinath, and H. Guo, *Introduction to Wavelets and Wavelet Transforms,* Prentice Hall, New Jersey, 1998.

26. Daubechies, I., *Ten Lectures on Wavelets,* SIAM, Pennsylvania, 1992.

27. Cohen, A., and R.D. Ryan, *Wavelets and Multiscale Signal Processing,* Chapman & Hall, Paris, 1992.

28. Pesu, L., P. Helisto, E. Ademovic, J. C. Pesquet, A. Saarinen, and A. R. A. Sovijarvi, "Classification of Respiratory Sounds based on Wavelet Packet

Decomposition and Learning Vector Quantization," *Technology and Health Care,* Vol. 6, pp. 65-74, 1998.

29. Hadjileontiadis, L.J., and S.M. Panas, "Separation of Discontinuous Adventitious Sounds from Vesicular Sounds Using a Wavelet-based Filter," *IEEE Transactions on Biomedical Engineering,* Vol. 44 , pp.1269 -1281, 1997.

30. Du, M., F.K. Lam, F.H.Y. Chan, and J. Sun, "Multi-resolution Decomposition Applied to Crackle Detection," *Systems, Man, and Cybernetics, IEEE International Conference on Computational Cybernetics and Simulation,* Vol. 5 pp. 4223 -4226, 1997.

31. Yerer, S., *"A Wavelet-based Instrument for Detection of Crackles in Pulmonary Sounds,"* MS. Thesis, Bogazici University, 2002.

32. Sankur, B., Y.P. Kahya., E.C. Guler, and T. Engin, "Feature Extraction and Classification of Nonstationary Signals Based on the Multiresolution Signal Decomposition," *Pattern Recognition, Proceedings of the 12th IAPR International. Conference on Computer Vision & Image Processing*, pp. 592 - 595, 1994.

33. Pittner, S., and S.V. Kamarthi, "Feature Extraction from Wavelet Coefficients for Pattern Recognition Tasks," *IEEE Transactions on Pattern Analysis and Machine Intelligence,* Vol. 21, pp. 83 -88, 1999.

34. Charleston, S., M.R. Azimi-Sadjadi, R. and Gonzalez-Camarena, "Interference Cancellation in Respiratory Sounds via a Multiresolution Joint Time-Delay and Signal-Estimation Scheme," *IEEE Transactions on Biomedical Engineering*, Vol.44, pp. 1006 -1019, 1997.

35. Bahoura, M., M. Hubin, M. Ketata, "Respiratory Sounds Denoising Using Wavelet Packets," *Proceedings of the 2nd International Conference on Bioelectromagnetism*, pp. 11 -12, 1999.

36. Charbonneau, G., J.L. Racineux, M. Sudraud, and E. Tuchais, "An Accurate Recording System and Its Use in Breath Sounds Spectral Analysis," *Journal of Applied Physiology,* Vol. 55, pp.1120-1127, 1983.

37. Güler, E.Ç., *"Observation, Parametric Modeling and Classification of Respiratory Sounds,"* MS. Thesis, Bogazici University, 1992.

38. Kraman, S.S., G.R. Wodicka, Y. Oh, and H. Pasterkamp, "Measurement of Respiratory Acoustic Signals: Effect of Microphone Air Cavity Width, Shape, and Venting," *Chest*, Vol. 108, pp. 1004-1008, 1995.

39. Guler, E.C., *"Classification, Visualization and Transient Analysis of Respiratory Sound Pattern,"* Ph. D. Dissertation, Bogazici University, 1998.

REFERENCES NOT CITED

Aldrobi, A. and M. Unser, editors, *Wavelet in Medicine and Biology,* Boca Raton: CRC Press, 1996.

Aleksanyan, V., Teshiste Temel Bilgi <Propedotik>, Istanbul: Filiz Kitabevi, 1982.

Beyon, J. Y., *LabVIEW Programming, Data Acquisition and Analysis,* New Jersey: Prentice-Hall, 2001.

Chugani, M. L., A. R. Samant, and M. Cerna, *LabVIEW Signal Processing,* Prentice-Hall, New Jersey, 1998.

Demuth, H., and M. Beale, *Neural Network Toolbox User's Guide,* Massachusetts: MathWorks, 2000.

Hudson, D., and M. E. Cohen, *Neural Networks and Artificial Intelligence for Biomedical Engineering*, New York: IEEE Press, 2000.

Misiti, M., Y. Misiti, G. Oppenheim, and J. M. Poggi, *Wavelet Toolbox User's Guide*, Massachusetts: MathWorks, 2000.

Stearns, S. T., and R. A. David, *Signal Processing Algorithms in MATLAB,* New Jersey: Prentice-Hall, 1996.